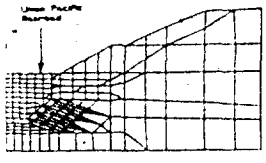

TECHNICAL REPORT ITL-90-4

FINITE ELEMENT STUDY OF TIEBACK WALL FOR BONNEVILLE NAVIGATION LOCK

by

Reed L. Mosher, Virginia R. Knowles

Information Technology Laboratory

DEPARTMENT OF THE ARMY
Waterways Experiment Station, Corps of Engineers
3909 Halls Ferry Road, Vicksburg, Mississippi 39180-6199

May 1990
Final Report

Prepared for DEPARTMENT OF THE ARMY
US Army Engineer District, Portland
Portland, Oregon 97208-2946

Destroy this report when no longer needed. Do not return it to the originator.

The findings in this report are not to be construed as an official Department of the Army position unless so designated by other authorized documents.

The contents of this report are not to be used for advertising, publication, or promotional purposes. Citation of trade names does not constitute an official endorsement or approval of the use of such commercial products.

2

Unclassified
SECURITY CLASSIFICATION OF THIS PAGE

REPORT DOCUMENTATION PAGE

Form Approved OMB No. 0704-0188

1a. REPORT SECURITY CLASSIFICATION Unclassified	1b. RESTRICTIVE MARKINGS
2a. SECURITY CLASSIFICATION AUTHORITY	3. DISTRIBUTION/AVAILABILITY OF REPORT Approved for public release; distribution unlimited.
2b. DECLASSIFICATION/DOWNGRADING SCHEDULE	
4. PERFORMING ORGANIZATION REPORT NUMBER(S) Technical Report ITL-90-4	5. MONITORING ORGANIZATION REPORT NUMBER(S)
6a. NAME OF PERFORMING ORGANIZATION USAEWES Information Technology Laboratory 6b. OFFICE SYMBOL (If applicable) CEWES-IM-D	7a. NAME OF MONITORING ORGANIZATION
6c. ADDRESS (City, State, and ZIP Code) 3909 Halls Ferry Road Vicksburg, MS 39180-6199	7b. ADDRESS (City, State, and ZIP Code)
8a. NAME OF FUNDING/SPONSORING ORGANIZATION US Army Engineer District, Portland 8b. OFFICE SYMBOL (If applicable) CENPP-EN-G	9. PROCUREMENT INSTRUMENT IDENTIFICATION NUMBER
8c. ADDRESS (City, State, and ZIP Code) PO Box 2946 Portland, OR 97208-2946	10. SOURCE OF FUNDING NUMBERS See reverse. PROGRAM ELEMENT NO. / PROJECT NO. / TASK NO. / WORK UNIT ACCESSION NO.
11. TITLE (Include Security Classification) Finite Element Study of Tieback Wall for Bonneville Navigation Lock	
12. PERSONAL AUTHOR(S) Mosher, Reed L.; Knowles, Virginia R.	
13a. TYPE OF REPORT Final report 13b. TIME COVERED FROM _____ TO _____	14. DATE OF REPORT (Year, Month, Day) May 1990 15. PAGE COUNT 120
16. SUPPLEMENTARY NOTATION Available from National Technical Information Service, 5285 Port Royal Road, Springfield, VA 22161.	
17. COSATI CODES FIELD / GROUP / SUB-GROUP	18. SUBJECT TERMS (Continue on reverse if necessary and identify by block number) See reverse.

19. ABSTRACT (Continue on reverse if necessary and identify by block number)

This study of the Bonneville Navigation Lock temporary tieback wall was performed to analytically confirm the design of the wall and to predict its performance during construction operations. The method chosen to do this involves finite element (FE) soil-structure interaction analysis. This method of modeling the wall-soil relationship provides a detailed and accurate representation of the system and its response to various loadings.

The objectives of the study were met through both the development and analysis of a finite element model with the program SOILSTRUCT and assessment of the measured field performance of the wall. The analysis and instrumentation results showed that the wall section studied deflected less than the 0.1-ft limit set by design critieria. In addition, the incremental analysis allowed prediction of wall performance during construction. The analysis results were used in conjunction with the instrumentation results to verify both the FE model and the instrumentation.

(Continued)

20. DISTRIBUTION/AVAILABILITY OF ABSTRACT ☐ UNCLASSIFIED/UNLIMITED ☒ SAME AS RPT. ☐ DTIC USERS	21. ABSTRACT SECURITY CLASSIFICATION Unclassified
22a. NAME OF RESPONSIBLE INDIVIDUAL	22b. TELEPHONE (Include Area Code) / 22c. OFFICE SYMBOL

DD Form 1473, JUN 86 Previous editions are obsolete. SECURITY CLASSIFICATION OF THIS PAGE
Unclassified

90 06 27 312

10. SOURCE OF FUNDING NUMBERS (Continued).

Intra-Army Order for Reimbursable Services No. E86870164, dated 3 August 1987, and No. E86880032, dated 21 October 1987.

18. SUBJECT TERMS (Continued).

Anchored/tieback wall
Diaphragm wall
Instrumentation data
Nonlinear finite element analysis
Performance prediction
Slurry trench construction
Soil-structure interaction
Temporary wall

19. ABSTRACT (Continued).

The results produced by the FE analyses are wall deflection, bending moment, earth pressure distribution, anchor loads, ground surface movement, and soil stresses.

EXECUTIVE SUMMARY

This study of the Bonneville Navigation Lock temporary tieback wall was performed to analytically confirm the design of the wall, to predict its performance during constuction operations, and to assist in instrument data interpretation. The method chosen to do this is finite element (FE)* soil-structure interaction analysis. This method of modeling the wall-soil relationship provides a detailed and accurate representation of the system and its response to various loadings. The objectives of this study were met through the development of an FE model, an analysis with the program SOILSTRUCT, and the assessment of the measured wall performance.

The FE analyses predicted that the constructed wall would meet the criteria (maximum 0.1-ft** deflection). The instrument results showed that the wall section studied did indeed deflect much less than 0.1 ft. In addition, the incremental analysis allowed prediction of wall performance during construction.

The results from the FE analyses are wall deflection, earth pressures, bending moment, anchor loads, ground surface movement, and soil stresses. The wall and a summary of the analyses performed are described briefly in the following text.

Wall Description

The purpose of the tieback wall is to retain soil from the open excavation for the new Bonneville lock channel. The wall is a reinforced concrete diaphragm structure built by the slurry trench method in 20-ft-wide adjoining panels. The FE study is of an instrumented section of the wall at Panel 6, a 50-ft-high panel with four anchors, retaining 30 ft of cohesionless compact slide debris, 20 ft of sedimentary soft rock, and seated in competent diabase. All wall anchors are proof-tested to 150 percent of their design load and locked off at about 100 percent design load.

---

* For convenience, symbols and abbreviations used throughout this report are listed and identified in the Notation (Appendix E).

** A table of factors for converting non-SI units of measurements, used throughout this report, to SI (metric) units is presented on page 13.

Initial FE Model

The initial FE model, described in Parts I and II, is the model developed and analyzed prior to construction for prediction of the wall behavior. The soil parameters used in this initial model were deliberately chosen conservatively. As discovered at a later date, the properties modeling the wall were also slightly conservative. Because of this, the results from the initial FE model were expected to show a worst-case situation. Each stage of excavation and anchor installation was analyzed incrementally. At the final stage, the FE results show the top part of the wall deflected 0.065 ft into the soil. This is opposite the behavior expected for anchored or braced walls; these walls frequently deflect into the excavation. However, this worst-case prediction is well below the 0.10-ft criteria limit. The resulting bending moment is predicted as 133 k-ft; this is also well below its design maximum of 191 k-ft. The ground surface behind the wall is shown to heave upward slightly, then taper off to negligible movement at the railroad tracks. The earth pressure distribution is roughly triangular and slightly greater than the initial pressure before construction. Pressure concentrations can be observed at anchor levels. The anchor prestressing was great enough to pull the wall into the soil and increase the soil pressures to just above at-rest conditions.

The FE calculated anchor loads varied only slightly from their lockoff load level throughout the sequence of construction operations.

This initial FE model was concluded to be a valid representation of the wall and soil section at Panel 6. The results verified the wall design and provided a conservative estimate of behavior of the wall during the construction operations. It was concluded that construction of the wall would have a negligible effect on the railroad tracks.

Following this initial study, the model was used to conduct other analyses. In one analysis, it was found that anchor prestress level had a direct effect on the magnitudes of wall deflection, bending moment, and earth pressures. In another analysis, failure of the top anchor was simulated to show the relative influence of this support on the stability of the system. With full loss of anchor capacity, the wall moved out into the excavation 0.065 ft at the top, and 13 percent of its load was redistributed to the remaining anchors.

Field Performance and FE Model Refinement

After wall construction, instrumentation data were received and reduced to study field performance. Wall deflection and bending moment were plotted for several load cases. Comparison of this to the FE results showed a close qualitative resemblence of behavior in corresponding load cases. This close agreement in the nature of the response was not repeated in the magnitude of the response. The wall was measured to move a maximum of 0.01 ft into the soil, at the top. The FE study predicted 0.065 ft of movement at the top. The FE results appeared to be off from the observed results by some numeric factor but showed close qualitative agreement. The FE model could be refined by modifying one of the conservative soil parameters to more closely match the measured behavior numerically. It was found that stiffening the soil, by increasing the soil modulus, produced results that best matched instrumentation. This nonlinear unload-reload soil modulus parameter was increased by a factor of three to achieve an appropriate soil model. The increase is valid, because this parameter was initially chosen conservatively at the lower end of a range of possible parameter values associated with this type of soil. With this model, the ground surface movement was hardly discernible. The maximum bending moment was greatly reduced from that of the initial analysis. The earth pressure distribution remained about the same as the initial model but decreased in the soft rock zone along the bottom one-third of the wall. A more uniform shape was observed.

Interesting results were also found from a study conducted with K_o, the initial horizontal earth pressure coefficient, being increased from 0.5 to 1.0 to 2.0 for all of the soils. As K_o increased, the wall bulged increasingly toward the excavation, the bending moments increased, and the earth pressure distribution became erratic and of large magnitude. Increasing K_o produced behavior that diverged from the measured response of the wall during construction; therefore, the initial value for K_o, 0.5, was determined to be appropriate.

Panel 11 Analysis

Another FE model was developed for a section of the wall at Panel 11. The purpose was to see the behavior of this 80-ft panel, as compared to that

of the 50-ft Panel 6. Panel 11 has six anchors, retains only the cohesionless slide material, and, like Panel 6, is seated in the diabase. Three analyses were performed on Panel 11: one using the same parameters as for the initial Panel 6 model, a second with the soil modulus parameter tripled as with the final Panel 6 model, and a third with this parameter increased six times.

FE results for Panel 11 were similar to those of Panel 6, but were of a greater magnitude. Although Panel 11 was not instrumented, the results from the tripled stiffness analysis are considered most appropriate of the three, based on the Panel 6 study. Again, the wall was pulled into the soil 0.153 ft at the top. Although this exceeds the criteria limit of 0.10 ft for wall deflection, the fact that the wall moved into the soil and not into the excavation, as assumed, decreases the likelihood for problems at the railroad tracks. Any heave behind the wall will be supressed by vertical surcharges, such as equipment and trains, not included in the analyses.

The maximum bending moment predicted for Panel 11 from the FE analysis is 236 k-ft. The design moment for this panel is not available for comparison. The earth pressures on Panel 11 assumed a fairly uniform distribution through the soil, then very rapidly became quite large at the soil-diabase interface. This is due to the stress transfer and different degrees of movement between the strong, stiff, cohesive diabase, and the less stiff, cohesionless soil.

The tieback anchor loads in Panel 11 remained fairly consistent throughout the FE-modeled construction steps. The responses to each load case were similar to the Panel 6 anchor responses.

Conclusions on Panel 6 and Panel 11 Analyses

The Panel 11 analysis is useful in displaying the relative differences between the reactions of the two panels of different sizes. In general, the greater height of excavation caused larger pressures, deflections, and moments in Panel 11. The Panel 11 response, as predicted from the FE analysis, might be considered a worst-case reaction for the entire wall section, because it is one of the tallest and most anchored of the panels. The results from Panel 6 might be considered a more typical response of this wall.

A main outcome of this study is that the FE soil-structure interaction method of analyzing a tieback wall is an effective approach for determining

significant details of the behavior of the system. For this particular case, it was found that the soil is stiffer than originally estimated. However, the key aspects of the wall-soil response were accurately modeled from the very beginning. This information can be incorporated into the design and construction of future walls at the Bonneville Navigation Lock site or in similar geologic areas.

PREFACE

This report presents the investigation of the temporary tieback wall at the new Bonneville Navigation Lock construction site. The US Army Engineer Waterways Experiment Station (WES) was authorized to conduct this investigation by the US Army Engineer District, Portland (NPP), through Intra-Army Order for Reimbursable Services No. E86870164, dated 3 August 1987, and E86880032, dated 21 October 1987. The investigation was coordinated through Mr. Patrick Jones, Project Engineer, Soils Section, Geotechnical Branch (GS), NPP, under the general supervision of Mr. Richard Hannon, Chief, Soils Section, GS, NPP.

The work was performed at WES by Ms. Virginia Knowles, Scientific and Engineering Applications Center, Computer-Aided Engineering Division (CAED), Information Technology Laboratory (ITL), and Mr. Reed Mosher, Interdisciplinary Research Group, CAED, ITL, with assistance from Dr. John Peters, Soils Research Facility, Soil Mechanics Division, Geotechnical Laboratory. This report was prepared by Ms. Knowles and Mr. Mosher. Many valuable comments were provided by Dr. Peters. Mr. Joseph Jenkins, CAED, ITL, assisted in plotting results for the report. All work was accomplished under the general supervision of Dr. Edward Middleton, Chief, CAED, and Dr. N. Radhakrishnan, Chief, ITL. This technical report was published by ITL, WES.

COL Larry B. Fulton, EN, is Commander and Director of WES. Dr. Robert Whalin is the Technical Director.

CONTENTS

LIST OF TABLES

LIST OF FIGURES

CONVERSION FACTORS, NON-SI TO SI (METRIC) UNITS OF MEASUREMENT

Non-SI units of measurement used in this report can be converted to SI (metric) units as follows:

Multiply	By	To Obtain
degrees (angle)	$\pi/180$	radians
feet	0.3048	metres
inches	2.54	centimetres
kips	4,448.0	newtons
kip-feet	1,355.75	newton-metres
kips per square foot	0.48824	kilograms per square centimetre
miles (US statute)	1.609	kilometres
pounds (force) per square foot	47.88	pascals
pounds (force) per square inch	6.894757	kilopascals
tons (short)	0.9072	tons (metric)

FINITE ELEMENT STUDY OF TIEBACK WALL FOR BONNEVILLE NAVIGATION LOCK

PART I: INTRODUCTION, PROJECT DESCRIPTION, OBJECTIVES, AND METHODS

1. This report describes the model, analysis method, and results for the investigation of a temporary, anchored, retaining wall. This temporary wall is used to retain soil from the excavation for the construction of a new navigation lock at Bonneville Lock and Dam on the Columbia River, between the states of Washington and Oregon. The new structure is located landward of the existing lock and requires an open excavation for the new lock and channel construction. The US Army Engineer District, Portland, is responsible for planning, design, and construction of this wall. The US Army Engineer Waterways Experiment Station has been providing assistance to the US Army Engineer District, Portland, by conducting a finite element (FE) study of the wall. The study was performed to provide an analytical measure of wall and soil behavior. The results will help assess the wall design and instrumentation data.

2. This additional study was initiated because adjacent to the upstream portion of the excavation lies the Union Pacific Railroad's (UPRR) main transcontinental railroad tracks for the northwestern United States. The design of the wall has come under scrutiny due to its proximity to the railroad line. The temporary tieback wall was designed to limit settlement of the soil behind the wall, upon which the adjacent railroad tracks are founded. To ensure that the wall would perform as designed, a reevaluation of the wall was conducted using state-of-the-art engineering techniques.

Project Description

Site

3. The Bonneville Lock and Dam is located on the Columbia River, about 146 miles* from its mouth at the tidewater head and 42 miles east of Portland, OR. Because the Oregon-Washington state boundary follows the Columbia River channel, the lock and dam site is divided between the two states. The new

* A table of factors for converting non-SI units of measurement to SI (metric) units is presented on page 13.

lock is under construction on the Oregon side of the river and landward (southwest) of the old lock. The new lock will have a greater lockage volume (30-million-ton capacity) than the old lock (13-million-ton capacity) and will help reduce shipping bottlenecks at this location on the river.

4. The temporary tieback wall will retain the sides of the excavation for construction of the upstream miter gate section and lock channel. This wall will adjoin a permanent guard wall that protects the upstream channel. Both walls are installed by the slurry trench method of construction. Parallel to and 50 ft landward from the temporary wall lies the main northwest rail line of the UPRR. At the beginning of this project, the railroad was relocated landward, away from the construction site for the new lock. This relocation required the excavation of a large volume of the slope and highway fill materials. A plan view of the site is shown in Figure 1.

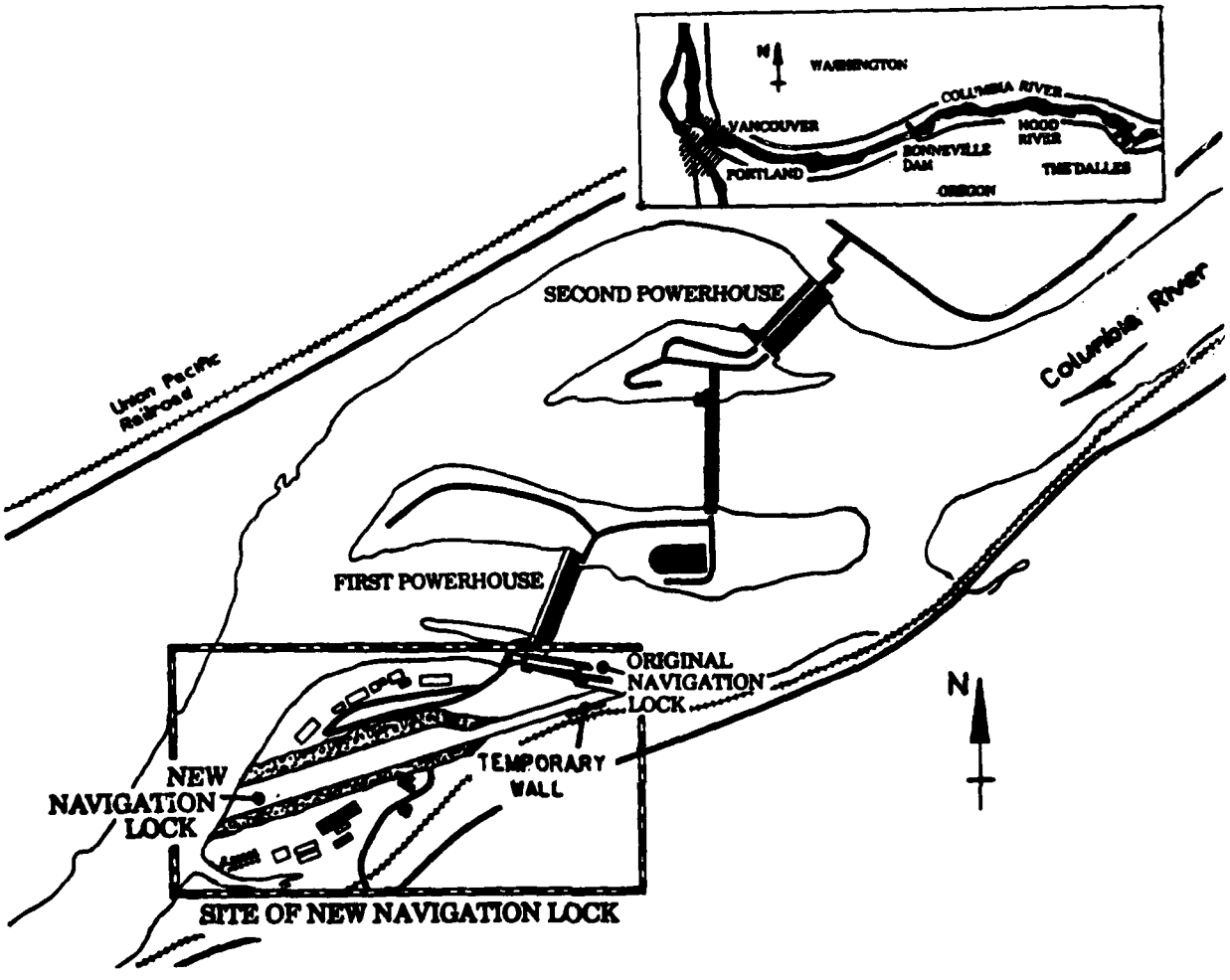

Figure 1. Plan view of the project site

Geology

5. The temporary wall is located near the toe of the Tooth Rock Landslide. Much of the material retained by the wall is debris from the slide. The Tooth Rock Landslide is a Pleistocene age, deep-seated slump consisting primarily of large displaced slide blocks (SB) and unconsolidated slide debris (SD). Slope stability analyses, along with evaluation of surface movement, indicate that this slide unit is stable. The slide blocks are derived mainly from the underlying Weigle formation (Tw). These blocks range from tens to hundreds of feet across. The slide debris is a mixture of decomposed clayey rock materials ranging from granular deposits to boulders as large as 20 ft across. Erosion and river work on the SD have produced a new distinct material called reworked slide debris (RSD), a medium-dense granular deposit. RSD is a combination of gravels, cobble- to boulder-size rounded rocks, and a mixture of fine sands and silts. Ancient flood deposits of silt and sand cover much of the ground surface above the RSD.

6. Under the Tooth Rock Landslide are two intact rock units: (a) the Tw, a sedimentary, "soft rock," material consisting of volcanic derived mudstone, siltstone, and claystone, and (b) the Bonney rock intrusive (Ti), a large, irregular, diabase unit with columnar jointing intruding the older Weigle formation. The permanent lock structure itself is to be built on a large monolithic mass of this diabase. A geologic profile at the wall section under study was developed from boring logs and section profiles. This profile is displayed in Figure 2.

Wall description

7. The temporary retaining wall is approximately 440 ft long. It will be constructed in two phases: a 180-ft-long section and a 260-ft-long section. The first section is made up of nine 20-ft-long, 3-ft-thick, reinforced concrete panels. The heights of the panels range from 20 to 110 ft, depending on the depth to the diabase. The top of each panel in this section is at elevation (el) 89 ft.* Each panel is seated at least 2 ft in the diabase for stability and seepage control. Dewatering efforts upstream and behind the wall have minimized seepage effects; however, there are weepholes in the wall panels to relieve any water buildup.

---

* All elevations (el) cited throughout this report are in feet referred to the National Geodetic Vertical Datum (NGVD) of 1929.

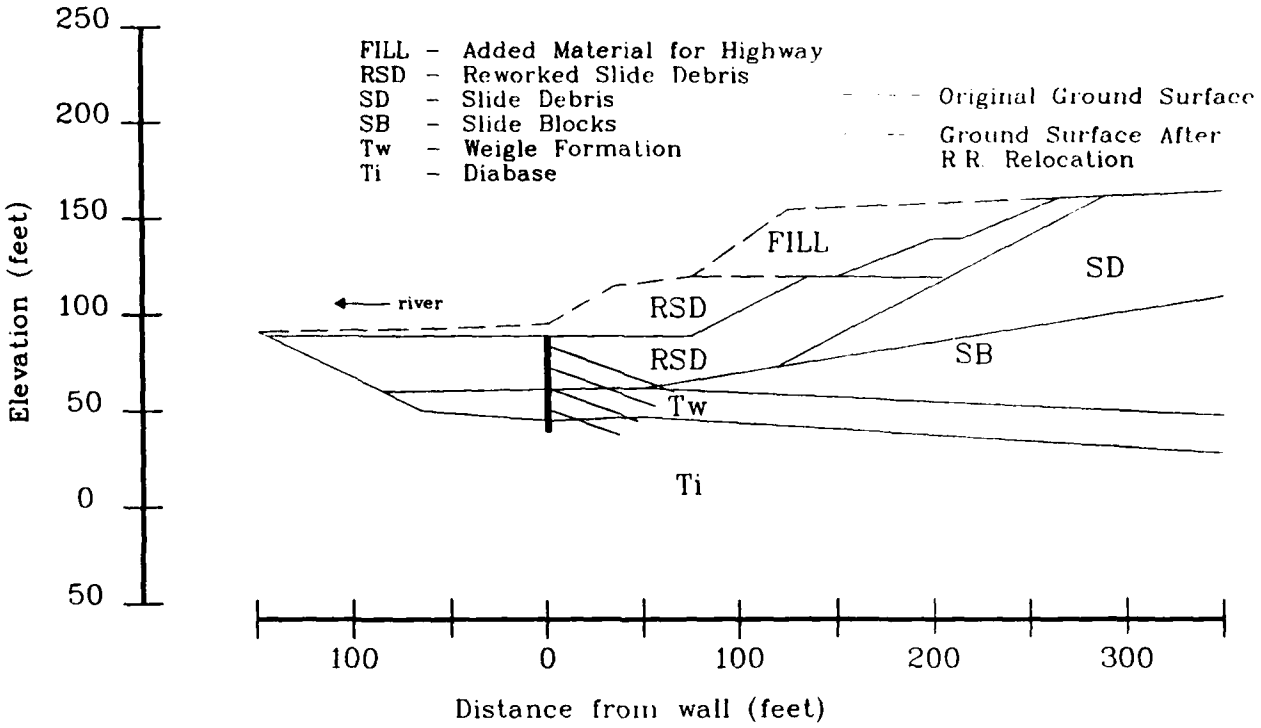

Figure 2. Geologic profile at Panel 6, looking upstream

8. The diaphragm wall was constructed by the slurry trench method. In this method, each of the panels was individually built according to the following procedure. A 3- by 20-ft concrete form was placed at the ground surface in the location of the panel. This form guided a clamshell bucket as it excavated soil for the panel construction. As excavation progressed, a bentonite slurry head was maintained in the hole. Excavation continued until a minimum of 2 ft of diabase was recovered from the bottom of the hole. Due to irregular and steeply sloped diabase, some panel bottoms were "stair stepped" to reduce the volume of diabase excavated. A crane then placed the steel reinforcing cage into the slurry-filled excavation, and concrete was tremmied in, displacing the slurry. This concluded the construction of one panel. The panels were constructed in an alternating order so that adjacent panels were not built sequentially, but were joined by a shoulder pipe to panels that were already built. Figure 3 shows a front view of the temporary wall.

9. After the wall was completed, excavation for the lock channel was initiated. Soil was removed on the north face of the wall from the ground surface down to the top of the diabase. The material removed consisted mainly

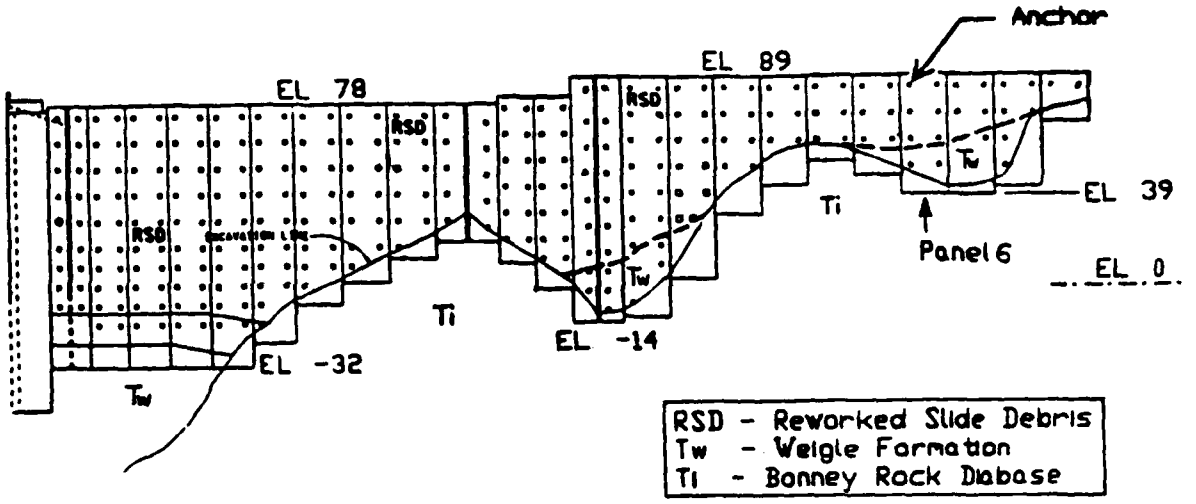

Figure 3. Front view of temporary tieback wall

of RSD and varying amounts of the Weigle. Anchors were installed as excavation progressed. Panel 6 of this wall (Figure 3), a 50-ft-tall panel, was instrumented with strain gages and a slope inclinometer. The data from these instruments will be used to evaluate wall performance and provide information for future construction.

Anchors

10. Tiebacks were installed in a grid pattern of approximately 10 ft horizontal by 11 ft vertical. All anchors at the same elevation were installed before anchors at the next lower row were installed. The installation procedure consisted of drilling, grouting, prestressing (and proof-testing), and lockoff. The tieback was a 19-strand 0.6-in.-diam high-strength steel tendon. The anchorage in the soil was formed by pressure grouting. The unbonded length of the tie varied with each anchor from 37 to 74 ft, depending on the distance past the critical slip plane as determined from limit equilibrium methods. The minimum bonded length is 30 ft for anchorage in the RSD and 35 ft in the Tw. Tieback corrosion protection includes cement-grout protection over the bonded length and a grease-filled sheath over the unbonded length. All grout strengths tested above the minimum design strength of 3,000 psi. Each anchor was prestressed for a proof test and creep test by the application of a load 50 percent above the design load (DL) of the anchor. The design loads are approximately one-half (safety factor = 2) the ultimate load capacities for the anchors as determined by the field tests detailed in the Tieback Test Program, Phase II Report (US Army Engineer District, Portland

1986). The design bond stress for RSD is 60 psi and for the Weigle is 35 psi. Following the prestressing, anchors were locked off at loads near their design load. Figure 4 displays a section view of Panel 6. Information for the four anchors of Panel 6 is listed in Table 1.

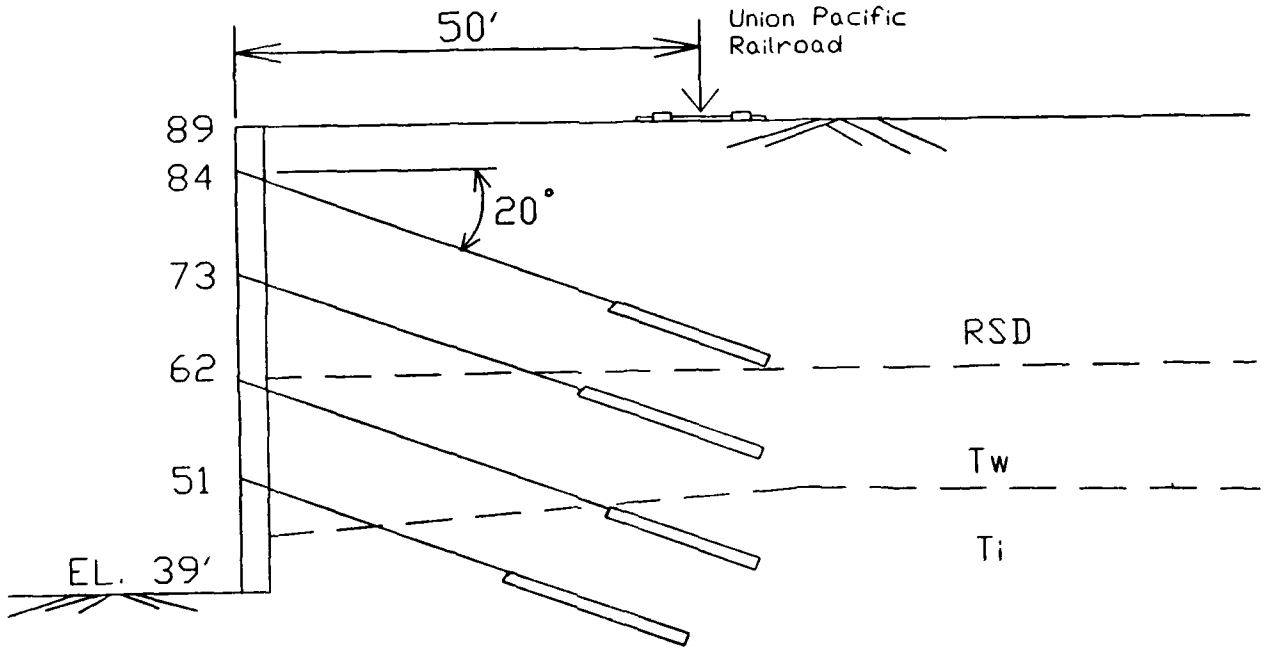

Figure 4. Section view of Panel 6 of the tieback wall

Table 1
Panel 6 Anchor Loads

Anchor Elevation feet	Anchor Length* feet	Design Load (DL) kips	Prestress Load 150% DL	Lock-off Load
84.	89	281.	421.5	272.
73.	79	281.	421.5	292.
62.	68	281.	421.5	290.
51.	52	358.	537.0	356.

* Anchor length = unbonded + half of bonded lengths.
Area of steel anchor strand = 0.217 sq in.

Study Objectives

11. The purpose of this study was threefold: (a) to provide a means for additional confirmation of the procedures used in designing the wall; (b) to predict potential wall performance during excavation and tieback installation; and (c) to assist in the interpretation of instrumentation results. To accomplish these, Panel 6 was analyzed.

12. Results from the study depict wall behavior in terms of lateral deflection and internal bending moment. Earth pressures on the wall are also presented. Due to proximity of the railroad tracks to the wall, movement of the ground surface behind the wall is assessed as well. Soil response to the loadings is evaluated by studying the stresses (horizontal, vertical, and shear) and the deflections experienced by the soil during each load increment.

Analysis Description

13. The computer program SOILSTRUCT was used for the analysis. SOILSTRUCT was specifically developed to model complex soil-structure interaction problems by the FE method. This program was developed by Prof. G. Wayne Clough, Virginia Polytechnic Institute (VPI), and his colleagues over a period of 20 years and has been used to analyze a wide variety of problems, including navigation locks, retaining walls, supported excavations, dams, tunnels, foundations, and cofferdams. The element types and material relationships in SOILSTRUCT will be explained in the context of the model developed for this study.

Model

14. The FE mesh developed to model Panel 6 and surrounding soil is shown in Figure 5. The model approximates the soil profile at Panel 6 shown in Figure 2. This grid has 395 elements and 389 nodes. Preliminary studies in formulating the model revealed the need to extend the grid far beyond the wall to ensure that proper in situ stresses were developed. Nodes along the bottom of the grid were fixed in both the horizontal and vertical directions, while nodes on the two sides of the grid were fixed horizontally only. All other nodes were free to move in both directions.

15. The soil and wall were modeled by a two-dimensional, plane-strain, subparametric, quadrilateral element, QM5. The QM5 element is of the linear

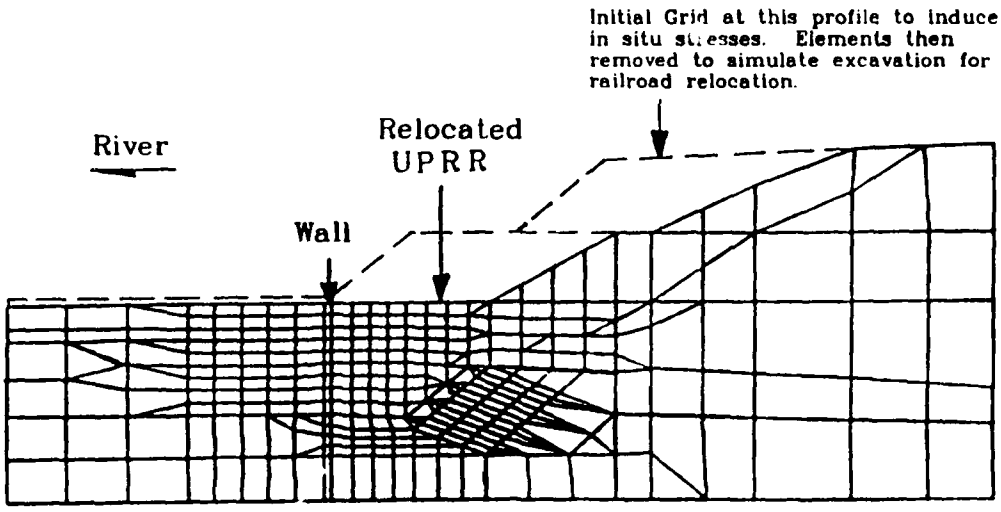

Figure 5. FE grid model of Panel 6 and geologic section

variety with reduced integration for the shear terms. The element has five nodes; four corner nodes and one internal node at the center. It has been shown to be efficient and accurate in modeling bending and shear response (Doherty, Wilson, and Taylor 1969).

16. In the model, slip elements were supplied at all interfaces between soil and the wall. The slip element employed in SOILSTRUCT is the four-node, zero-thickness element developed by Goodman, Taylor, and Brekke (1968). It allows for controlled relative movements on the interface between materials with different properties, such as soil and concrete. This response between the soil and concrete is an essential aspect of the analysis of soil-structure interaction problems.

17. The bar element in SOILSTRUCT is a one-dimensional truss member that can respond by either compression or tension, or both compression and tension. The bar elements were utilized in two ways in the model: (a) to represent the anchors, and (b) as strain gages attached to the surfaces of wall elements to directly determine bending moment from their movement (Peters et al. in preparation). Appendix A describes the use of bar elements as strain gages.

18. The anchors were first modeled as bar elements surrounded by two-dimensional elements with grout properties within the soil mass. Initial analyses showed that the small movements of the soil surrounding these anchorages had little effect on soil stresses in the wall vicinity, therefore in

subsequent analyses, the anchor was simply modeled as a bar element connected from the wall to a fixed boundary along the model base. Appendix B explains the studies used in developing the wall and anchor models for the FE grid.

Materials

19. Soils are known to have a complex stress-strain response. The constitutive model in SOILSTRUCT attempts to capture all of the key aspects of soil behavior. The model used in the program is a variation of the commonly applied Duncan and Chang (1970) hyperbolic scheme. For primary and/or initial loading, the soil response is represented by a nonlinear, hyperbolic curve, the shape of which is a function of confining stresses and the Mohr-Coulomb strength parameters of the soil. During unloading or reloading, the soil behavior is approximated by a linear response. If reloading brings the stress level back to the original point achieved during primary loading, then increasing the stresses beyond this level results in behavior that follows the nonlinear, primary curve until failure is reached. This stress-strain model is presented in Figure 6.

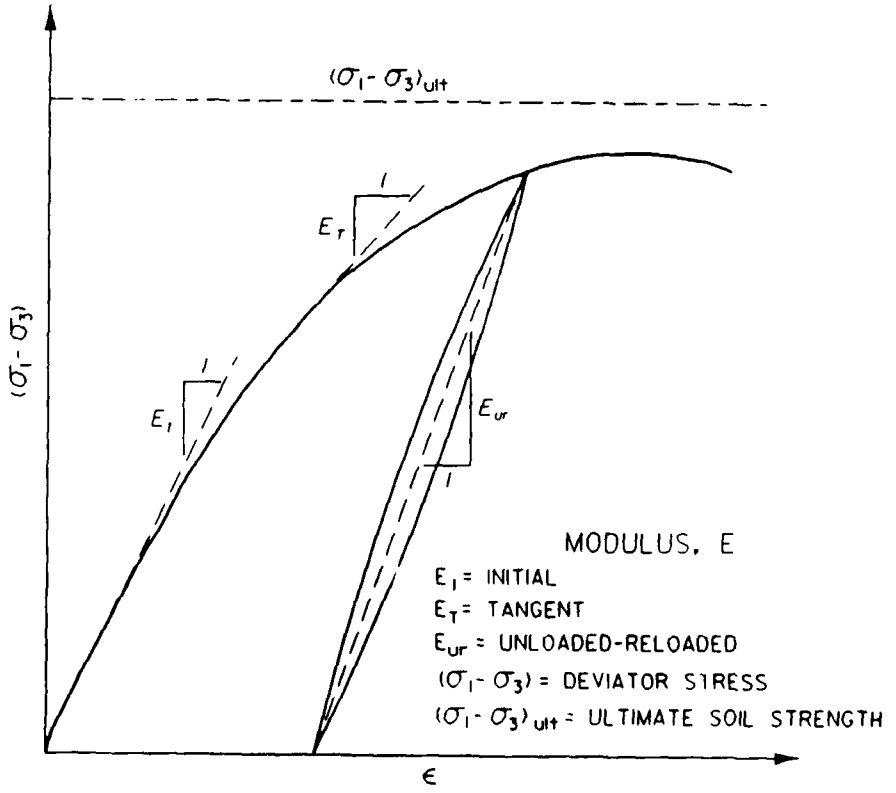

Figure 6. Hyperbolic representation of stress-strain curve for soil

20. In the soil model, the strength of the soil is defined by the conventional Mohr-Coulomb criterion, with the soil strength parameters specified by the friction angle and the cohesion. If the stresses in an element are equal to or exceed those allowed by the Mohr-Coulomb limits, the modulus is set to a very low value so that the element will not take on any additional shear stresses; however, hydrostatic stresses can be increased. This particular type of nonlinear elastic model is the most widely used in finite element studies of soils because of its relative simplicity and its ability to model key aspects of the soil response.

21. Structural materials, such as the wall and the anchors, are assumed to behave in a linear elastic manner. The interface between structural materials and soils is represented with the one-dimensional slip element. To define the proper response of this interface, a stress-displacement relationship is required, similar to that used for modeling stress-strain behavior in the soil. A bilinear representation is used, with the stiffness of the interface depending upon the normal stress on the interface. The interface strength is defined in terms of the Mohr-Coulomb criterion.

22. The material properties and parameters of the soils modeled in the analysis are listed in Table 2. Soil properties were obtained from laboratory test data (Headquarters, Department of the Army 1987), and the parameters needed for the hyperbolic model were estimated based on published data found in the report by Duncan et al. (1980). These parameters were deliberately chosen on the low side to provide a worst-case scenario.

23. Properties of the panel section provided by the Portland District were:

concrete strength = 3,000 psi

section stiffness (EI) = 1,012,500 k-ft/lin ft

section modulus (S) = 1.5 ft^3/lin ft

Interface element properties are determined in accordance with properties of the materials adjacent to the interface. The wall-soil interface for this study is modeled as a cohesionless surface of high shear stiffness, with a friction angle of 30 deg.

Loading Sequence

24. SOILSTRUCT is designed so that the actual construction process can be simulated in the FE analysis. Simulation of the actual sequence of construction is important because the soil stress-strain response is nonlinear

Table 2
Soil Properties and Parameters

Property	Slide Block (SB)	Slide Debris (SD), Reworked Slide Debris (RSD), Fill Material	Weigle Formation (Tw)	Bonney Rock, Diabase (Tl)
Friction angle (deg)	32	34	30	0
Cohesion (psf)	750	0	10,000	100,000
Unit weight (pcf)	130	125	130	175
Poisson's Ratio	0.45	0.45	0.40	0.40
Initial horizontal earth pressure coefficient	0.5	0.5	0.5	0.5
Initial tangent modulus parameter, K_m	200	300	1000	20,000
Unload modulus parameter, K_{ur}	200	300	1000	20,000
Strength ratio, R	0.7	0.7	0.7	0.7
Modulus exponent, N	0.6	0.3	0.5	0.5
Minimum initial tangent modulus (psf)	100	100	100	100
Tangent modulus at failure (psf)	100	100	100	100

and stress-path dependent. SOILSTRUCT provides for simulation of initial stresses, fill placement, material excavation, dewatering, and placement of structural materials in a series of incremental loading steps. Incremental stresses and displacements are computed after each load step. Table 3 lists the loading steps used to model the sequence for the wall construction and lock channel excavation. This procedure is discussed subsequently.

25. The original soil surface of the FE grid was horizontal at el 89 ft. The slope behind the wall was gradually built up to simulate natural loading and develop accurate in situ stresses before any construction started.

Table 3
Loading Steps in SOILSTRUCT Analysis

Step Number	Description
1	Build natural slope, first increment
2	Build natural slope, second increment
3	Build natural slope, third increment
4	Build natural slope to preexcavation profile
5	Excavate for R.R. relocation (current profile)
6	Build wall
7	Excavate el 78.5 ft (in front of wall)
8	Prestress first tieback, el 84 ft (150% design load)
9	Excavate to el 67.5 ft, lock off first tie at field load
10	Prestress second tieback, el 73 ft
11	Excavate to el 56.5 ft, lock off second tie
12	Prestress third tieback, el 62 ft
13	Excavate to el 45 ft, lock off third tie
14	Prestress fourth tieback, el 51 ft
15	Excavate to bottom of wall, el 39 ft, lock off fourth tie
16	Release top anchor in failure simulation analysis

To model the slope excavation for the railroad relocation, elements corresponding to the excavated section were removed from the grid, and the loads resulting from this stress release were applied to the remaining elements. The displacements resulting from these loadings were reset to zero to correspond with conditions in the field prior to placement of the wall. To model the slurry construction, material properties were changed from soil to concrete in the appropriate location, and corresponding loads were applied to the system as a result of the difference between the unit weights of the soil and concrete. Displacements of the wall from this step were zeroed as well. This coincides with the zero reading for the instrumentation placed in the wall.

26. Once the wall was in place, the simulated excavation for lock construction began. First, a layer of soil (about 10 ft) was excavated (step 7, Table 3). Excavation is modeled in the program by changing designated elements to air and applying the stresses released from these elements to nodes of the adjacent unexcavated elements. The grid was designed so that the rows

of elements in front of the wall corresponded to the excavation lifts and the nodes of the wall to the locations of the tiebacks.

27. During the next load case (step 8, Table 3), the first row of anchor placements was modeled by applying a load, equal to 150 percent of the design anchor load, to the wall at the first anchor elevation, at the proper inclination (20 deg). With excavation of the second layer (step 9, Table 3), the stiffness of the first anchor was added to the system by attaching a pre-stressed bar element to the wall at the anchor elevation and to a fixed boundary. Also, during this step, a loading was applied again at the first anchor elevation to reduce the anchor load from the proof-test level, used to test the anchor, to the design load level. The actual in situ anchor loads at lockoff varied slightly from the design load. This process of excavation and anchor placement was repeated until the excavation reached the bottom of the wall. Figure 7 illustrates the procedure.

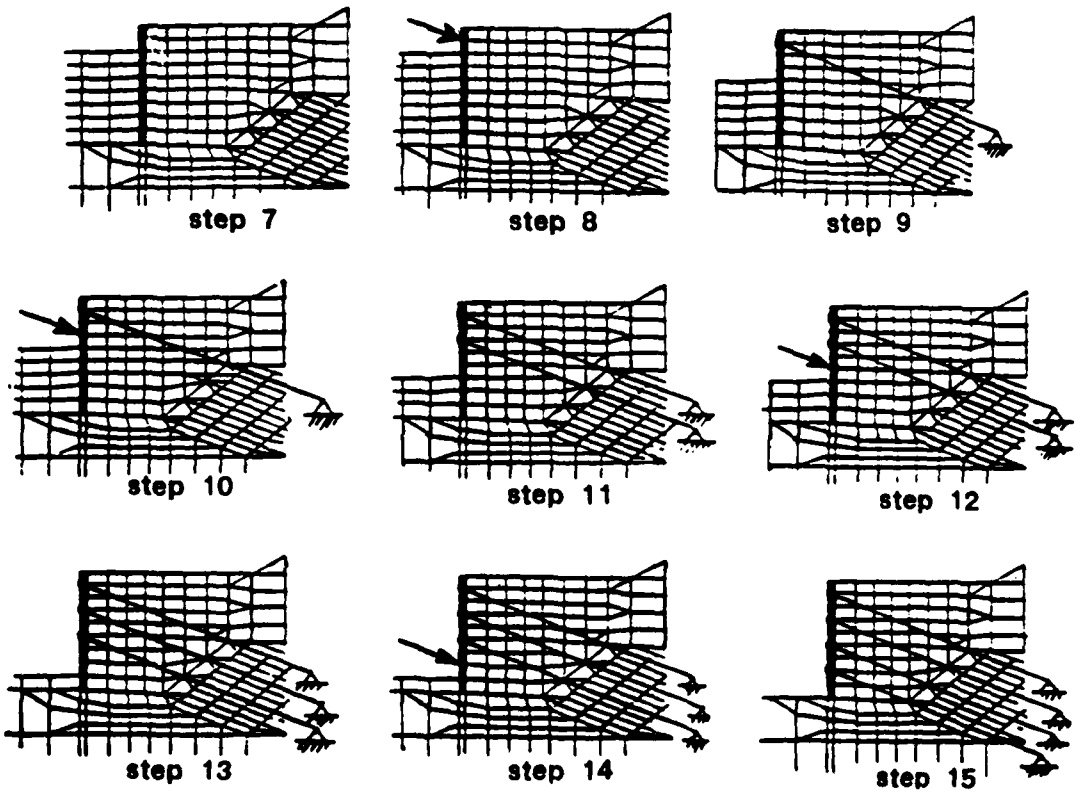

Figure 7. Models of the loading sequence used in SOILSTRUCT to represent construction operations at Panel 6

Organization of Documentation

28. The contents of this report are presented in chronological order, according to the progression of work accomplished. The study was divided into three phases. Phase 1 involved the development and analysis of a model of the wall prior to its construction in the field. The analysis results were used to predict field performance and to provide assistance in locating potential problem areas, if any existed, so that the design or construction procedure could be modified before work began. Part I describes the background, the site, the study objectives, and the model development. Part II presents the results of the analysis on this model, including predictions of wall deflection, bending moment, and earth pressures, among other details that completed Phase 1 of the project.

29. Phase 2 is the reanalysis of the model for different construction and field conditions. This was done immediately following Phase 1 to provide an indication of possible behavior due to: anchor prestress load variations, failure of the top anchor, and different soil conditions. Part III gives a discription of these analyses and a discussion of the results.

30. Phase 3 was initiated when the wall construction was completed and instrumentation data from the site were received. This work phase involved reduction of the field data to show wall deflection and bending moment and comparison of these results to the predicted analytical results. The model was then refined to more closely match the measured performance by modifying soil characteristics. The description of this work, the analyses, and results are presented in Part IV.

31. The remainder of the report, Parts V through VII and the appendixes, were developed after Phase 3 in the process of completing the study and report. Part V contains a detailed discussion of the wall model and its properties and the method of reducing strain gage data to obtain bending moment.

32. Part VI shows the field measurements from the completion of construction to 7 months later. Various aspects of the measured behavior are discussed.

33. In Part VII, an account of modeling and analysis results from another section of the wall is presented. This is a taller section with more anchors and differing soil conditions. This work began shortly after the

Phase 1 work was concluded and continued as part of Phase 2.

34. Appendix A describes the method by which one-dimensional bar elements are used in the FE program to determine the bending moment of structural elements.

35. Appendix B presents studies performed to develop certain aspects of the FE grid, namely the wall and the anchor models.

36. Appendix C lists the data from the wall instrument readings.

37. Appendix D shows the calculation of various values presented in Part V.

38. Appendix E lists and identifies the symbols and abbreviations used throughout the report in the Notation.

PART II: RESULTS FROM INITIAL STUDIES OF PANEL 6 (PHASE 1)

39. The analysis results of the Panel 6 model described in Part I are presented and discussed in Part II. Results include soil stresses, wall deflections, bending moments, earth pressures on the wall, and ground surface movement behind the wall. This analysis was performed before construction of the wall began, thereby allowing any problem areas found in the wall design or construction procedure to be modified prior to construction.

40. The results for each construction step were studied, from the in situ state and wall construction through the excavation and tie installation procedure. Trends, maximums, and other significant features, as well as final results, are presented and discussed.

Phase 1 Results

Soil stresses

41. Stresses in the soil, horizontal (σ_H), vertical (σ_V), and shear, display the soil reactions to the various loadings. Figures 8a through 8e show the ratio of horizontal to vertical stress, σ_H/σ_V, for soil elements in the vicinity of the wall. This ratio can be thought of as a horizontal earth pressure coefficient. Figure 8a shows the initial soil stress ratios, or at-rest earth pressure coefficients, prior to any construction. The horizontal stresses are equal to and up to three times as great as the vertical stresses near the soil surface at the toe of the slope. This is due to the rotation of principal stresses caused by the slope. The stress ratio decreases with depth and appears to stablize around 0.6 to 0.7 at a depth of 30 ft. After the excavation for the railroad relocation and construction of the wall (Figure 8b), this stress ratio increases in most areas. This increase is due to: (a) overburden removal, which decreases vertical stress and locks in horizontal stress, and (b) construction of the wall, which slightly increases horizontal stress due to differences in material densities.

42. Figure 8c shows these stress ratios after the first layer of soil has been excavated in front of the wall. The wall moved toward the excavation, decreasing confining pressure of the soil behind it, and increasing confining pressure of the soil in front of it. The soil in front of the wall also experienced a decrease in vertical stress due to the excavation. The

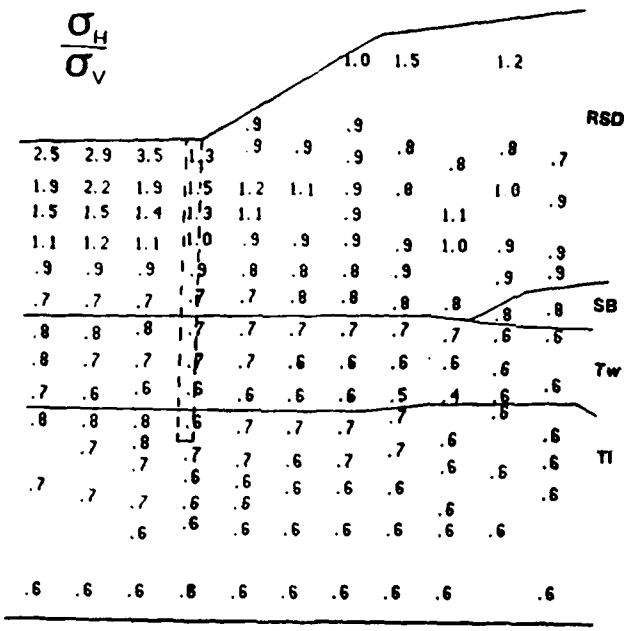

a. Initial state, at rest

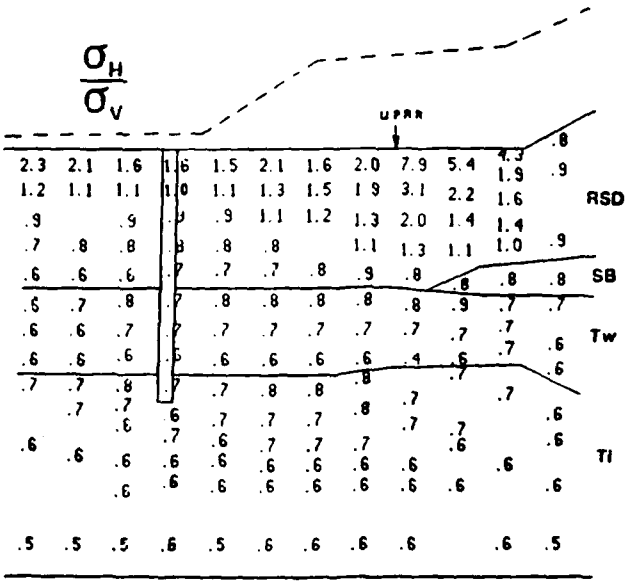

b. Surface excavation for railroad relocation and construction of Panel 6

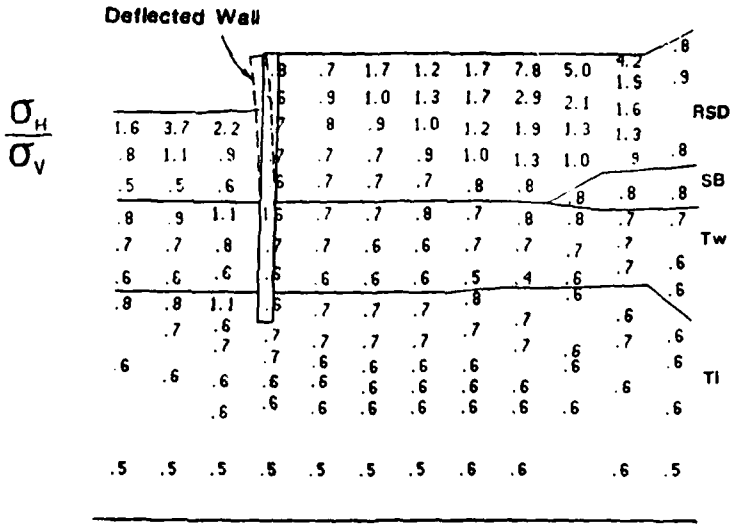

c. First excavation in front of wall, to el 78.5 ft

Figure 8. Ratio of horizontal to vertical soil stress during construction operations at Panel 6 (Continued)

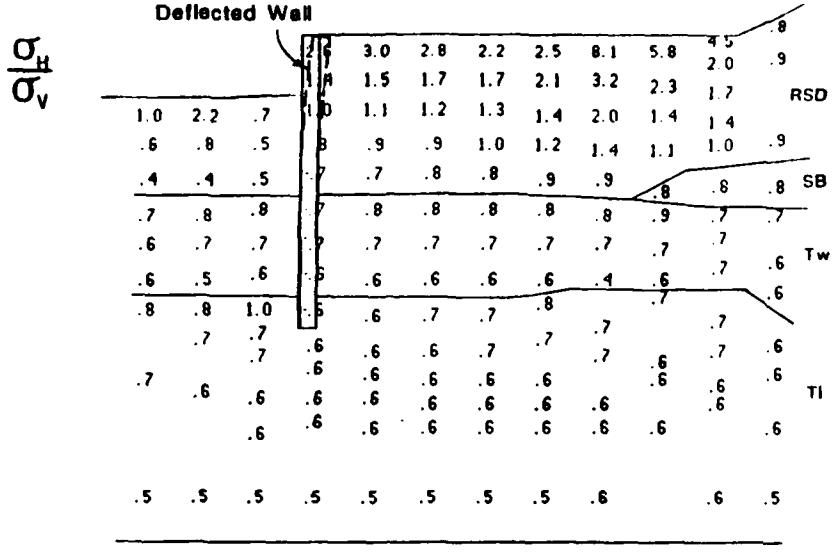

d. Prestressing of first anchor at el 84 ft

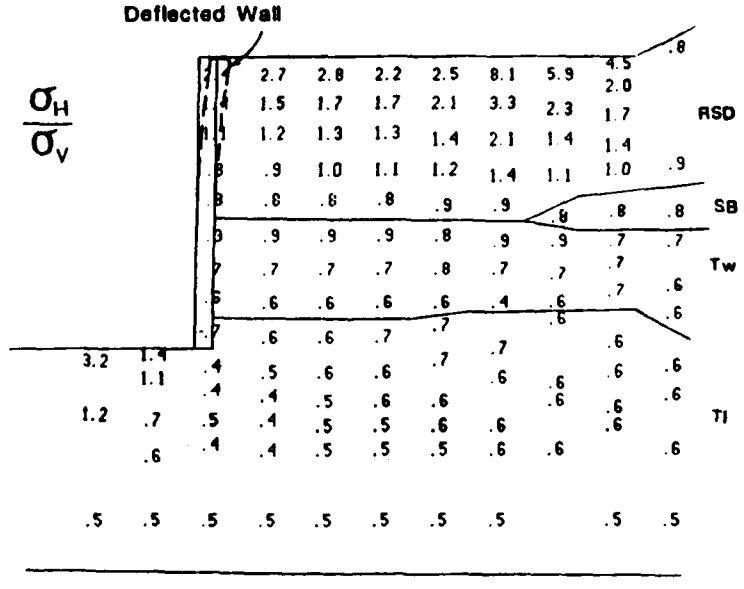

e. End of construction

Figure 8. (Concluded)

change in the stress ratios from Figures 8b to 8c reflect the response of the soil to the changing loads.

43. Figure 8d shows the stress ratios after the proof-test load (150 percent DL) has been applied to the wall. The effect of this on soil stresses is opposite that in the previous step. The stress ratio increases behind the wall because of horizontal stress increase as the wall moves into the soil. In front of the wall, the stress ratio decreases as the wall moves away from the soil and decreases horizontal stress.

44. The behavior just described repeats, to a lesser degree, with each subsequent excavation and anchor placement. The horizontal-to-vertical stress ratios at the end of construction are shown in Figure 8e. These stress ratios behind the wall are almost the same as those from the first anchor prestress, Figure 8d.

45. The ratio of mobilized shear stress to maximum available shear stress can also be used to assess the soil response to various loadings in the construction procedure. This ratio represents the percentage of mobilized shear strength. This is shown in Figures 9a through 9e. Locations where the shear strength is at 100 percent means that the soil is at a state in which all of its shear resistance has been mobilized or activated. In Figure 9a, stresses of 100 percent can be observed at the toe of the lower slope. This is the soil state prior to any construction; therefore movements may have occured at this location at some time in the past. After the overburden is removed to relocate the railroad line and build the wall, the highly stressed elements appear at the toe of the new slope, Figure 9b. Full mobilization of the shear strength at the toe does not indicate a potential collapse of the slope. Instead, it simply means that the combination of overburden removal and slope movements were sufficient to cause a localized high-stress condition. Field instrument readings at this area indicated some movement of the slope.

46. As construction continues with excavations and anchor installations, change in the mobilized shear strength is observed most in the soil near the ground surface on both sides of the wall. Behind the wall, shear stresses are reduced during excavations and are increased during anchor prestressing. In front of the wall, the opposite is true. This response is shown in Figures 9c and 9d, in which excavation and anchor prestressing occur consecutively. Figure 9e shows the final mobilized shear strength at the end of construction. A distinct

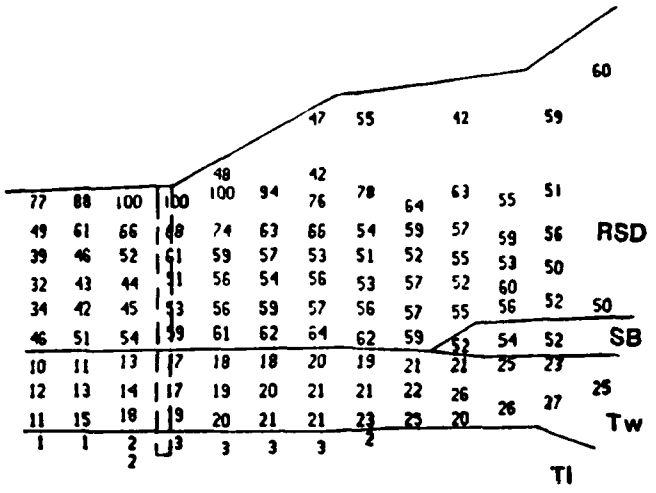

a. Initial state, at rest

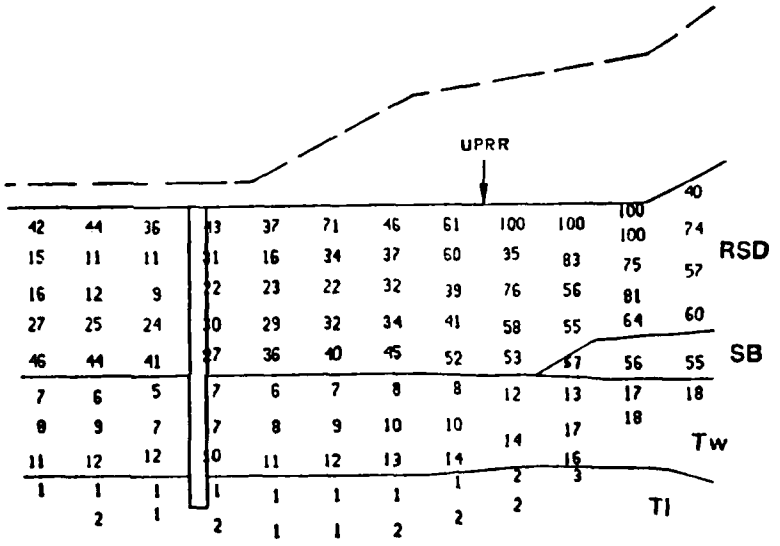

b. Surface excavation for railroad relocation and construction of Panel 6

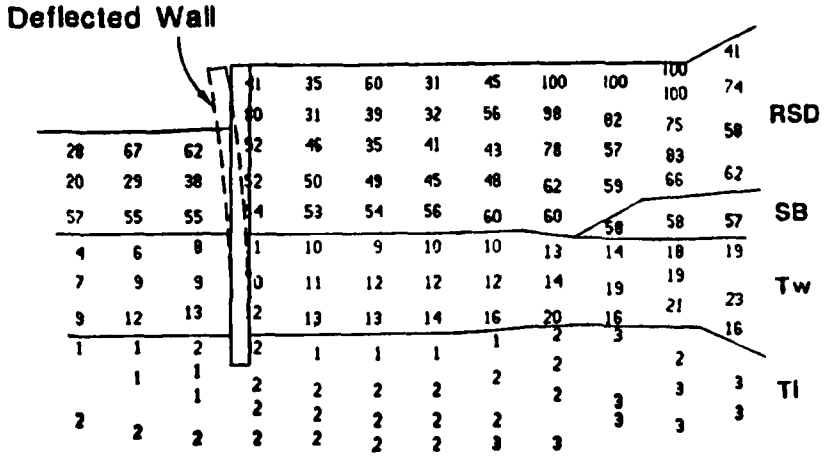

c. First excavation in front of wall, to el 78.5 ft

Figure 9. Percent of mobilized shear strength during construction operations at Panel 6

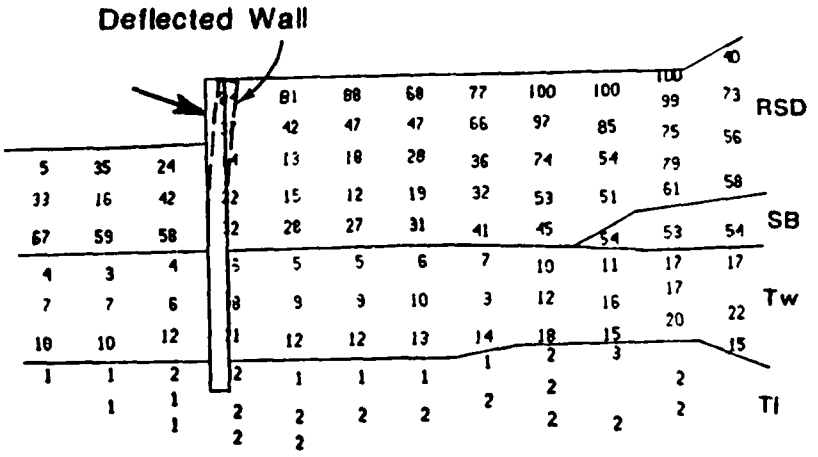

d. Prestressing of first anchor at el 84 ft

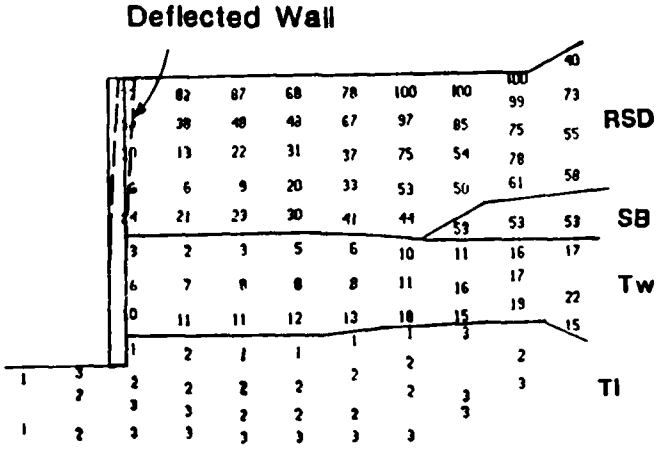

e. End of construction

Figure 9. (Concluded)

difference in magnitude of percent mobilized shear is seen on either side of soil layer boundaries (RSD-Tw, Tw-Ti) in all of Figures 9a through 9e. This response is representative of the relative strengths of the materials.

Wall deflection

47. Lateral movement of the wall from the SOILSTRUCT analysis is shown in Figures 10a through 18a for each construction step, beginning with the first excavation in front of the wall. In this first excavation to el 78.5 ft, Figure 10a, the wall moves 0.5 in. toward the excavation. With prestressing of the first tieback at el 84 ft, shown in Figure 11a, the wall is pulled into the soil 0.78 in. past the vertical position. This is the greatest deflection experienced by the wall throughout all the construction procedure. In subsequent construction steps, Figures 12a through 18a, there is little change in the deflected position of the wall. In general, the wall moves into the soil with each anchor pull and back toward vertical with each excavation. The final deflected position, Figure 18a, is 0.67 in. into the soil at the top of the wall. This analysis showed that the diabase provides firm support for the wall. Maximum deflection at the base of the wall is never greater than 0.012 in. toward the excavation.

48. The predicted deflection at end-of-construction with respect to wall height is (0.67 in./12)/50 ft = 0.11 percent of wall height. This compares well with results from other tieback wall observations and analyses: 0.19 percent predicted and 0.11 percent observed (Clough, Weber, and Lamont 1972), 0.38 percent from full-scale test in clay (Tamano 1985). In a diaphragm wall case study (Schultz 1981), 85 percent of the cases of anchored or braced walls retaining granular soils show a maximum lateral deflection, normalized to wall height, of less than 0.10 percent.

Wall moment

49. Figures 10b through 18b show the bending moment diagram for the wall from the FE analysis. Moment was calculated from strain in the extreme fibers of the wall section. This procedure is explained in Appendix A. The sign convention is: tension is positive, compression is negative.

50. Except for the first excavation (Figure 10), the moment diagram for the wall retains the same general form throughout the construction procedures. The upper one-third of the wall experiences negative moment, and the lower two-thirds of the wall, positive moment. The maximum moment is always positive and varies during the construction sequence from 62 to 133 k-ft. The

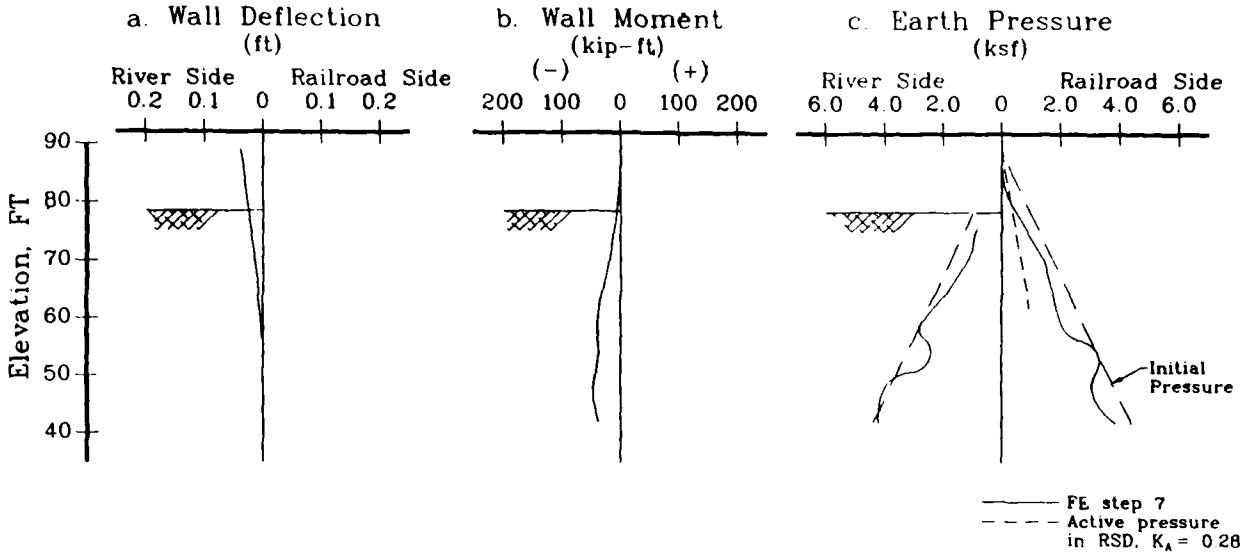

Figure 10. Deflection, moment, and earth pressure for load step 7; excavation to el 78.5 ft

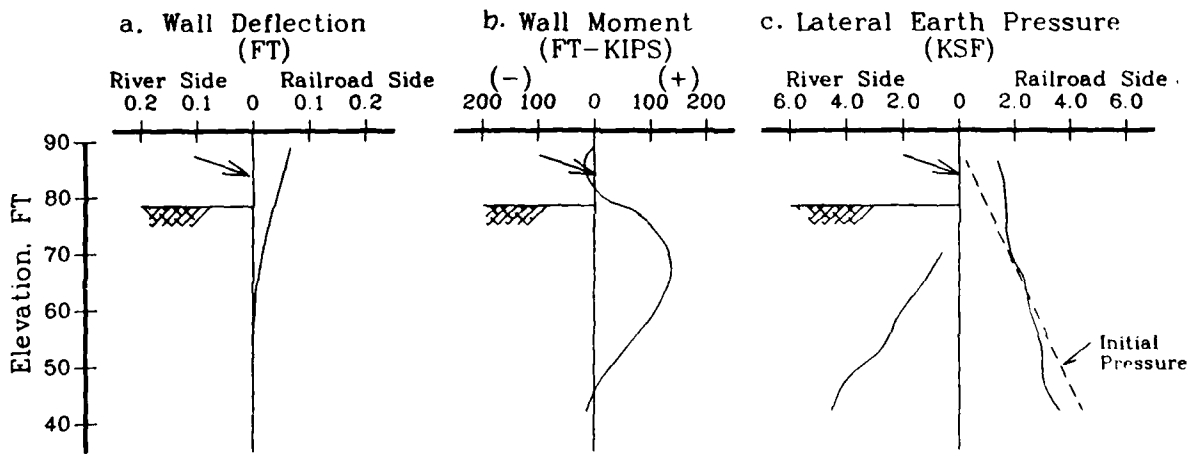

Figure 11. Deflection, moment, and earth pressure for load step 8; prestress anchor at el 84 ft

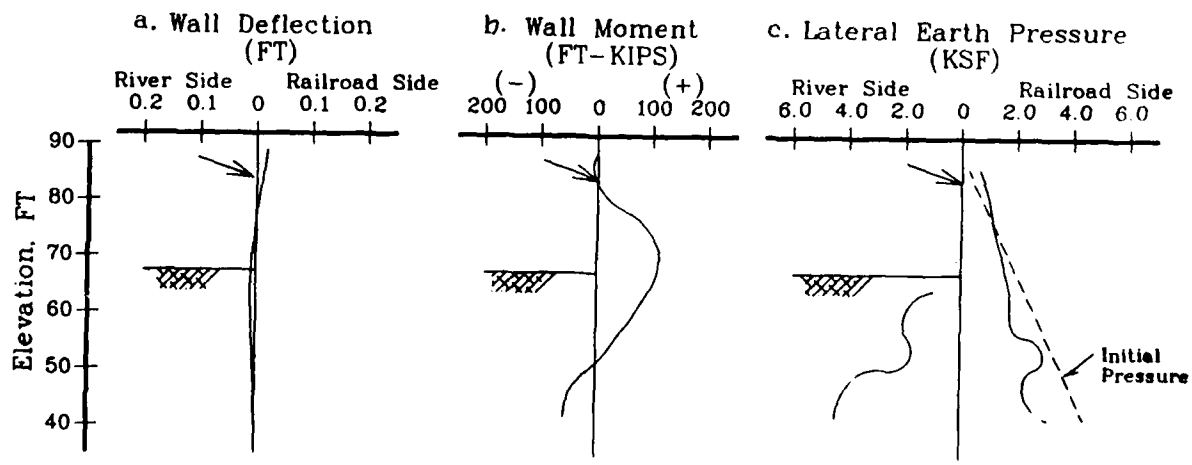

Figure 12. Deflection, moment, and earth pressure for load step 9; excavation to el 67.5 ft, lock off anchor at el 84 ft

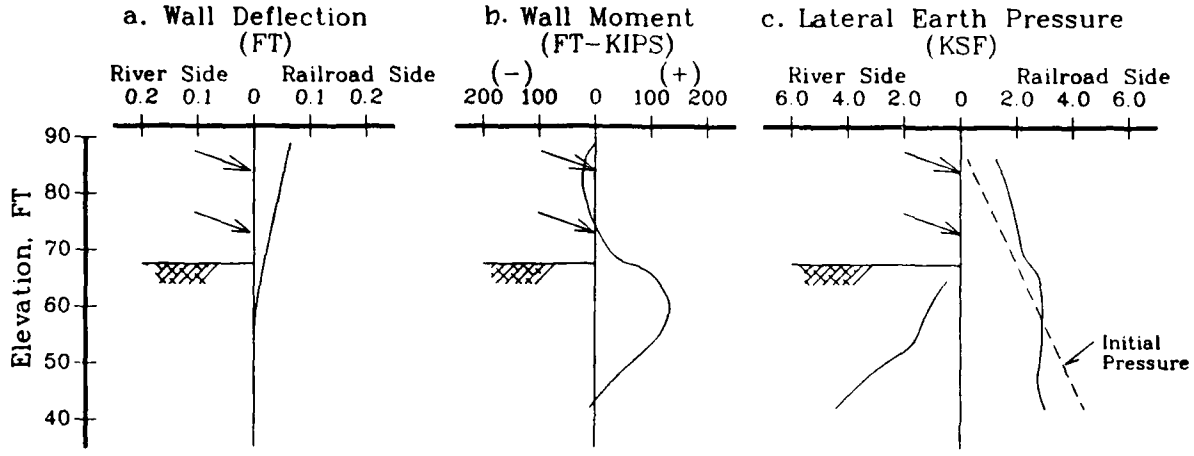

Figure 13. Deflection, moment, and earth pressure for load step 10; prestress anchor at el 73 ft

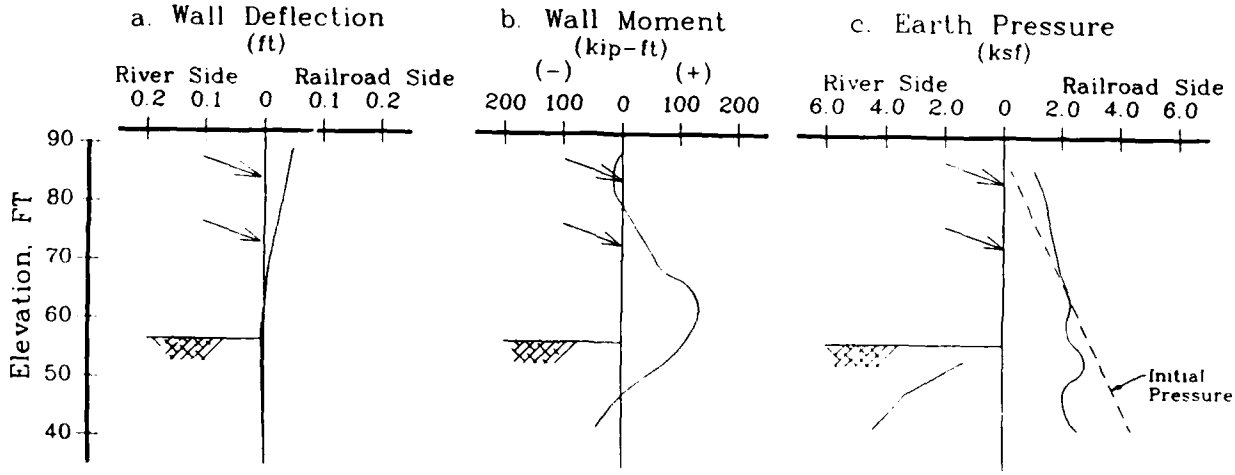

Figure 14. Deflection, moment, and earth pressure for load step 11; excavation to el 56.5 ft, lock off anchor at el 73 ft

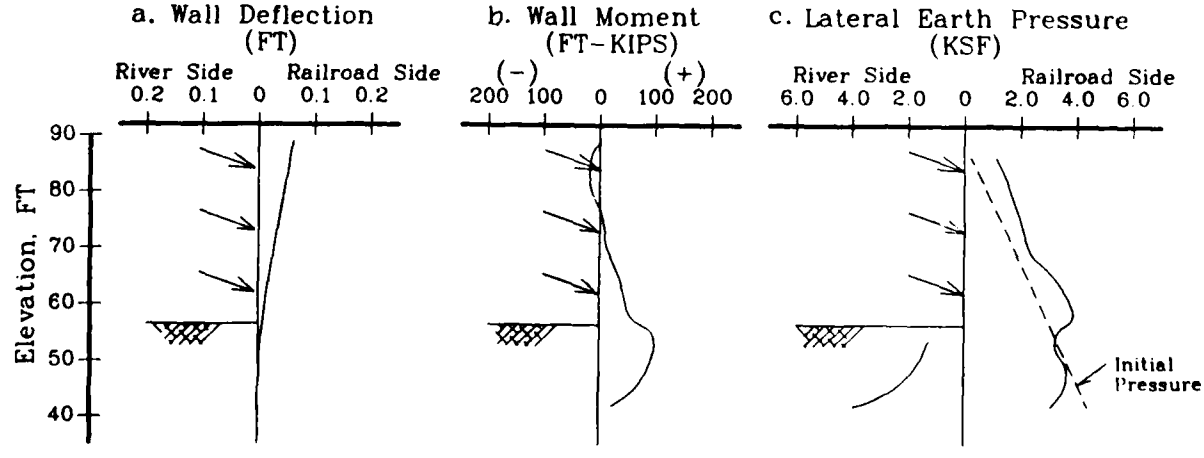

Figure 15. Deflection, moment, and earth pressure for load step 12; prestress anchor at el 62 ft

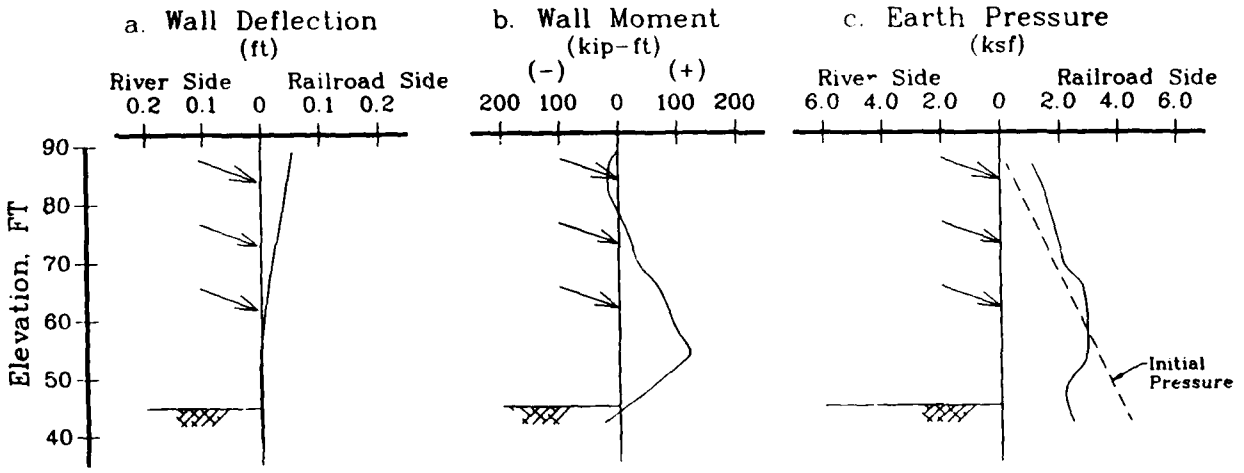

Figure 16. Deflection, moment, and earth pressure for load step 13; excavation to el 45 ft, lock off anchor at el 62 ft

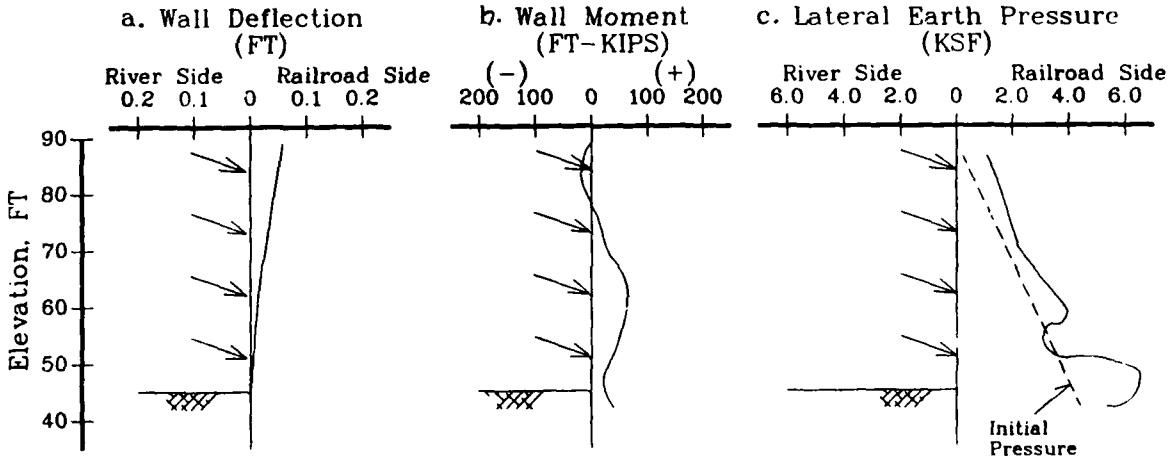

Figure 17. Deflection, moment, and earth pressure for load step 14; prestress anchor at el 51 ft

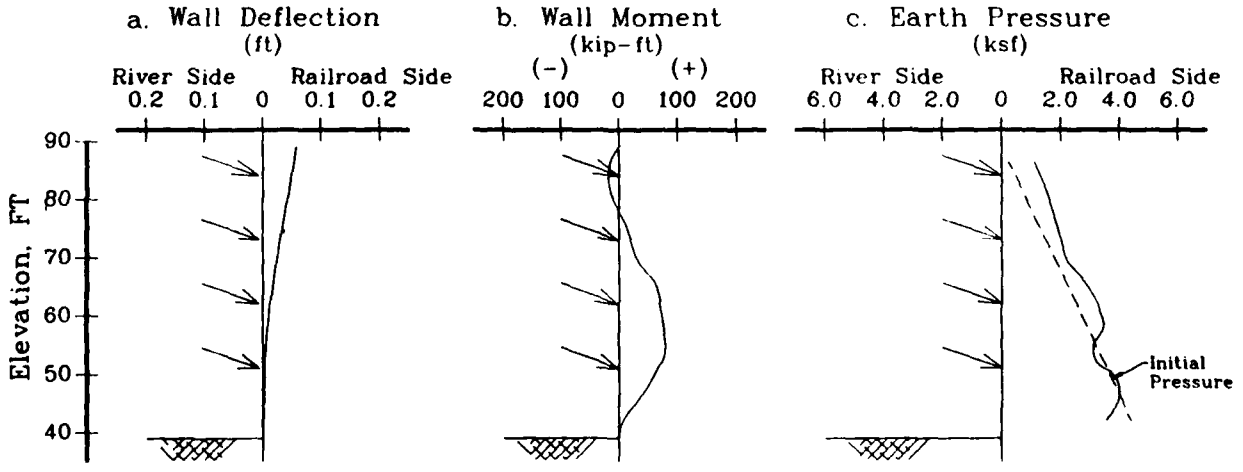

Figure 18. Deflection, moment, and earth pressure for load step 15; final excavation to el 39 ft, lock off anchor at el 51 ft

overall maximum moment (133 k-ft) occurs when the second anchor is prestressed at el 73 ft, Figure 13b.

51. Panel 6 was designed for a maximum moment of 191 k-ft. The analysis results indicate that the moment design for this panel is safe by 44 percent. Figure 18b shows the moment diagram after the final excavation and anchor load lockoff.

Earth pressures

52. Lateral earth pressures on the wall from the FE analysis are shown in Figures 10c through 18c and 19. The effect of overconsolidation is seen in the initial pressures on the wall after it was built (Figure 19). This pressure is approximately 50 percent greater than the pressure computed as $\sigma_h = 0.5\ \sigma_v$, shown for comparison. This increase in initial pressures can also be attributed to the replacement of the soil by the concrete wall. Schultz (1981) found that the earth pressures measured after concrete wall construction by the slurry trench method were slightly greater than at-rest pressures measured prior to placement of the wall. This is partially attributed to the difference in unit weights of the materials and partially to the loadings encountered in the process of excavation, slurry placement, and concrete tremie.

53. The earth pressure distribution changes throughout the construction sequence as a result of anchor prestressing, excavations, and the response to these loadings from the different soils. The FE analysis initial pressure diagram (Figure 19), is also shown with the pressure diagram of each load step (Figures 10c through 18c), for comparison.

54. After the first excavation to el 78.5 ft (Figure 10c) the soil behind and near the top of the wall is in an active state. This is caused by the excavation of soil in front of the wall and the resulting wall movement away from the soil behind it. The displacement of the top of the wall is 0.004 D (D = the depth of excavation at this point). Movement of only about 0.001 to 0.003 D is required to mobilize soil to the active pressure state. The Rankine active earth pressure coefficient for the RSD is computed as $K_a = \tan^2 (45\text{-}\phi/2) = 0.28$. The pressure distribution for this is also plotted in Figure 10c. Further down the wall, the lateral earth pressure is greater than active, but less than the initial pressure on the wall after construction. The analysis shows that with prestressing of the first anchor, Figure 11c, earth pressures increase to greater than initial pressures behind the upper

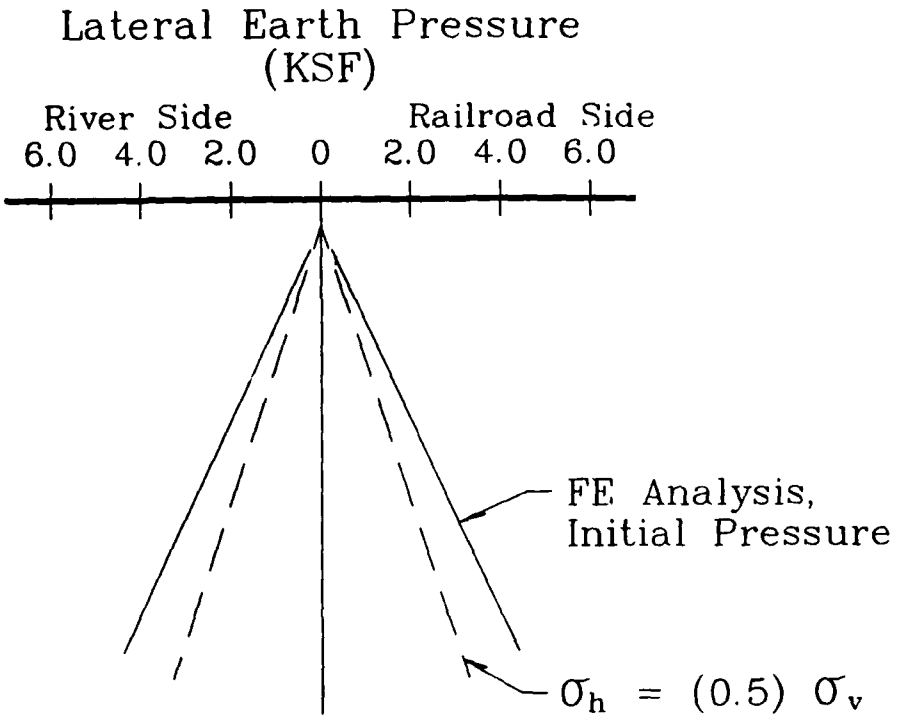

Figure 19. Earth pressures before excavation in front of wall

one-third of the wall. Subsequent excavations and anchor prestressings (Figures 12c through 18c) show decreases and increases, respectively, of the earth pressure along the wall. Bulging of pressure around the anchors appears in the lower one-half of the wall. This reflects a pressure concentration caused by the prestressing loads, also noted by Clough (1976).

55. In general, the earth pressures on this wall decrease below the initial lateral pressure on the wall (Figure 19) during excavations and increase above the initial lateral pressure during anchor prestressing.

56. Figure 20 shows the combined plots of earth pressures on the wall from Figures 18c and 19, and the pressure diagram used in design of the wall. The rectangular design pressure was calculated according to the Naval Facilities Engineering Command Design Manual 7.2 (Department of the Navy 1982) and includes soil pressure and surface load pressure on the wall for the at-rest condition. This is an apparent pressure diagram used to compute anchor prestress loads and is not an expected earth pressure distribution.

57. The results from consecutive load steps are shown together in Figures 21a and 21b for comparison.

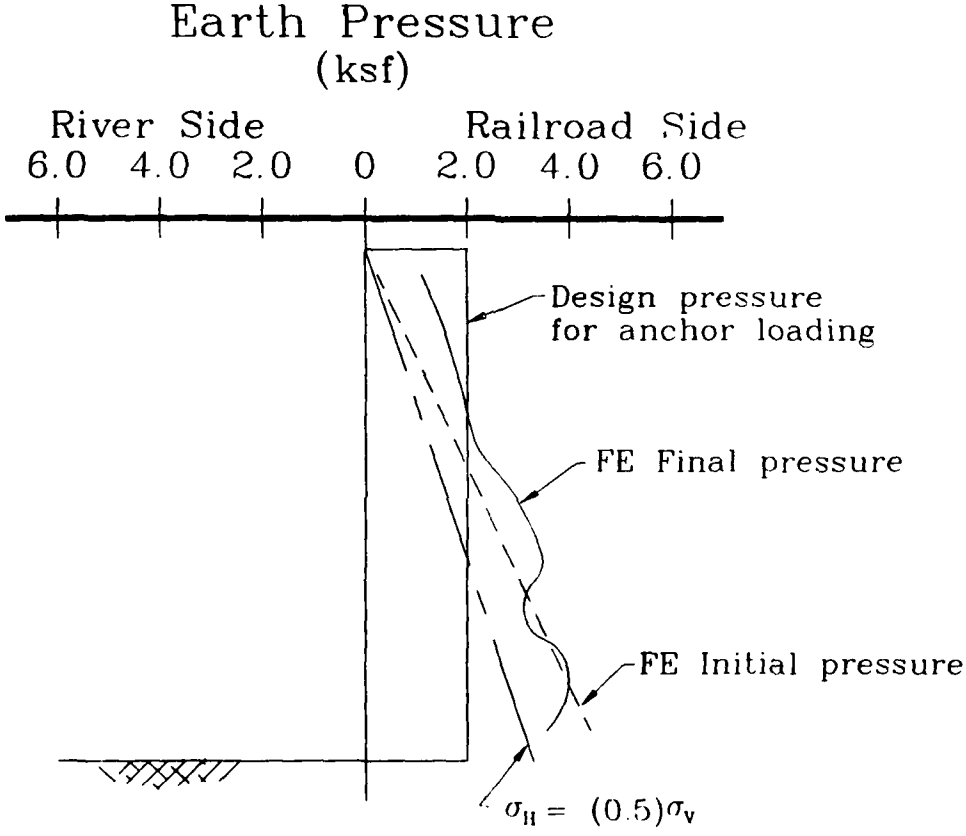

Figure 20. FE earth pressures on tieback wall and apparent pressure diagram used to design anchor loads

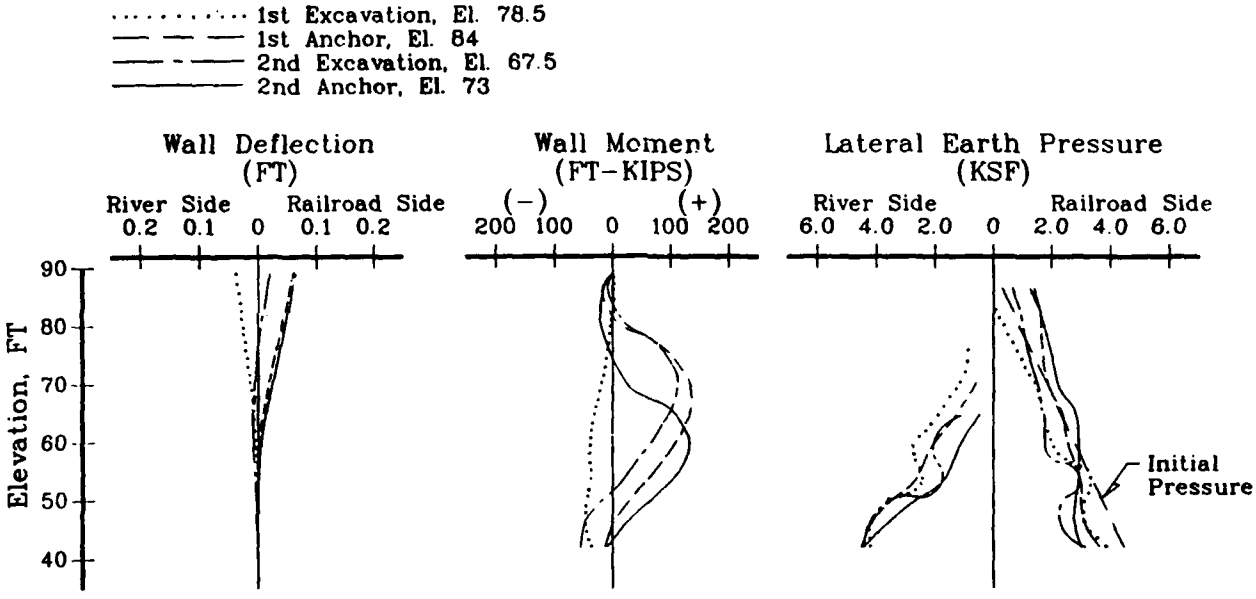

a. Results from Figures 10 through 13 (load steps 7-10)

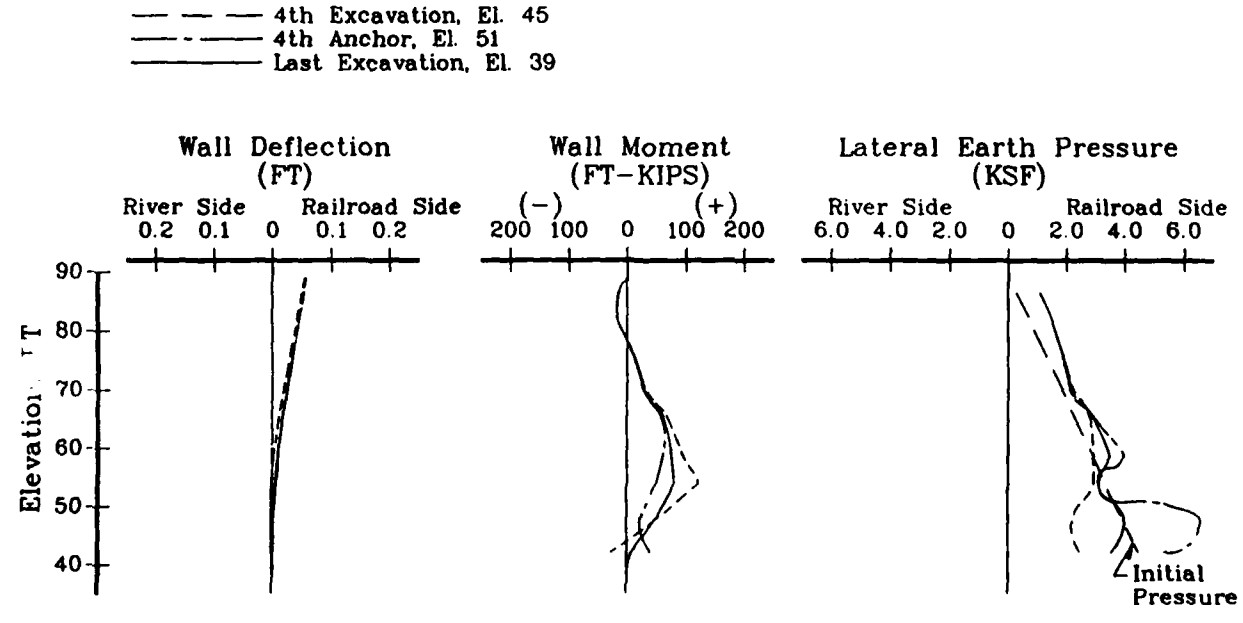

b. Results from Figures 16 through 18 (load steps 13-15)

Figure 21. Deflection, moment, and earth pressure for groups of load steps

Anchor loads

58. Table 4 lists loads in the anchors for each construction step, from anchor installation to the end of construction. After an anchor was installed, an excavation was performed. This operation caused the wall to move outward slightly and, thus, increase the anchor load from its lockoff value. Following prestressing of the next lower anchor, the upper anchor loads decrease. These changes can be noted in Table 4.

Table 4
FE Anchor Loads During Construction Steps

Anchor Elevation	Lockoff Load (kips)	step 9	step 10	step 11	step 12	step 13	step 14	step 15
84.'	272	298	270	280	270	275	272	273
73.'	292	---	---	302	289	295	291	293
62.'	290	---	---	---	---	297	290	294
51.'	356	---	---	---	---	---	---	361

NOTES:
Refer to Table 3 for description of construction steps.
Anchor loads in kips (tension).

59. Overall, the FE anchor loads varied only slightly from their lockoff load value throughout the sequence of construction operations. The greatest change occuring in the analysis was an increased load of 9.4 percent in the top anchor, el 84 ft, after soil was excavated in front of the wall. At the end of construction, the top two anchors carry almost the same loads as when they were locked off, while the bottom two anchors have only about 1 percent greater load than their lockoff load.

Ground movement

60. Deflection of the ground surface behind the wall is studied for effects it may have on the adjacent railroad line. The maximum vertical deflection at the tracks is predicted to be approximately 0.10 in. of heave, and occurs with placement of the third anchor. The ground surface under the tracks at the end of construction is 0.08 in. above the original horizontal

position. Plots of the maximum and final vertical ground surface deflections behind the wall are shown in Figure 22.

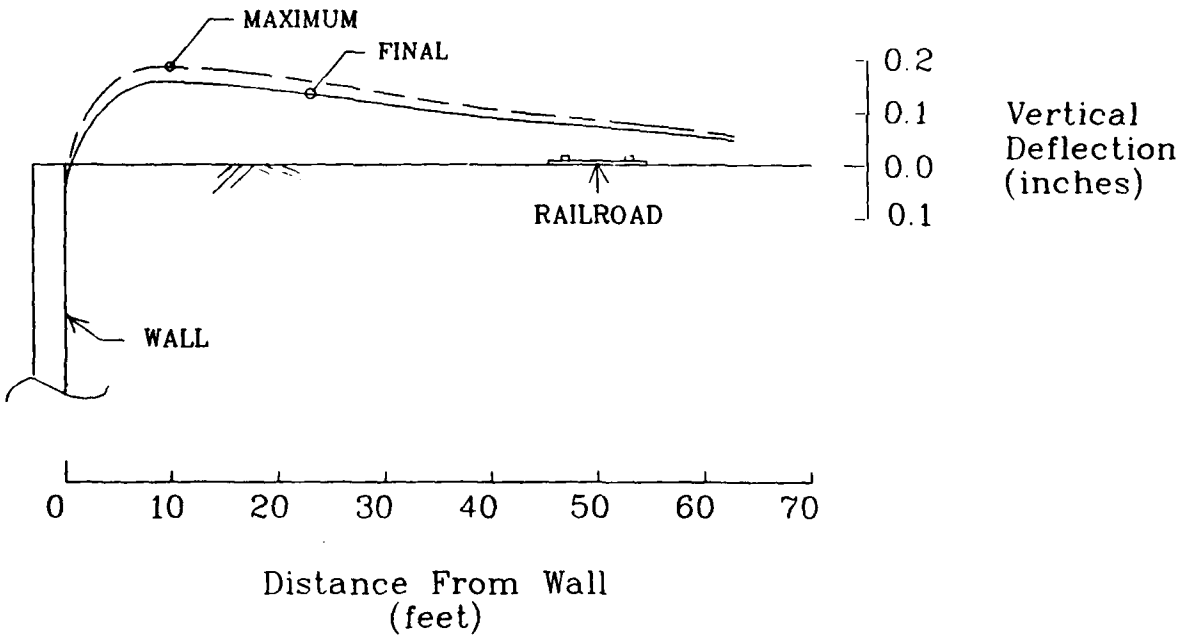

Figure 22. Ground surface deflection behind Panel 6 from FE analysis

Discussion of Analytical Results

61. In general, the wall responded satisfactorily to the various loadings it experienced. Expected wall behavior is seen qualitatively in the results for each construction operation; the wall moves toward the excavation when the first volume of material is removed, then is pulled back into the retained soil when the first anchor is prestressed. All subsequent wall movements remained on the railroad side of vertical, and away from the excavation. The wall design is conservative with respect to bending moment. The analysis shows the section modulus to be more than sufficient, therefore the wall should not experience structural problems during the loading processes. The results of this finite element analysis show that the excavation for the lock should have no effect on the alignment of the railroad tracks. The ground moves a negligible amount at the tracks.

62. Shear stresses in the soil were fully mobilized at the toe of the slope after overburden excavation. After this, no areas of the soil mobilize

more than 90 percent of maximum stress throughout the remaining construction sequence.

Conclusions of Phase 1 Study

63. This initial FE soil-structure interaction analysis has confirmed the adequacy of the wall design. The soil stiffnesses were chosen conservatively so that the deflections predicted by the analysis should be greater than those actually experienced by the wall.

64. Results of this study are satisfactory and reasonable. Comparison with the instrumentation results should help confirm the model's validity, as well as explain and interpret instrumentation data. The functionality and value of this model and analysis procedure are enhanced by realizing its potential for use in parametric studies. One can readily change the material properties, loading steps, or other features for a variety of desired results. Parts III and IV describe the outcome of variations and parametric studies performed with this model of Panel 6.

PART III: VARIATIONS ON THE INITIAL FE MODEL (PHASE 2)

65. This part describes a second phase of the temporary tieback wall study in which various aspects of the initial FE model of Panel 6 (Phase 1, Parts I and II) have been modified. Specifically, analyses were performed for: (a) anchor loads of different magnitudes, (b) reduced capacity and failure of the top anchor, and (c) reduced stiffness parameter for all the soils. These analyses were performed during the period of construction, but prior to instrument readings of Panel 6.

66. The latter two analyses were requested by the Portland District. The first group of results, different sets of anchor loads, were obtained from preliminary analyses performed before the actual anchor loads were known. The purpose of these analysis variations is to determine the sensitivity of the wall-soil system to each parameter and to assess the range of behavior associated with a range of possible values for a soil model parameter such as the soil stiffness constant.

Phase 2 Results

Anchor loads

67. An analysis was performed on the Panel 6 model using anchor loads approximately double the actual in situ anchor loads. This was done to see the effect of anchor prestress levels on the system.

68. Table 5 lists the two sets of anchor lockoff loads used in the analyses, and lists maximum wall deflections and moments resulting from each. The wall deflection, moment, and earth pressure at the end of construction are plotted for each anchor load set in Figure 23. The magnitudes of the first set of anchor loads are about twice as great as the as-constructed (in situ) loads. This difference is reflected in almost direct proportion in the resulting wall deflection and bending moment magnitudes. Earth pressures become very large and display large bulges with the high anchor loads of set 1, as compared to the more linear distribution of pressure from the lower loads of set 2. This shows that the anchor load magnitude has a direct effect on wall behavior and the resulting earth pressures. These pressure bulges are seen in the Weigle layer (Tw), (el 44 to el 62 ft) but not in the RSD. This may or

Table 5
Anchor Load Sets for Panel 6 Analyses

Anchor Elevation	SET 1 200% DL (kips)	SET 2 In situ loads 100% DL (kips)
84'	562	272
73'	562	292
62'	562	290
51'	562	356
Maximum wall deflection (ft)	.126	.065
Maximum moment (ft-kips)	246	133

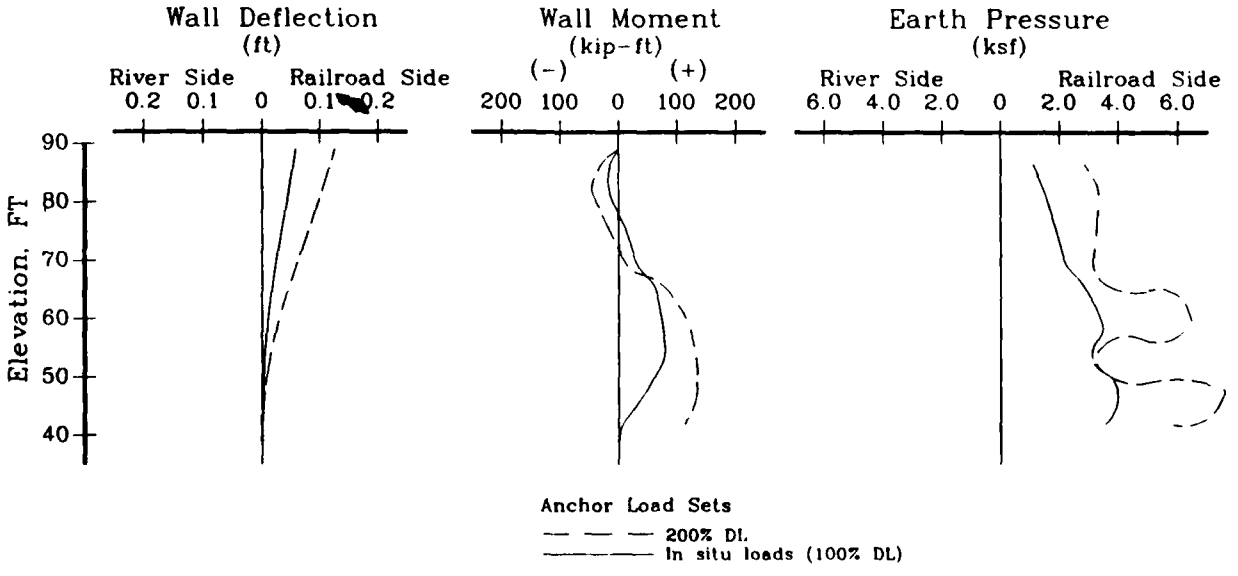

Figure 23. Wall behavior with different magnitudes of anchor loads (end of construction)

may not have to do with the material property differences. The Panel 11 analysis (Part VI) addresses this again.

Failure of top anchor

69. The second study performed was a simulated failure of the top anchor at the end of construction. This was modeled by deleting the top anchor bar element from the FE grid. In doing so, the bar force was applied as equal and opposite forces to the nodes where the bar was connected. Results were obtained for one-half- and zero-load capacities of the anchor. These, along with results prior to anchor failure, are shown in Figure 24.

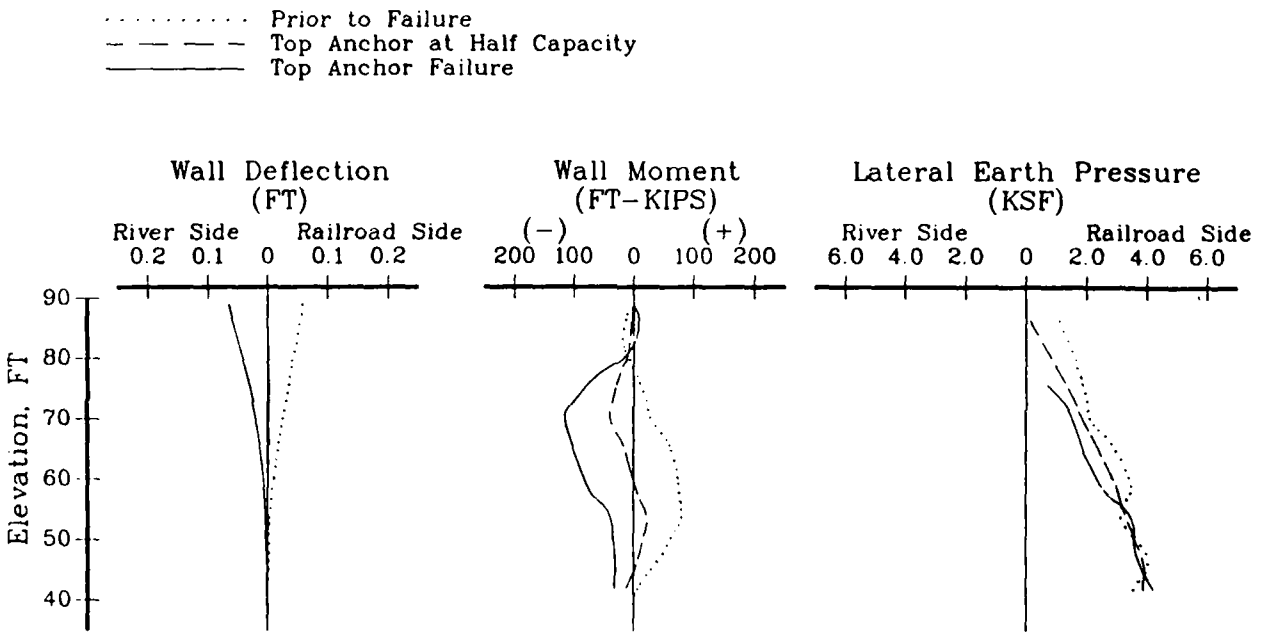

Figure 24. Wall reaction to failure of top anchor

70. With failure of the top anchor, the wall moves 0.78 in. past vertical toward the excavation. The earth pressure has lowered in the top part of the wall, and the bending moment has shifted from positive to negative values, with a maximum of -115 k-ft. The bending moment and deflection plots after top anchor failure are almost mirror images about the vertical axis of the plots before anchor failure.

71. A small portion, 13.5 percent of the failed anchor's load was distributed to the remaining anchors: 8.8 percent in the second anchor, 3.6 percent in the third anchor, and 1.1 percent in the bottom anchor. The rest of the load was transferred to the soil through mobilization of shear as the wall

moved outward. Design stress for the anchorage included a safety factor of 2, so that this small increase in load would not overstress the remaining anchors. Similar results were obtained in a full-scale performance test of a multitied sheet-pile wall in a 34-ft excavation (Tamano 1985). In this test, the top row of four rows of anchors was released, and 9.13 percent of the load was redistributed to the remaining three anchor rows. Broms (1988) discusses the case of load redistribution using field examples of anchored sheet-pile walls in soft clay. In one case, 36 percent of the failed anchor's load was redistributed to surrounding anchors, and the maximum for one anchor was only 9 percent. A 64-percent decrease in the lateral earth pressure on the wall was computed. In another case, 35 percent of the failed anchor's load was redistributed to other anchors, but a 32-percent increase in lateral earth pressure occurred on the wall. Broms attributes this difference in behavior to the differences in mobilized shear strength in the clay behind the wall prior to anchor failure and to the safety factor used in design.

72. In this analysis, the ground surface under the railroad tracks settled to 0.06 in. below the original horizontal position due to the downward and outward movement of the soil with failure of the top anchor.

Reduced soil stiffness

73. A third analysis was performed with the hyperbolic modulus constant, K_m, for all the soil types reduced to one-half the value used initially. K_m determines the initial tangent modulus value, or stiffness of the soil, for primary loading. Figure 25 shows a comparison of wall deflection,

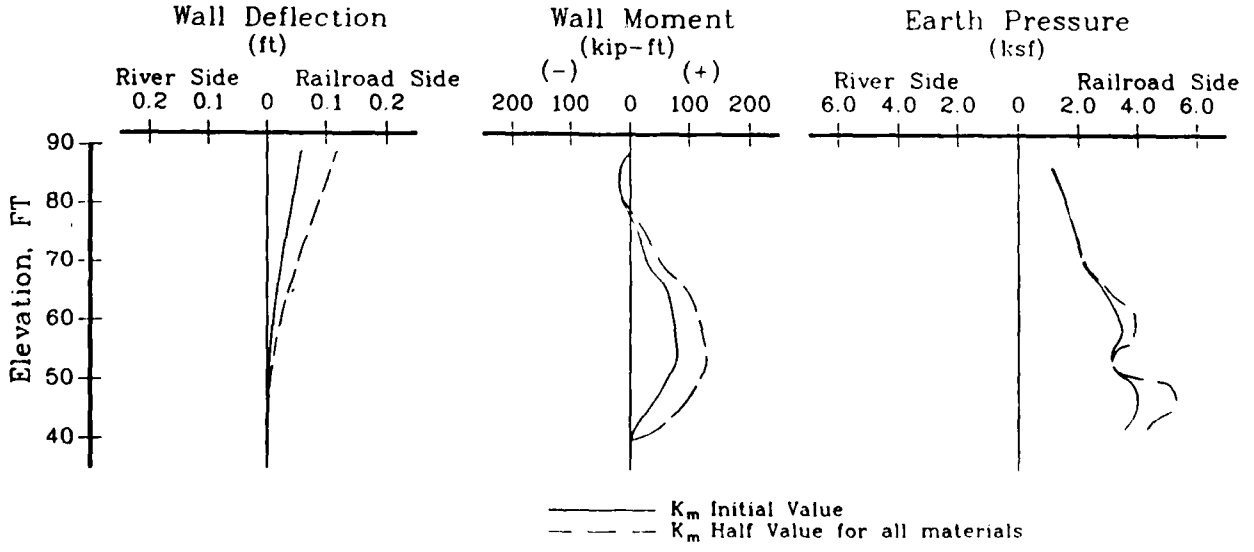

Figure 25. Wall behavior with reduced soil stiffness (end of construction)

moment, and earth pressures at the end of construction for both the original analysis and the softer soil analysis. Wall deflections are about 65 percent greater and moments about 40 percent greater in response to loadings on the softer soil than those in the initial analysis. Ground surface deflection is greater as well, with a maximum heave of 0.16 in. under the railroad tracks. Earth pressures remain essentially the same, showing little reaction to this soil property change. It is probable that the earth pressures measured on a tieback wall may be more directly related to anchor loads than to the actual soil pressures mobilized. The wall deflection and moment show structural sensitivity to the soil stiffness.

Conclusions After Analysis Variations

74. It is obvious from the results of the anchor load variations that the response of the system is related to the magnitude of load and to the relative stiffnesses of the materials being loaded. This relation between anchor load and the deflection, moment, and earth pressure is almost directly proportional. That is, the anchor loads of set 1 (Table 5) are almost twice as large as loads of set 2, and the resulting deflections, moments, and pressures of the wall are up to twice as great.

75. The soil stiffness reduction to 50 percent of its initial value for all the soils is somewhat of an exaggeration of a possible range of values that may be chosen for this parameter. However, in some cases, this range of difference may exist between the modulus constant used and one that is more representative of the material. The sensitivity of the system to this parameter is observed in the deflection and moment of the wall. Earth pressures are little affected. Variations with this parameter are addressed more fully in later analyses (Part IV).

76. The analysis in which the top anchor fails reveals the importance of this anchor in the soil retention system. However, the movement of the wall into the excavation is not relatively large (0.13 percent of excavation height), the new moment in the wall is not excessive, the remaining anchor loads increase by only a small amount, and the ground surface at the railroad tracks settles to only 0.06 in. below horizontal. Remedial action can be taken without fear of complete failure or stoppage of railroad traffic if this situation occurs.

PART IV: INSTRUMENTATION RESULTS AND FE MODEL REFINEMENT (PHASE 3)

77. The third phase of study is presented in Part IV. At this point in the study, the instrumentation data from slope inclinometers and strain gages had just been received and reduced to wall deflections and bending moments. This phase of the study involves the comparison of measured values to the FE results and the refinement of the FE model to obtain results more closely resembling observed behavior. Various modifications to the soil parameters were analyzed to determine the influence of these parameters on the wall-soil response to the loadings.

Instrumentation Results

78. Instrumentation reports were received from the Portland District containing data from strain gages and slope inclinometers (BCA Geophysics, Inc. 1988). These data for Panel 6 were used to produce the deflection and moment curves shown in Figure 26 for the end of construction case. Instrumentation results corresponding to other load steps are discussed later in paragraph 92. For comparison, FE analysis results for the end of construction for the initial Panel 6 analysis of Part II are shown in Figure 26 as well. The

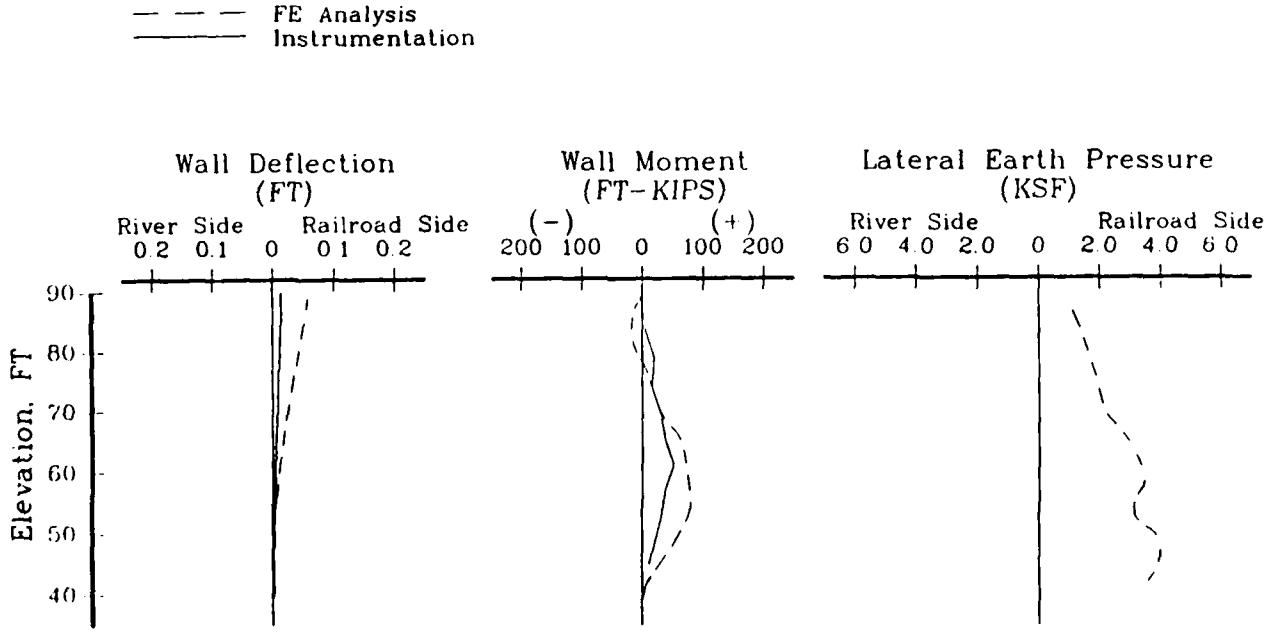

Figure 26. Instrumentation and FE analysis results for Panel 6 at the end of construction

results are very close. It appears that the FE predictions are unmatched to the measured behavior only by a numeric factor. Since the structural properties are known with a high degree of certainty, and the soil properties (hyperbolic parameters) were selected conservatively, it is likely that one of the soil parameters could be adjusted to represent a stronger or stiffer material and bring the FE results closer to the observed behavior.

Parametric Study

Variation of K_o

79. In previous analyses of Panel 6 (Parts II and III), the initial at-rest earth pressure coefficient for the RSD, Weigle, and diabase materials was 0.5. This was used in the program SOILSTRUCT to compute initial soil stresses before loading begins. To determine the response of the soil to loading due to this property, K_o was increased. This is a feasible variation because the materials could possibly have a higher K_o than 0.5 due to overconsolidation. Also, pressuremeter testing indicated a high K_o (Smith 1985).

80. Two additional analyses were performed on the Panel 6 model; one using $K_o = 1.0$ and the other using $K_o = 2.0$, for the RSD material only. The wall deflection, moment, and earth pressures from these analyses are plotted with the initial results ($K_o = 0.5$) and instrumentation data for the end of construcion case. Figure 27 shows these results.

81. As K_o is increased from 0.5 to 2.0, the final wall deflection bulges more toward the excavation, and the wall moment increases almost three times. The earth pressures have an erratic distribution of lows and highs in the lower two-thirds of the wall, while they are almost the same for all the values of K_o in the upper one-third of the wall. This type of behavior is noted in an investigation by Potts and Fourie (1984) of a propped retaining wall, where large soil and wall movements were observed with high initial K_o values, and bending moments were much greater than those predicted from conventional methods.

82. This behavior diverges from the in situ performance and does not predict deflections or moments any closer to the instrumentation results than $K_o = 0.5$ from the initial analysis. Therefore, the value of K_o is left at 0.5 for all subsequent work.

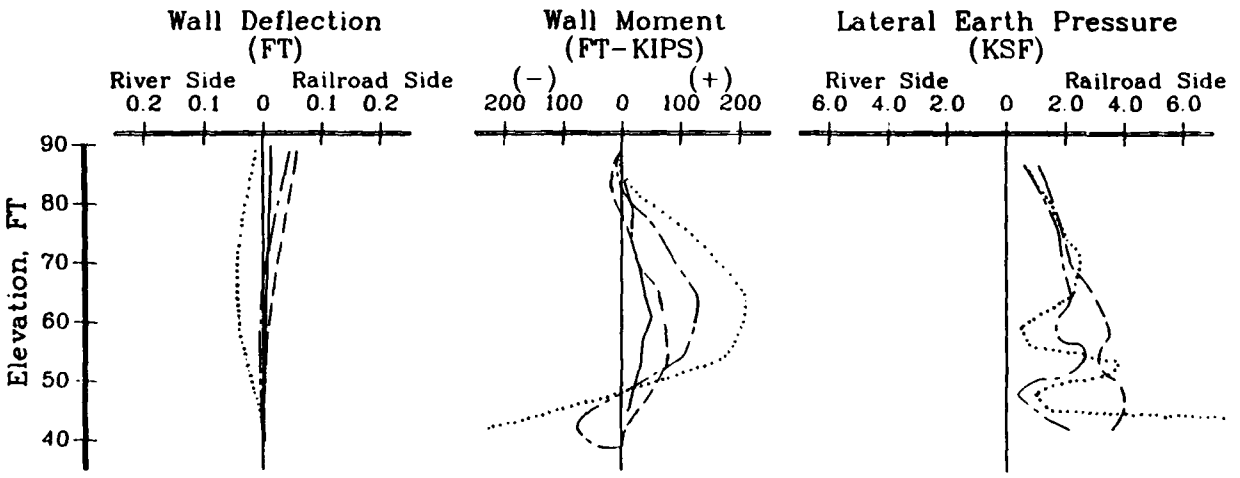

Figure 27. Wall response to increases in K_o (end of construction)

Variation of K_m

83. The modulus constant, K_m, is a parameter used in the nonlinear hyperbolic response model for soil in SOILSTRUCT (Figure 6). This parameter is the soil modulus stiffness constant and is directly proportional to the soil modulus value. The K_m values used in the initial analyses are found in Table 2. As noted in Part I, the hyperbolic parameters were chosen to give conservative results; therefore, two more analyses were performed where the K_m value, hence the stiffness of the RSD and Tw materials, was increased from the initial value used. In one, K_m was doubled, and in the next, it was tripled. (The unload-reload modulus, K_{ur}, was set equal to the K_m of each analysis.) The resulting wall deflection, moment, and earth pressures at the end of construction are plotted in Figure 28, along with results from the initial analysis and the instrumentation results.

84. With increasing soil stiffness, the FE-predicted wall deflection and moment approach the observed response. Earth pressures vary by little, with their distributions becoming more linear than in the initial analysis. The wall deflection shows more sensitivity to the increases in the K_m than

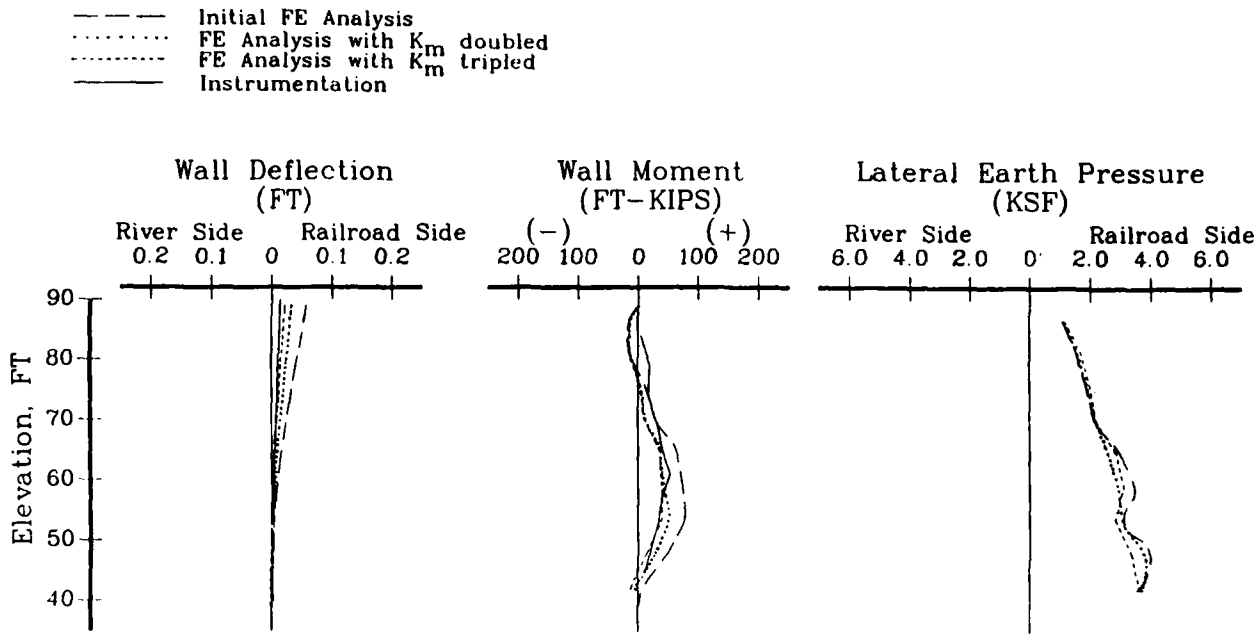

Figure 28. Wall response to increases in hyperbolic parameter K_m (end of construction)

does the moment. It is reasonable to conclude from these results that the soil stiffness is the deciding factor in reproducing the observed behavior with the FE results. Because of the initially conservative choice of this parameter's value and because of the range it can have for similar soils, it is not unreasonable to increase these values by three times.

Significance of K_m variation

85. Since the stiffness parameter, K_m , affects the initial tangent modulus of the soil's stress-strain curve, then the stiffer soil (higher K_m) will have a different stress-strain curve. The soil stress-strain response depends on the confining pressure, σ_3 , at that point in the soil. To show the sensitivity of the soil response to the variation of the K_m parameter, stress-strain curves are plotted in Figure 29 for each of the three values of K_m used in the analyses, at three different confining pressures. The three confining pressures correspond to a certain overburden pressure at a location behind the wall. Those shown in Figure 29 are for a 5-ft depth (σ_3 = 312.5 psf), a 25-ft depth (σ_3 = 1,562.5 psf), and a 40-ft depth (σ_3 = 2,532.5 psf), using a horizontal earth pressure coefficient of 0.5.

86. Figure 29 shows that as K_m increases, the initial slope of the stress-strain curve increases. This causes smaller changes in strain for the

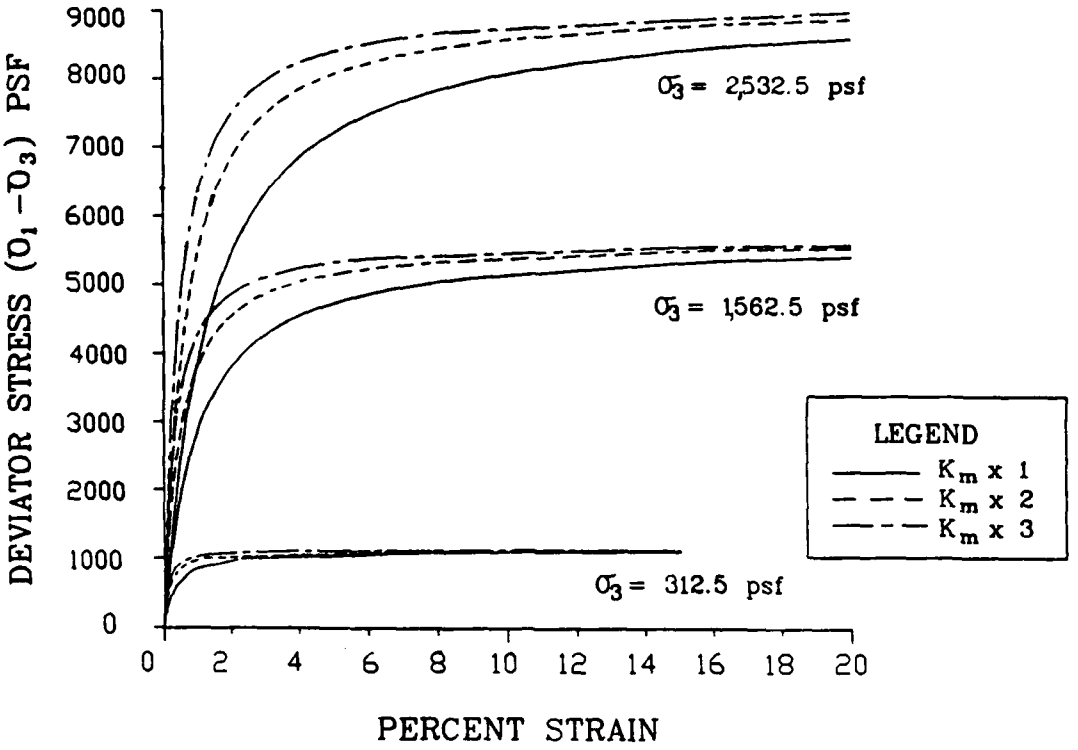

Figure 29. Hyperbolic stress-strain response of soil with increased stiffnesses at three different confining pressures

same change in deviator stress. This is what is meant by the term stiffer soil.

Variation of K_{ur}

87. The hyperbolic soil parameter, K_{ur} , is similar in function to the K_m parameter. However, K_{ur} describes the soil modulus during unloading and reloading situations. Due to the cycles of loads on the wall and soil occurring in this analysis (excavations and anchor installations), the K_{ur} parameter is applied more often than the K_m parameter to describe the soil response.

88. When K_m was increased in the preceeding analyses, K_{ur} was increased to the same value. According to Duncan et al. (1980), the unload-reload soil modulus parameter, K_{ur} , can range from $1.2K_m$ for stiff, dense soils, to $3K_m$ for softer, loose soils.

89. To see the effect of different values for K_{ur} and K_m on this model, an analysis was performed with the unload-reload parameter, K_{ur} , tripled and the initial parameter, K_m , kept at the original value (Table 2)

for the RSD and Tw materials. The results of this, at the end of construction, are presented in Figure 30, along with the results of the previous analysis in which both modulus parameters were tripled. Little difference is seen in the deflection and moment plots for the two analyses. This shows that, essentially, it is the unload-reload modulus controlling the soil response to loads in both models, although the initial modulus has some effect. Earth pressures show a notable variation in the Weigle material for the two different models.

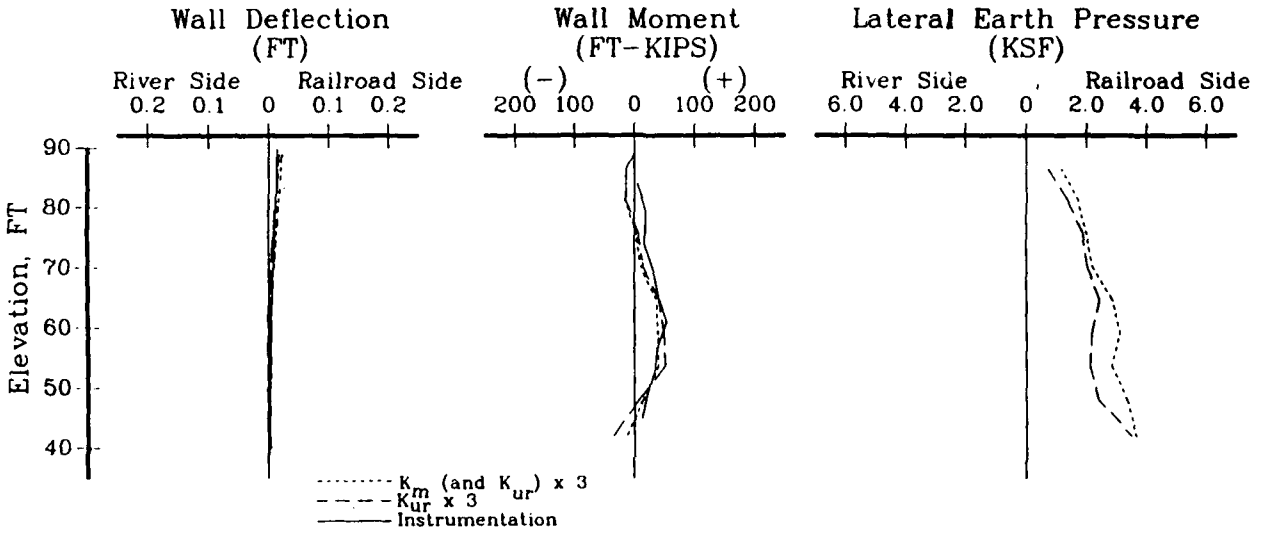

Figure 30. Comparison of results for the increased modulus values, K_m and K_{ur}

90. The effect of the unload-reload modulus parameter on the hyperbolic stress-strain model is shown in Figure 31. A stiffer soil modulus, E_{ur}, results from the increased K_{ur}.

91. The FE analyses using the tripled unload-reload modulus for RSD and Tw are presented in the subsequent comparisons with the instrumentation results. Figures 32a through 32c show these results, along with results from the initial FE model of Part II.

Instrumentation during construction

92. The strain gage and slope inclinometer readings were obtained at various construction stages. Wall deflection and bending moment were computed from these and plotted with the initial and tripled K_{ur} FE analysis results. These are shown in Figures 33 through 36. Not all the load steps analyzed in

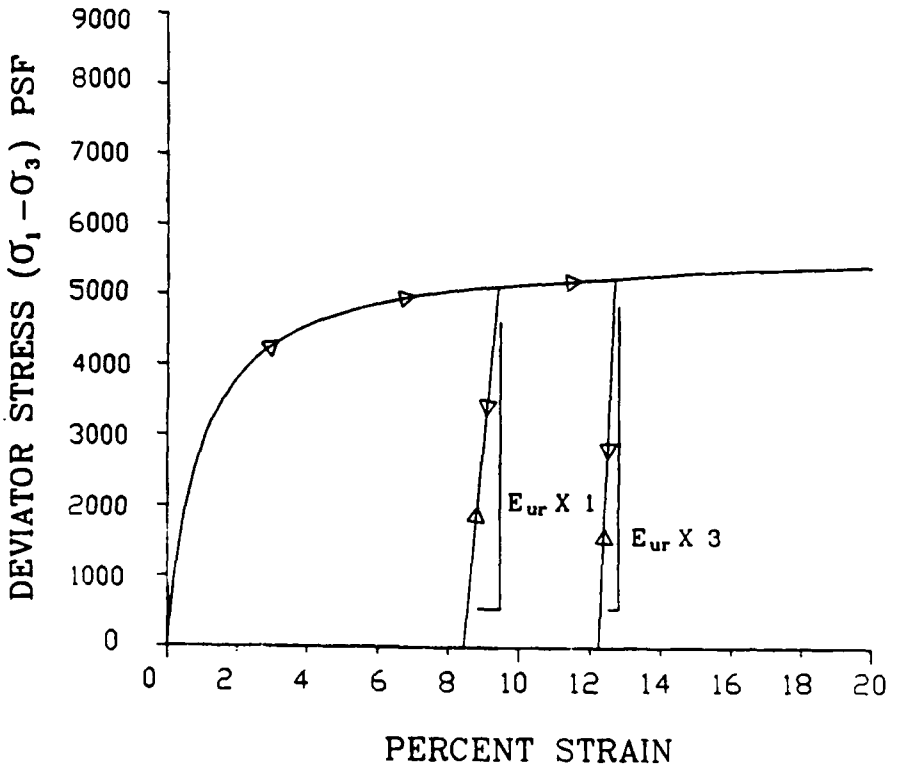

Figure 31. Unload-reload soil modulus, E_{ur} , for different stiffness parameters, K_{ur}

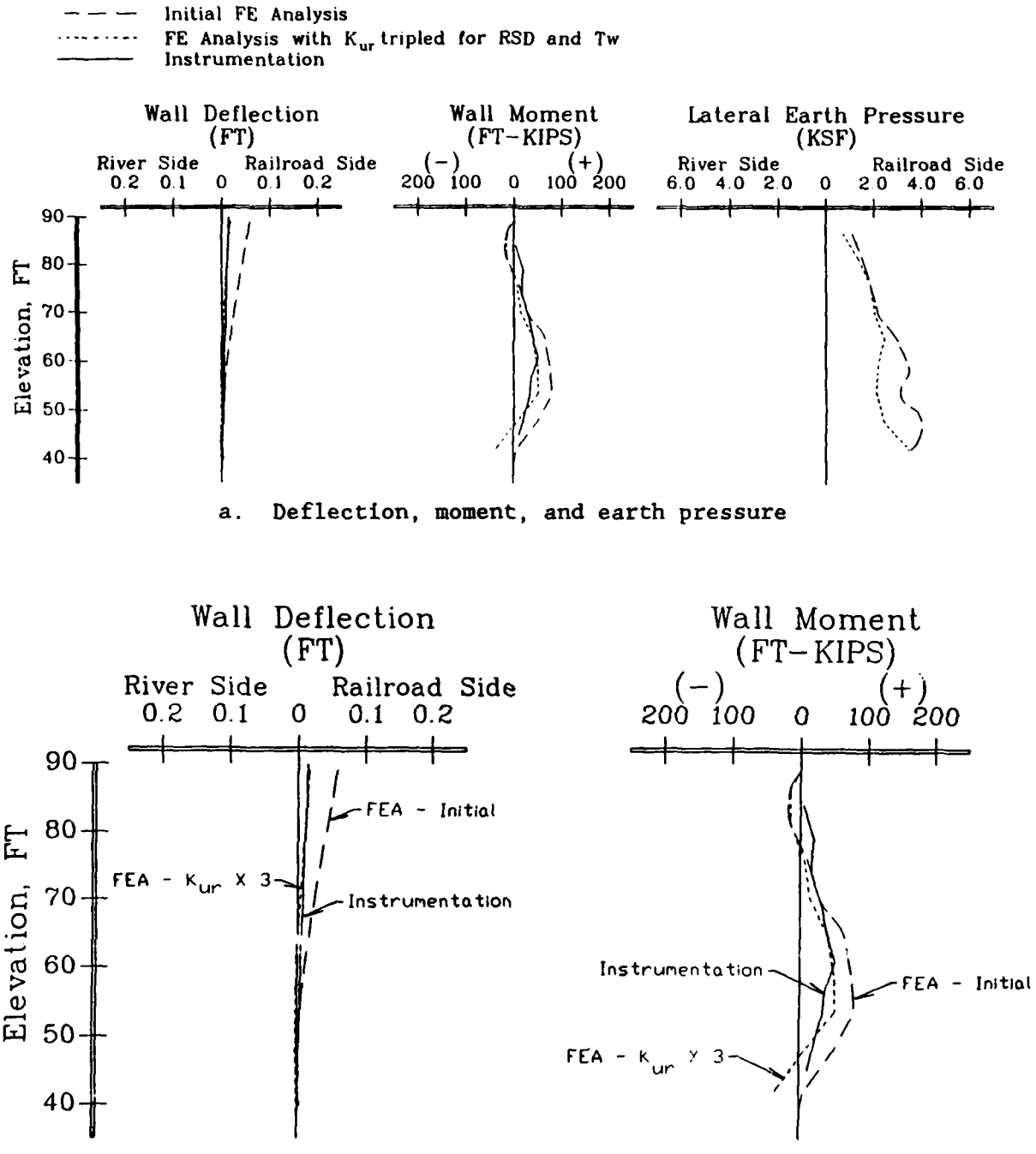

Figure 32. Comparison of end-of-construction results from instrumentation, the initial FE analysis, and the tripled K_{ur} (RSD and Tw) FE analysis

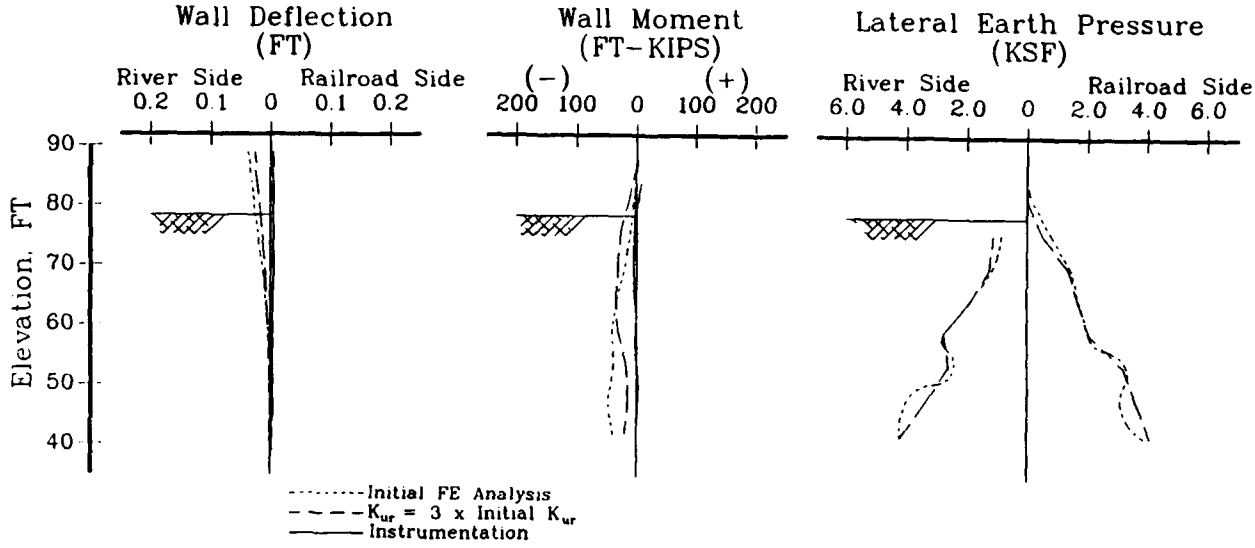

Figure 33. Results from instrumentation, initial FE, and K_{ur} × 3 analyses for the first excavation to el 78.5 ft (step 7)

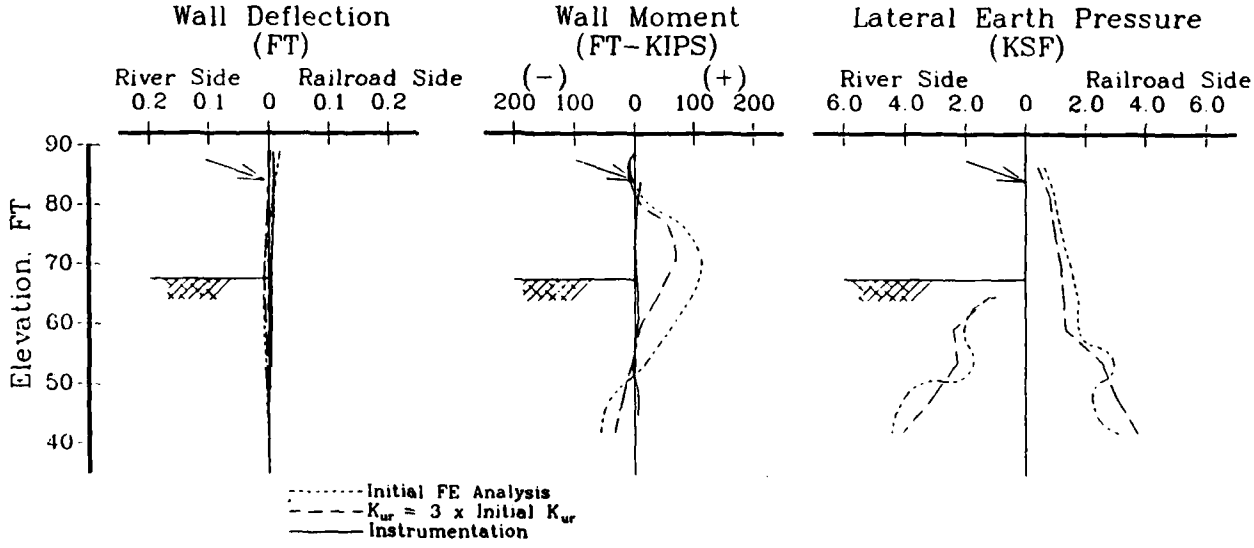

Figure 34. Results from instrumentation, initial FE, and K_{ur} × 3 analyses after the first anchor lockoff and second excavation to el 67.5 ft (step 9)

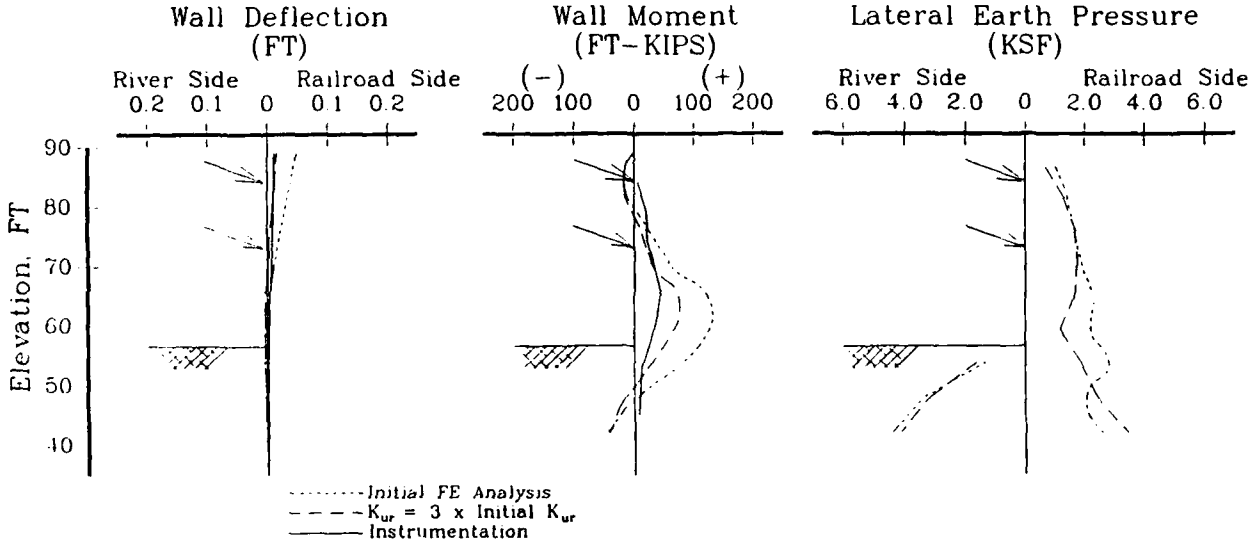

Figure 35. Results from instrumentation, initial FE, and K_{ur} × 3 analyses after the second anchor lock-off and third excavation to el 56.5 ft (step 11)

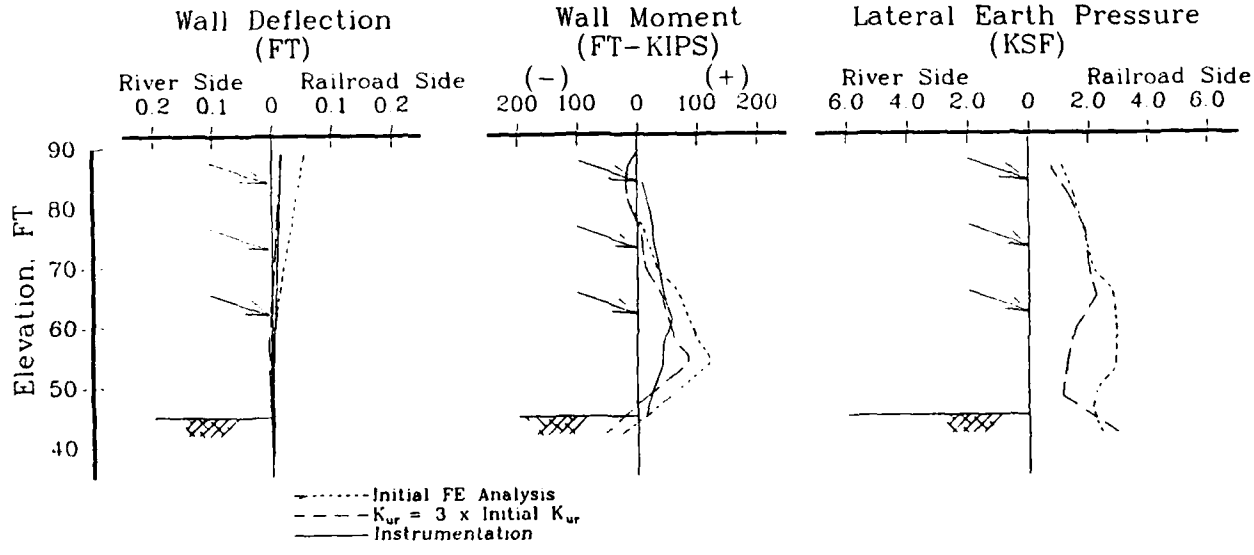

Figure 36. Results from instrumentation, initial FE, and K_{ur} × 3 analyses after the third anchor lockoff and fourth excavation to el 45 ft (step 13)

the study had corresponding instrument readings. Also, while the dates of the instrument readings were known, the exact field operation on that date was not always known with certainty; therefore, the instrumentation results are shown with the FE load steps to which they were determined to be closest, chronologically.

Increased K_{ur} six times

93. At the suggestion of Dr. J. M. Duncan, VPI, consultant to the Portland District on this project, the stiffness used in analyzing the RSD material could possibly be as much as six times the magnitude of the original value used. This was done in two analyses: in one both K_m and K_{ur} were increased, and in the other only K_{ur} was increased. These plots are shown with the results of tripled stiffness parameters and instrumentation, for comparison, in Figures 37 and 38.

94. Both deflection and moment from the analyses of K_m and $K_{ur} \times 6$ (Figures 37 and 38) overshoot the measured wall deflection and moment and are unconservative. Therefore, it appears that the soil is indeed stiffer than originally modeled, but only by about three or possibly four times. In addition, the K_m and K_{ur} values should not differ from each other by more than a factor of 2 or 3. For stiff, dense soils, Duncan et al. (1980) report K_{ur} values at approximately $1.2K_m$. Therefore, a more realistic set of parameters might be not only a tripled or quadrupled K_{ur} value from that originally used, but also a doubled or tripled K_m value from that originally used.

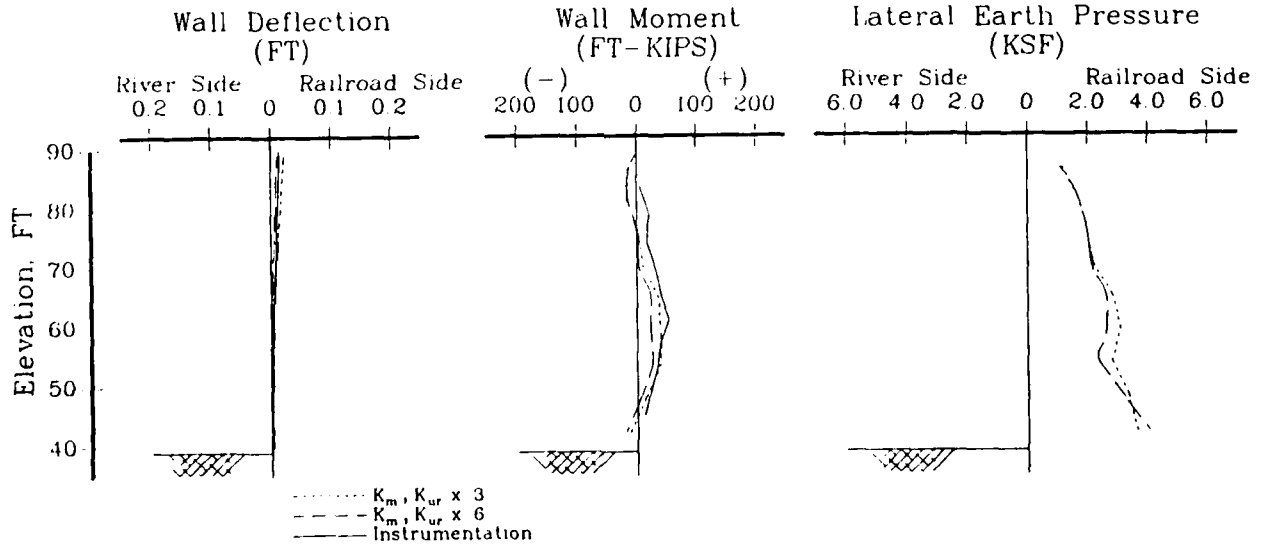

Figure 37. Hyperbolic modulus parameters K_m and K_{ur} increased by three and six times original values

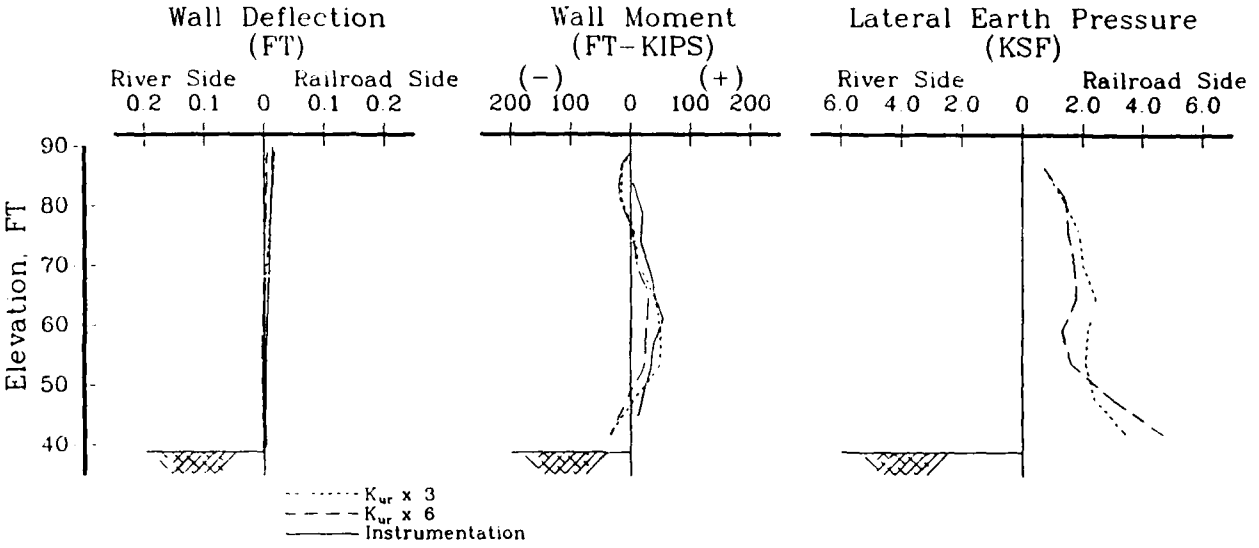

Figure 38. Hyperbolic modulus parameter K_{ur} increased by three and six times original value

Summary, Panel 6

95. Table 6 summarizes the resulting maximum values from all of the analyses performed on the Panel 6 model (Parts II, III, and IV) and lists the

Table 6
Summary of Results - Maximum Occurrences

Analysis Description	Maximum Wall Deflection (feet) - river, + land		Maximum Wall Moment (kip-ft./ft.) - ten., + compr.		Maximum Surface Movement at R.R. (inches) - down, + up	
Initial FE Analysis (Tab. 2 properties, Tab. 1 anchor loads)	0.065	+ (step 8)	133	(8,10)	0.10	(12)
Anchor loads at 200% design load	0.126	(15)	246	(11)	0.20	(15)
Top anchor failure	-0.065	(16)	-115	(16)	-0.06	(16)
K_o = 1.0 for RSD	0.071	(8)	173	(11)	0.06	(8)
K_o = 2.0 for RSD	0.048	(8)	-249	(13)	-0.11	(13)
$K_o/2$ (all soil)	0.123	(12)	202	(10)	0.16	(12,14)
K_o X 3 (RSD & Tw)	0.029	(8)	82	(8)	0.03	(12)
K_o X 3 (RSD & Tw)	0.028	(8)	84	(8)	0.04	(12)
K_o X 6 (RSD & Tw)	0.016	(8)	55	(8)	0.01	(12)
K_o X 6 (RSD & Tw)	-0.015 0.013	(7) (8)	56	(11)	-0.01 0.01	(7) (8)
Instrumentation	0.014	(~13)	57	(~13-14)	NA	

• Indicates load step where maximum occurred.
See Table 3 for load step description.

load step in which each maximum occurred. Table 7 summarizes maximum values at the end of construction for each analysis performed on Panel 6. The range of values obtained from these analyses provides a basis for comparing the wall and anchor design with a variety of soil and construction conditions.

Table 7
Summary of Results - End of Construction

Analysis Description	Final Maximum Wall Deflection (feet) - river, + land	Final Maximum Wall Moment (kip-ft./ft.) - ten., + compr.	Final Surface Location at R.R. (inches) - down, + up
Initial FE Analysis (Tab. 2 properties, Tab. 1 anchor loads)	0.056	79	0.07
Anchor loads at 200% design load	0.126 *	134	0.20 *
Top anchor failure	-0.065 *	-115 *	-0.06 *
K_o = 1.0 for RSD	0.044	128	0.02
K_o = 2.0 for RSD	-0.014	-226	-0.09
$K_m/2$ (all soil)	0.118	128	0.17
K_m X 3 (RSD & Tw)	0.022	41	0.02
K_{ur} X 3 (RSD & Tw)	0.017	52	0.03
K_m X 6 (RSD & Tw)	0.011	26	0.01
K_{ur} X 6 (RSD & Tw)	0.005	30	0.00
Instrumentation	0.011	52	NA

* Indicates overall maximum, as well as final maximum.

Conclusions of Phase 3 Study

96. The initial analysis results of Part II, while over-conservative in values, were qualitatively in good agreement with the instrumentation results (Figure 26). This led to the search for a soil parameter that would modify the results to better represent the measured behavior of the panel.

97. The parametric studies indicate that the relative value of the hyperbolic soil stiffness modulus is an influential parameter in the results of these FE analyses. Increases of the K_m and K_{ur} parameters provided results that closely approach the observed behavior, while variation of the

K_o value resulted in both qualitative and quantitative divergence from observed behavior. The best representative value of the soil stiffness parameter for RSD might be a combined increase of both the K_m and the K_{ur} values from those used in this study, for instance, K_m multiplied by two and K_{ur} multiplied by three. As noted in Part I, the soil parameters were initially chosen conservatively, and, given the range of this value for similar soils, this increase in the stiffness parameter is warranted.

98. The close agreement between the observed wall deflections and bending moment, and the analytical results confirm the accuracy of the nonlinear soil model, the FE technique, and the soil-structure interaction analysis of SOILSTRUCT in problems of this type.

PART V: INTERPRETATION OF STRAIN GAGE DATA

99. The method of interpreting the strain gage data for calculating bending moment in Panel 6 is discussed in Part V. The purposes of this discussion are to clarify the differences between the actual Panel 6 section properties and the model of Panel 6 used in the FE analyses, and to assess how the resulting bending moments are affected by this. The magnitude of strains experienced by Panel 6 in the field is also addressed, with respect to concrete tensile strength and cracking.

Summary of Analysis Procedures

FE wall model

100. The temporary tieback wall model used in the FE analysis was a 1-ft-deep section of the 3-ft-wide, 50-ft-high Panel 6. The properties used for the 1-ft reinforced concrete cross section were obtained from the Portland District at the beginning of the study: concrete strength = 3,000 psi; elastic modulus of concrete, $E_c = 3.12 \times 10^6$ psi; moment of inertia, $I = 2.25$ ft^4; and area = 3 ft^2 per lin ft. These properties were used to model the wall as a uniform material. The bending moments predicted from the FE analyses were derived from the strains occurring on the outside edges of the FE wall model. The method for doing this is described in Appendix A.

Strain gage data and moment calculaton for Panel 6

101. In the field, pairs of strain gages are located at 4- and 5-ft increments at 10 locations along the height of Panel 6, from approximately el 84 to el 45 ft. The pair consists of one gage on the excavation side of each reinforcing steel bar (front and back of wall). For 11 different dates during the construction process, the strains were read from the gages. The occasion for reading the strains was usually just after a major operation, such as an excavation or an anchor installation. These strains were used to calculate the bending moments in Panel 6. The moments were then compared with results from corresponding load cases in the FE analysis.

102. These observed wall bending moments presented in Part III of this report were calculated from the strain gage data in a manner similar to that used with the FE analysis strains. Strains from gages on the reinforcing bars

were linearly extrapolated to the outsides of the wall (approximately 7.5 in.). Stresses were calculated from the strains using the section elastic modulus, separated into axial and bending components, then the bending moments were calculated. The section properties used in the FE analysis were also used in the computations for the observed bending moment.

Revised Assessment of Panel 6

New section properties

103. The US Army Engineer Division, North Pacific (NPD), sent an example of calculating bending moment from Panel 6 strains. In this method, the section was transformed to a uniform steel section using the modular ratio $n = E_s/E_c = 7.2$, where E_s is the elastic modulus of steel. The E_c that was used reflected a higher-strength concrete (5,000 psi) than what was used in the FE model (3,000 psi). The original E_c used in the FE model is 3.12×10^6 psi, while the higher-strength E_c in the NPD calculations is 4.03×10^6 psi. These differences led to a reconsideration of the bending moments presented in Part III, in which the higher-strength concrete modulus and a representation of the steel in the panel cross section are accounted.

Better approximation of section properties

104. While strain distribution across a composite section is linear, stress distribution is not. Since the uncracked, or entire section, is used in considering stress distribution, a better approximation of the section properties, accounting for both steel and concrete stresses, and the higher concrete modulus is in order. The basis for the uncracked section assumption is explained later in this part.

105. A way to include both the steel and the concrete stresses in the moment calculation for the uncracked section is to use a composite or an effective modulus of elasticity (E_{eff}). This provides for weighted proportions of the steel and concrete properties in the section. One such expression, given in the report by Johnson (1988), is:

$$E_{eff} = \frac{E_s I_s + E_c (I_c - I_s)}{I_c}$$

where

$E_s = 29 \times 10^6$ psi

$I_s = 336.2$ in.^{4} , moment of inertia of the steel in the section

$E_c = 4.03 \times 10^6$ psi

$I_c = 46{,}656$ in.^{4} , moment of inertia of the concrete in the section

An effective elastic modulus of 4.21×10^6 psi is calculated for this section. This effective modulus is slightly greater than the high-strength concrete modulus (4.03×10^6 psi) and is quite a bit greater than the normal-strength modulus used in this study (3.125×10^6 psi). Calculations for I_s and I_c are provided in Appendix D.

106. The moment of inertia of a section, I , is also used in computing the bending moment from the extreme fiber strains. This value should also reflect both the steel and concrete materials in the composite section. While the effect of the steel on the moment of inertia is small, the consideration of it gives an effective moment of inertia, I_{eff} , of 2.36 ft^4/ft. The original value used (without steel) is 2.25 ft^4/ft. These calculations are shown in Appendix D.

Reassessment of FE results

107. An FE analysis of the Panel 6 model was again performed, this time employing the effective modulus shown in paragraph 105. The bending moment was calculated using this and the effective moment of inertia. These results are discussed in paragraph 108 through 123 and are shown in Figures 39 through 43.

108. The effect of the new moment of inertia is a directly proportional increase in the bending moments, by a factor of 2.36/2.25 = 1.05, a 5 percent increase in moment. This factor can be applied to all the moment diagrams presented in this report; both the moments derived from the instrumentation and the moments computed from the FE analyses.

109. Increasing the elastic modulus for the section has a different effect on the bending moment than does increasing the moment of inertia. In applying a larger elastic modulus to the strain-gage-moment calculations, larger stresses result from the same original strains, and therefore, larger bending moments are computed. However, the use of a larger elastic wall modulus in the FE analysis caused the panel elements to be stiffer and, therefore, experience lower strains from the loadings than those originally experienced. Even though stresses are higher because of the higher modulus, the overall

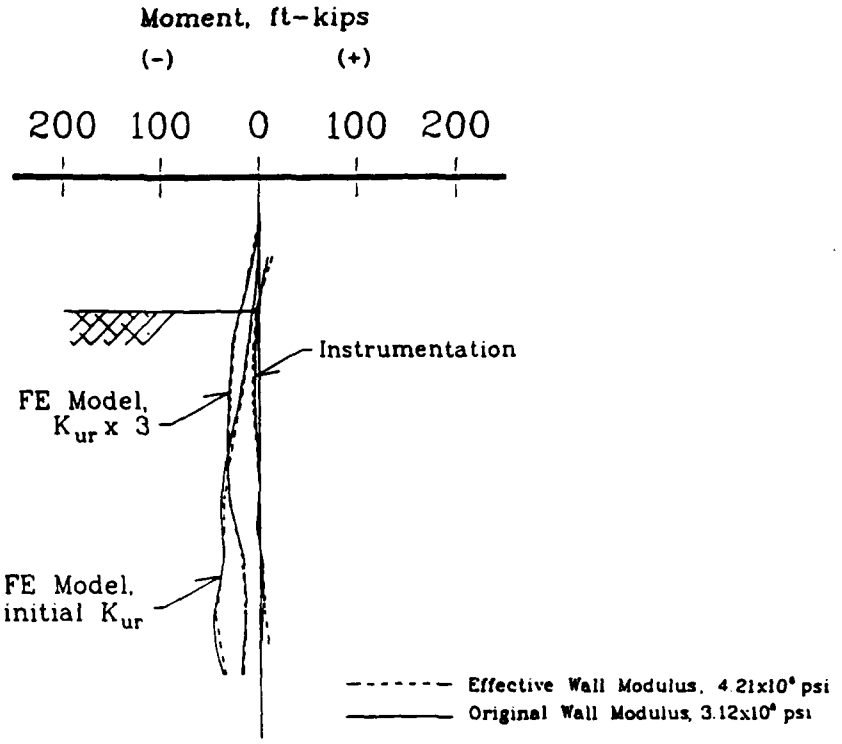

Figure 39. Bending moment change from original to effective modulus for instrumentation and two FE models; load step 7, first excavation to el 78.5 ft

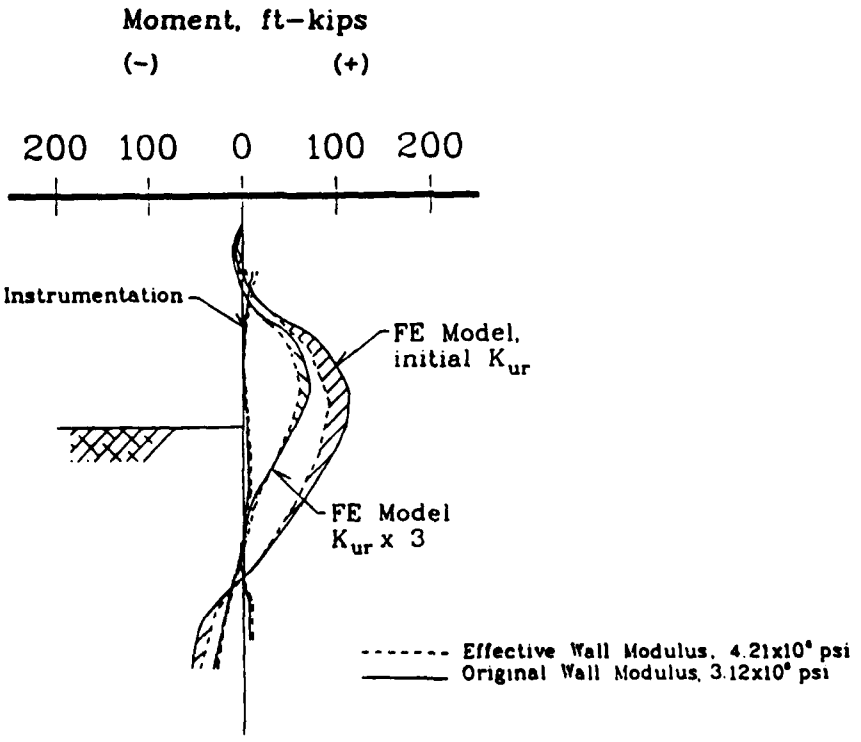

Figure 40. Bending moment change from original to effective modulus for instrumentation and two FE models; load step 9, second excavation el 67.5 ft, first anchor lockoff

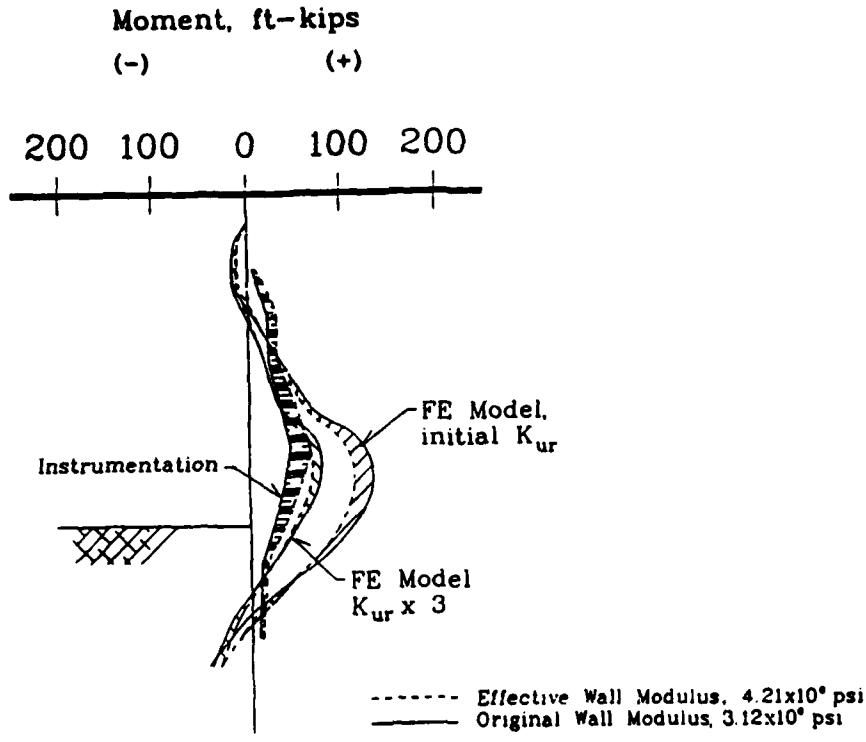

Figure 41. Bending moment change from original to effective modulus for instrumentation and two FE models; load step 11, third excavation to el 56.5 ft, second anchor lockoff

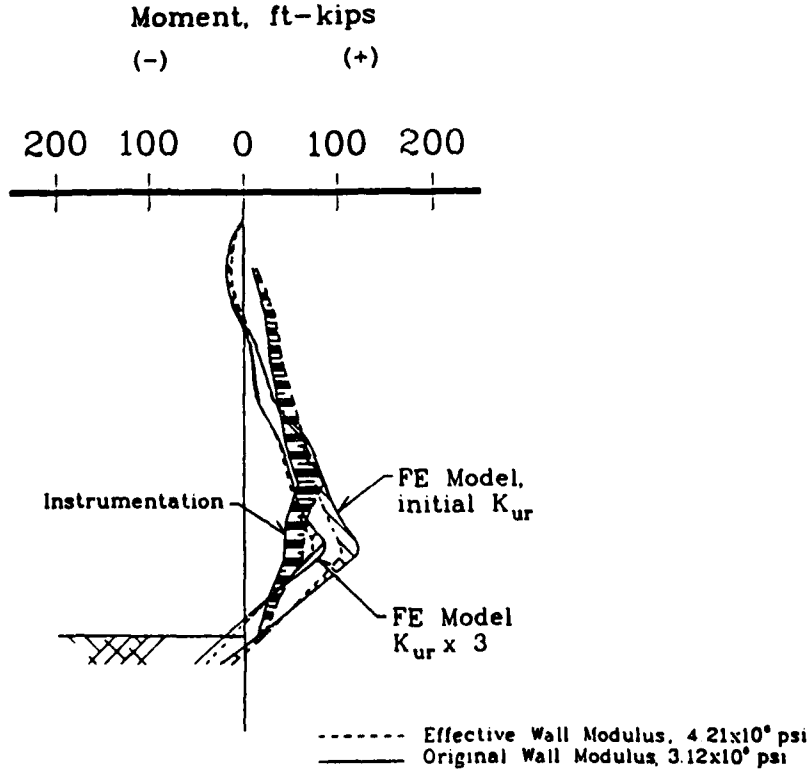

Figure 42. Bending moment change from original to effective modulus for instrumentation and two FE models; load step 13, fourth excavation to el 45 ft, third anchor lockoff

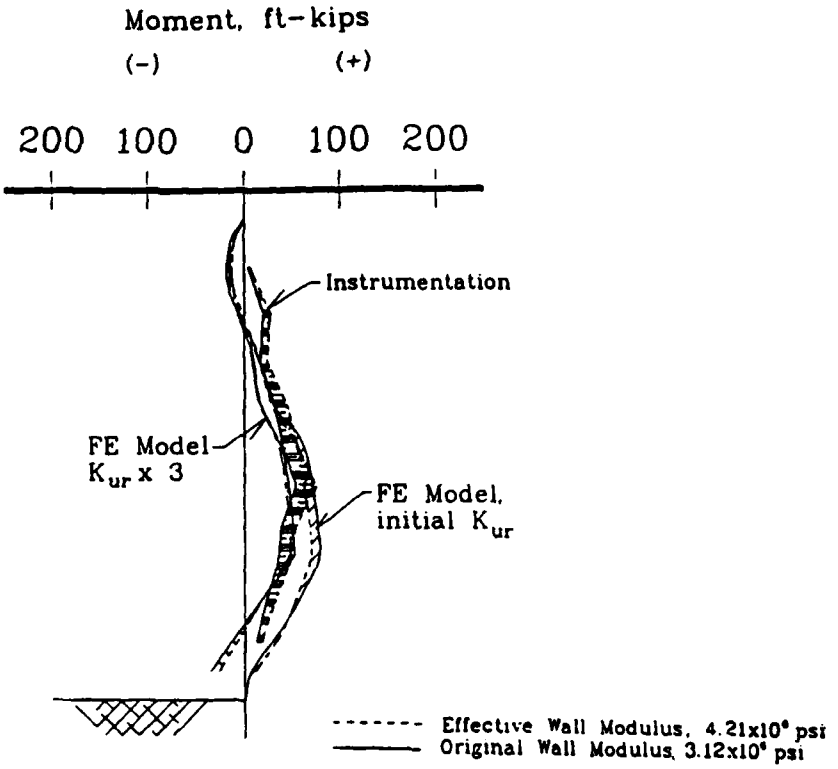

Figure 43. Bending moment change from original to effective modulus for instrumentation and two FE models; load step 15, last excavation to el 39 ft, fourth anchor lockoff

effect is lower bending moments because of the lower strains. The total effect is to bring the FE predicted moments and the measured moments closer together.

110. The resulting maximum moment from the initial FE model using the original E_c and I_c (Part II) is 133 k-ft. Using the larger (stiffer) wall modulus on the same model, the maximum moment is 115 k-ft. For the $K_{ur} \times 3$ model with the original elastic modulus, a maximum moment of 84 k-ft results, while for the larger modulus, a moment of 75 k-ft results. The average reduction in the maximum FE moment is 12 percent. Considering also the 5-percent moment increase due to the effective moment of inertia, these maximum bending moments are 121 and 79 k-ft, respectively. The effect of the larger wall elastic modulus on the FE-predicted wall deflection is negligible. Only the bending moment is notably affected.

111. The bending moments from strain gage data were then recalculated using the larger wall modulus. Results are also presented in Figures 39 through 43. This produced moments greater than those originally calculated.

The maximum moment calculated from strain gage data with the original wall modulus is 57 k-ft. For the same strain data, the maximum moment using the higher modulus is 84 k-ft. The use of the effective elastic modulus with the strain gage data in computing bending moment increases the moment over the original calculations by approximately 45 percent. A summary of these results is shown in Table 8.

Table 8

Maximum Bending Moment Comparison for the Original Elastic Modulus and the Effective Elastic Modulus of a Panel 6 Section. (E_{orig}= 3.12, E_{eff}= 4.21, x 10^6 psi)

Analysis	EOC * E_{orig} kip-ft/ft	EOC E_{eff} kip-ft/ft	EOC E_{eff} and I_{eff} kip-ft/ft	Overall E_{orig} kip-ft/ft	Overall E_{eff} kip-ft/ft	Overall E_{eff} and I_{eff} kip-ft/ft
Initial FE analysis, Original soil parameters (Tab.2)	79	70	74	133 (8,10)**	115 (8,10)	121
FE Analysis, K_{ur} X 3 for RSD and Tw	52	46	48	84 (8)	74 (8)	78
Instrumentation (Strain Gages)	52	75	79	57 (~13-14)	84 (~13-14)	88

* EOC = End of Construction condition.
** Indicates load step where maximum occurred. See Table 3 for load step description.

Concrete tension/cracking

112. The basis for analyzing an uncracked section of the wall is discussed in the following paragraphs. In most analyses of reinforced concrete members, a cracked section is assumed to exist because typical loading cases cause stresses in the tension side of the beam that exceed the concrete tensile strength. Analysis is then based on compression-only concrete, tension steel, and possibly compression steel.

113. Cracking or tensile strains for normal concrete are generally considered to be on the order of 0.010 to 0.012 percent, or 100 to 120 microstrain ($\mu\epsilon$) , where $1\ \mu\epsilon = 1 \times 10^{-6}\ \epsilon$. However, higher-strength concrete generally has higher tensile strength as well. Approximate tensile strains

can be calculated from equations relating tensile strength to compressive strength. Two such expressions are:

$$f_t' = 0.10\ f_c' \text{ (Ferguson 1979)}$$

and

$$f_t' = 2.1(f_c')^{2/3} \text{ (Leonhardt 1988)}$$

where

f_t' = concrete tensile strength

f_c' = concrete compressive strength, in psi

For the high-strength concrete (f_c' = 5,000 psi and $E_c = 4.03 \times 10^6$ psi), tensile strengths of f_t' = 500 psi and f_t' = 641 psi are obtained from the two expressions, respectively. These give tensile strains (f_t'/E_c) of 0.0124 and 0.0152 percent. These values, 124 to 152 $\mu\epsilon$, can be used to define a strain range in which tensile cracking may occur in Panel 6.

Panel 6 strains

114. Observation of the Panel 6 strains (linearly extrapolated from steel to face of concrete) shows only one occurrence of strain during construction that even approaches the lower bound of the 124 to 152 $\mu\epsilon$ cracking strain range. This is a strain of 117 $\mu\epsilon$, occurring on the excavation side of the panel near the third anchor elevation (el 62 ft). This strain was recorded after the third anchor was locked off. The strain at this location drops to 112 $\mu\epsilon$ in the reading following lockoff of the fourth anchor (el 51 ft). Strains from the gages to either side of this location remain below 100 $\mu\epsilon$. Because this maximum strain is less than the estimated minimum strain that may cause cracking of Panel 6, it is not likely that cracking has occurred. Therefore, the assumption of an uncracked wall section is appropriate for analysis of Panel 6.

Summary

115. Both the instrumentation and FE model bending moments described in Part III of this report are calculated from strains extrapolated to the extreme fiber of an uncracked uniform cross section, with properties of $E_c = 3.12 \times 10^6$ psi and $I_c = 2.25$ ft^4/ft .

116. The NPD example of moment calculation showed the need to consider a transformed section of uniform material. It also provided updated concrete material properties from the normal-strength concrete elastic modulus (3.12 ×

10^6 psi) to a high-strength concrete elastic modulus (4.03×10^6 psi).

117. Using the high-strength concrete elastic modulus, an effective modulus for the section was calculated. This includes weighted proportions of both steel and concrete in the section. The value of this effective modulus is 4.21×10^6 psi. Also, an effective moment of inertia was calculated from a transformed section to consider the effect of the steel. This is 2.36 ft^4/ft. These values were used in reanalysis of two of the Panel 6 models (initial, and $K_{ur} \times 3$) to determine the effect of this new section representation on the bending moments. Results are summarized in Table 8.

118. Assessment of the strains recorded on the faces of Panel 6 during construction shows that tensile cracking, as defined by the strain range of 124 to 152 $\mu\epsilon$, does not occur.

Impact of Section Properties Effects on Panel 6

119. These last paragraphs of this part serve to put in perspective the impact of each of the effects of the revised section properties on the bending moment assesment of Panel 6. For instance, the 5-percent moment increase due to I_{eff} is an almost negligible effect given the variations one might expect from errors in the modeling process and instrumentation. On the other hand, consideration of the proper elastic modulus is important for the correct interpretation of the bending moment sustained by Panel 6.

120. The use of the normal concrete section properties in the FE studies (Parts II through IV) produced overly conservative bending moments because the wall stiffness that was modeled is lower than the actual wall stiffness. The use of these same normal concrete section properties in the derivation of moment from the strain gage data has an opposite effect because the moments calculated are on the unconservative side of what was probably experienced.

121. Instrumentation results and FE results are more closely matched when the effective elastic modulus was used: the FE moments decrease, and the instrumentation moments increase to within a closer range of each other. These moment results, Figures 39 through 43, still indicate that the RSD material is stiffer than originally modeled in the initial studies.

122. The bending moment results of the parametric variations (Parts III and IV) are still very much valid because of their qualitative use in

assessing the influence of various parameters on the wall behavior. The FE moments shown for the various analyses can be viewed as conservative or upper-bound limits to the range of moments that may be experienced by the wall. In consideration of the revised wall section properties (effective elastic modulus), more accurate quantitative results could be obtained by mentally envisioning the FE moment diagrams at about 10 to 12 percent lower magnitude, and the instrumentation moment diagrams at about 45 percent higher magnitude.

123. While the purpose of this part is to investigate the effects of different section properties on the bending moment, it is important to keep the results of this study in perspective. The deflection of the wall is the key issue under question. Interpretation of the instrumentation data for wall deflection is straightforward. The observed behavior was well modeled by the FE analysis when the soil was stiffened (by the hyperbolic parameter, K_{ur}) by approximately three times its original value (Figure 32). Interpretation of the strain-gage data is less direct, and depends highly, as shown in this part, on the section properties and the method of assessing the section. Temperature variations in the concrete and nonuniform sections (due to caving, e.g.) can locally alter measured strains. One must also keep in mind that all of the computed moments, whether from FE analyses of instrumentation, and regardless of how conservative, show the wall to be well below its design bending moment capacity of 191 k-ft. It is the deflection criterion that has governed the wall design and initiated the concern leading to this investigation. The wall and ground surface deflections have been shown to cause no problems to the project site or railroad tracks nearby.

PART VI: LONG-TERM BEHAVIOR OF PANEL 6

124. Data from strain gages and the slope inclinometer of Panel 6 were recorded at various intervals following completion of the wall, Mar 14, 1988, until Oct 1988. These readings were received from the NPP Office, and the results are discussed in this part. A comparison between two readings of the wall deflection and bending moment, recorded on Mar 14 (end of construction) and Oct 4, 1988, is shown in Figure 44. The moment variations occurring between these times is described in paragraphs 125 and 126.

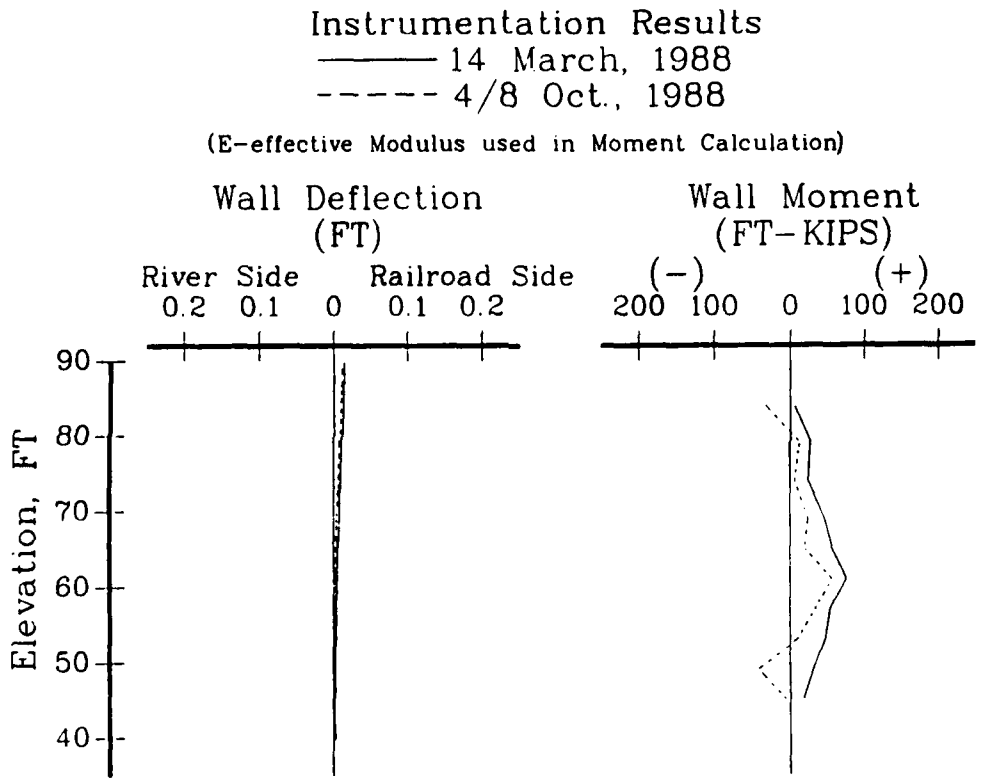

Figure 44. Comparison of observed deflection and bending moment of Panel 6 from end of construction, Mar 14 to Oct 8, 1988

Bending Moment and Strains

125. The strains in Panel 6 were recorded four to five times a month from the end of construction, Mar 14 to Oct 4, 1988. In general, the maximum moments calculated from these strains remain below 70 k-ft (computed with the effective elastic modulus discussed in Part V). However, the reading from

May 3, 1988, shows a point of high strain which would cause tension exceeding estimated tensile strength, about one-half way down the wall. This strain on the outside face of the panel is 223 $\mu\epsilon$, far exceeding the maximum estimated cracking strain of 152 $\mu\epsilon$ (Part V). If this reading is accurate, cracking has occurred at this point of the wall. The only other location at which a potential cracking strain is approached is at the top inside face of the wall, at a later date, Jul 27, 1988. This strain is only 125 $\mu\epsilon$, but indicates possible cracking because it falls just within the cracking strain range defined as 124 to 152 $\mu\epsilon$.

Deflection

126. The slope inclinometer readings of Oct 4, 1988, show only a very slight change in the deflected wall position since the end of construction. The maximum deflection at the top of the wall on Oct 4 is 0.13 in. (0.01 ft). At the end of construction, the maximum deflection at the top of the wall was 0.133 in. Slope inclinometer data from dates between these times are not available.

PART VII: PANEL 11 ANALYSIS

127. Panel 11 is another section of the temporary tieback wall analyzed in this investigation. This panel extends to over 80 ft in height and has six pairs of anchors. The model and methods of analysis for Panel 11 are similar to those of Panel 6. The results presented for Panel 11 are from an initial analysis and two other analyses in which the unload-reload stress-strain modulus of the RSD was increased, based on results from the Panel 6 study. The study of Panel 11 began shortly after the Phase 1 work on Panel 6 was completed.

Description

128. Panel 11 is similar to Panel 6 in its construction and size, but it differs in height. It is 82.3 ft on the upstream end and 65.3 ft on the downstream end. The base of this panel was stepped during construction due to the diabase inclination. The location of Panel 11 in the temporary wall is shown in Figure 45. Figure 46 shows the as-constructed panel.

129. The soil conditions behind Panel 11 are not like those at Panel 6 because the Weigle material does not come in contact with the wall at this point. Only the RSD material is retained by this panel. This is shown in the geologic section presented in Figure 47.

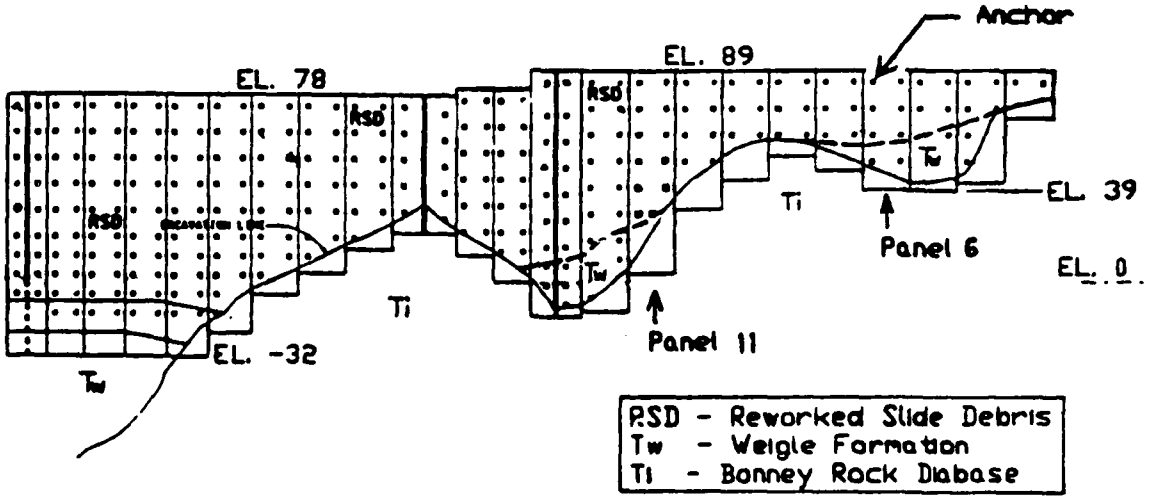

Figure 45. Front view of temporary tieback wall

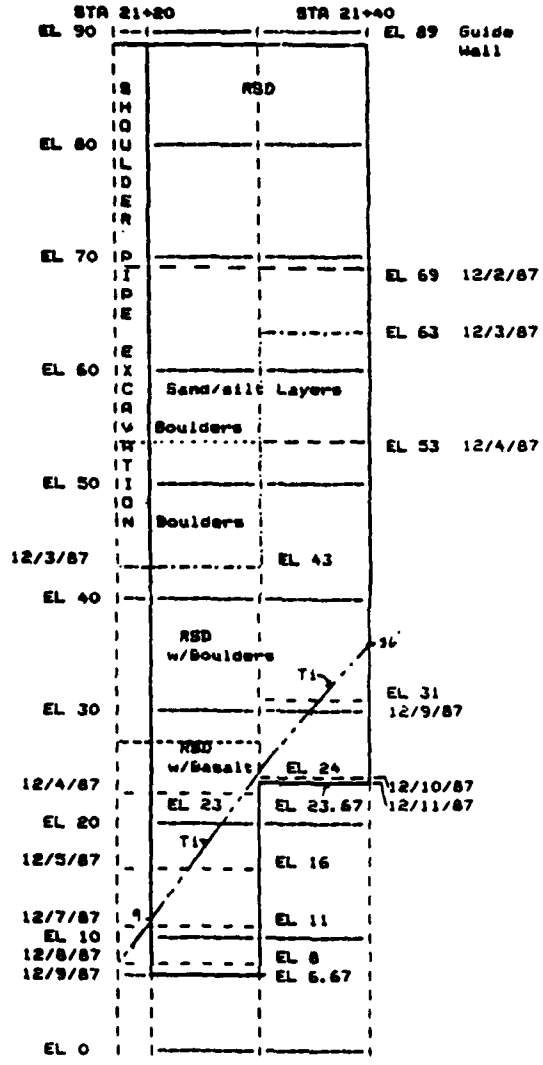

Figure 46. Panel 11, as-constructed

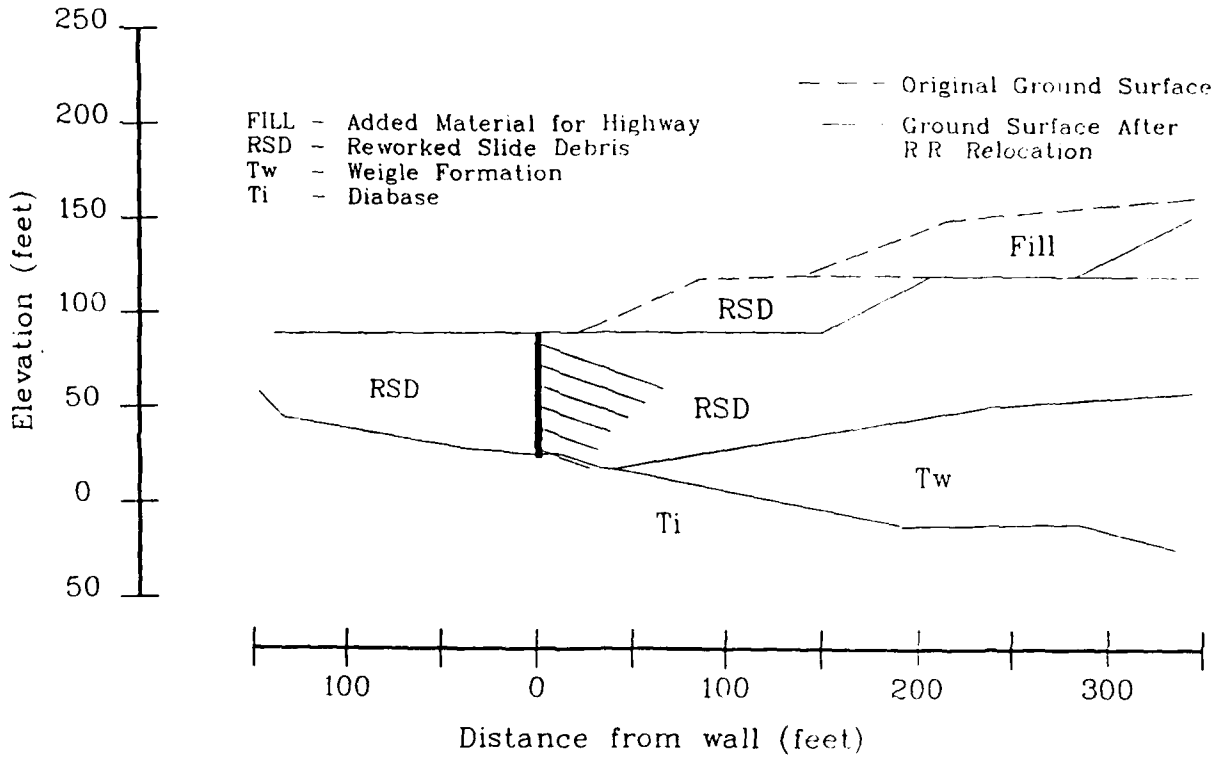

Figure 47. Geologic section at Panel 11

Model

130. Because the base of Panel 11 is stepped, only the right half of it is used in this study for ease of modeling. The model is a 1-ft-deep section along the center line of the right half, from el 89 to el 23.67 ft. Based on the construction report and boring logs, it was determined that the Weigle formation at Panel 11 begins about 25 ft behind the wall and extends further back. Therefore, the soil modeled in front of and immediately behind the wall at Panel 11 consists only of RSD resting on the diabase.

131. Figure 48 shows the front and side views of Panel 11. The anchors are installed in this panel the same as in Panel 6. The FE grid developed to model the wall and geologic section at Panel 11 is shown in Figure 49. This grid is denser than the Panel 6 grid in the vicinity of the wall.

Analysis

132. The Panel 11 model was initially analyzed using the same wall, soil, and interface properties and parameters as the ones used in the initial Panel 6 analysis (see Part I and Table 2). Based on instrumentation and the

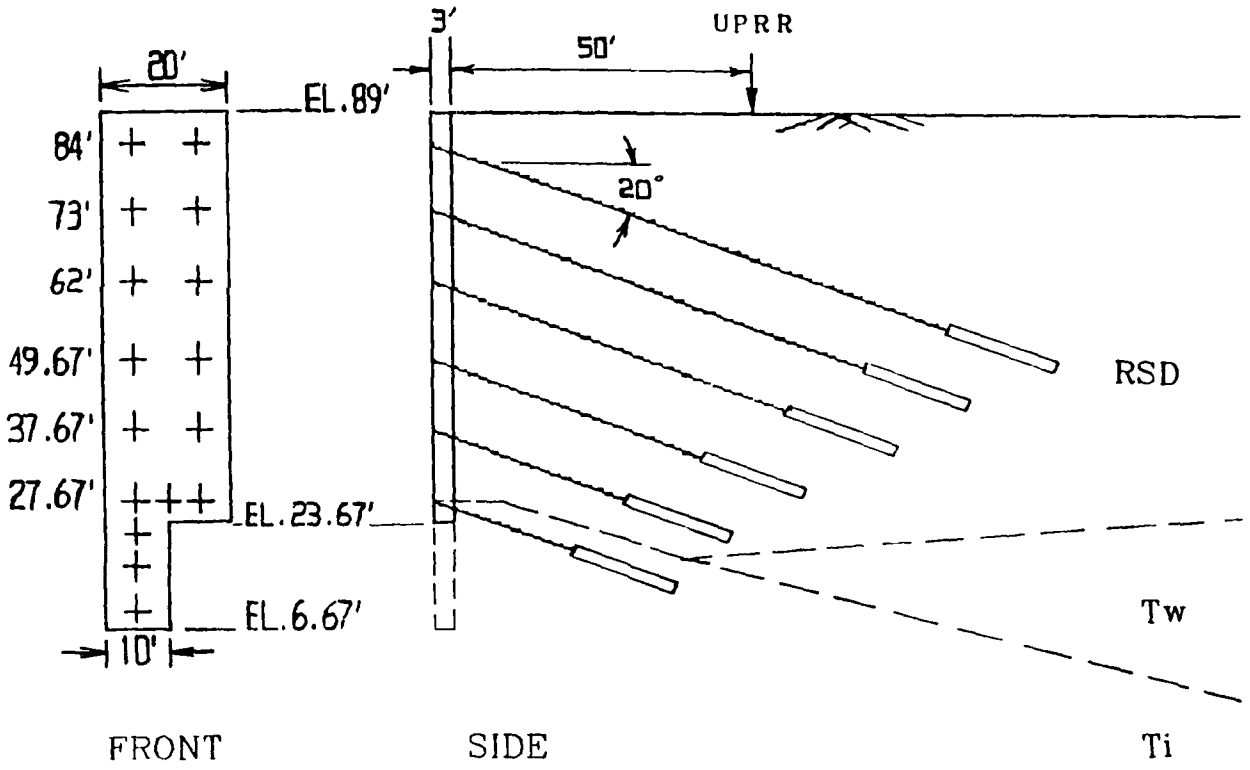

Figure 48. Front and side views of Panel 11

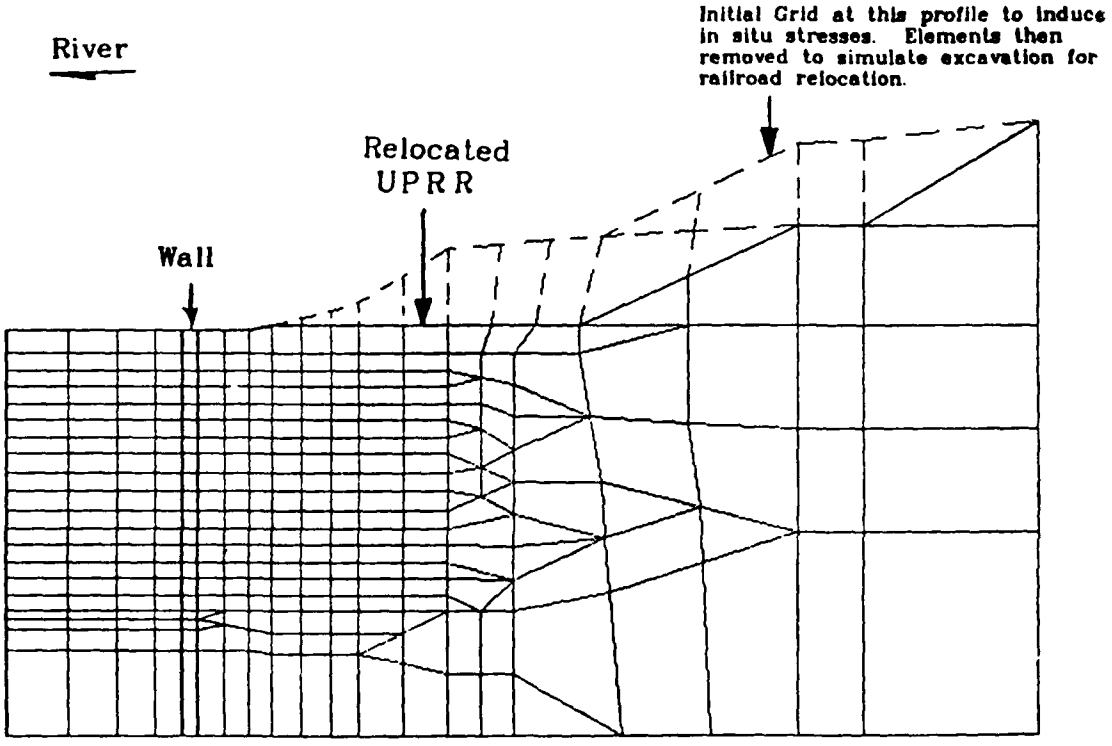

Figure 49. FE grid model of Panel 11 section

results obtained from K_m and K_{ur} variations for Panel 6, second and third analyses were performed on Panel 11 using three and six times the value of the initial unload-reload modulus, K_{ur} , for the RSD material.

Loading sequence

133. The loading sequence modeling the construction steps in the Panel 11 analysis is listed in Table 9. This is simply an extention of the load steps of the Panel 6 study, Table 3.

Table 9
Panel 11 Construction Steps

Step No.	Description
1	Build natural slope
2	Build natural slope
3	Activate interface elements
4	Excavate for railroad relocation
5	Build wall in soil
6	Excavate to el 80.3 ft (in front of wall)
7	Prestress 1st anchor at el 84 ft
8	Excavate to el 69.3 ft and lock off 1st anchor
9	Prestress 2nd anchor at el 73 ft
10	Excavate to el 57.9 ft and lock off 2nd anchor
11	Prestress 3rd anchor at el 62 ft
12	Excavate to el 46 ft and lock off 3rd anchor
13	Prestress 4th anchor at el 49.67 ft
14	Excavate to el 35 ft and lock off 4th anchor
15	Prestress 5th anchor at el 38.67 ft
16	Excavate to el 27.67 ft and lock off 5th anchor
17	Prestress 6th anchor at el 27.67 ft
18	Lock off 6th anchor

Results of Panel 11 Analyses

134. The results are presented together for the three Panel 11 analyses. The wall deflection, bending moment, and earth pressures resulting from each load step are shown in Figures 50 through 62. Anchor loads and the ground suface deflection are presented following the wall plots.

Wall deflection

135. The pattern of wall movement with the construction steps is similar to that seen in Panel 6. The wall moves out toward the excavation after the first excavation of soil in front of it (Figure 50), then is pulled back into the soil when the first anchor is prestressed (Figure 51). After this, all movement, toward or away from the excavation, stays on the railroad side of vertical. The stiffer the RSD, the less the wall deflects. The $K_{ur} \times 6$ RSD causes deflections to be approximately one-half of those with the $K_{ur} \times 1$ RSD. Maximum wall movement for the three analyses occurs at the top of the wall, with the prestressing of the fourth anchor (Figure 57). These values are 0.246, 0.153, and 0.130 ft, respectively, for $K_{ur} \times 1$, $K_{ur} \times 3$, and $K_{ur} \times 6$. The wall moves relatively very little after this load step, remaining essentially in the same deflected position from this point until the end of construction.

Bending moment

136. The bending moment diagrams have similar form for the three analyses, differing mainly in magnitude. The diagrams for the two increased RSD stiffnesses, $K_{ur} \times 3$ and $K_{ur} \times 6$, match very closely with only a small difference in magnitude between the two. The moment diagram from the initial analysis, $K_{ur} \times 1$, differs from the other two more in magnitude and also, at times, in form. The maximum bending moment in the wall occurs with the third excavation (Figure 54) in the three analyses. These values are 311, 236, and 213 k-ft, respectively, with each increased RSD stiffness. At the end of construction (Figure 62) the maximum moments from the two stiffer RSD analyses are slightly higher in value and higher in location on the wall than for the initial analysis. These values are 124, 142, and 140 k-ft for $K_{ur} \times 1$, $K_{ur} \times 3$, and $K_{ur} \times 6$, respectively.

Earth pressures

137. The earth pressure diagrams are very nearly the same for the three analyses performed on Panel 11. The increase in the RSD stiffness is

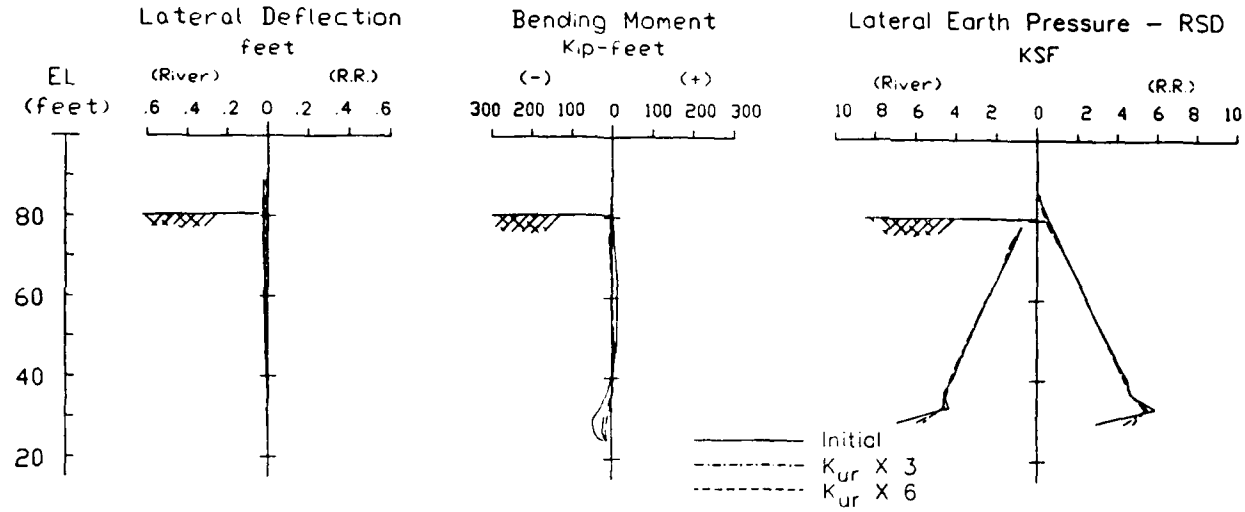

Figure 50. Deflection, moment, and earth pressure for Panel 11, load step 6; excavation to el 80.3 ft

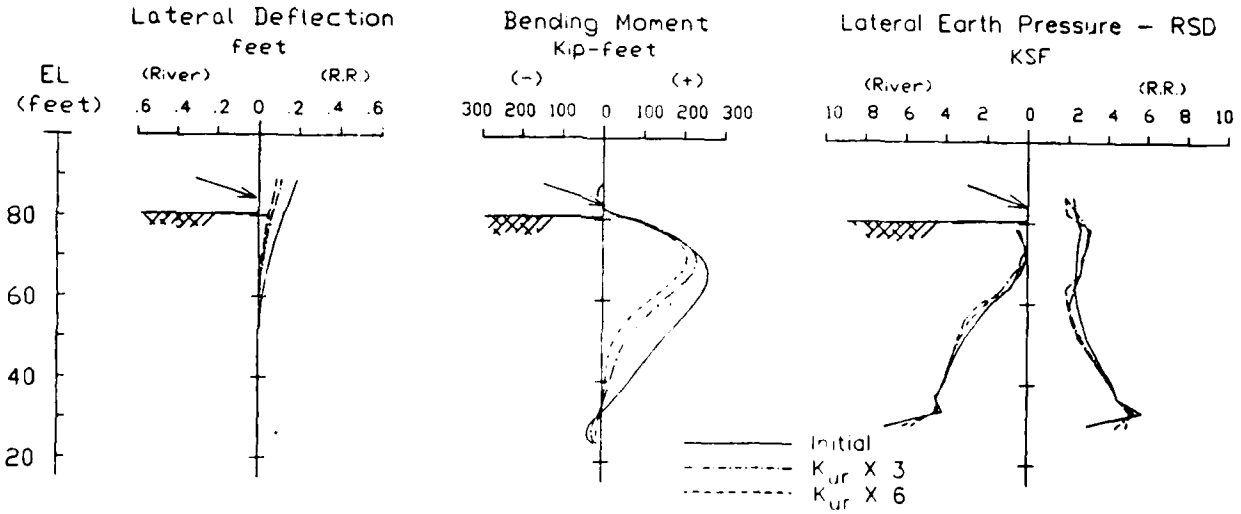

Figure 51. Deflection, moment, and earth pressure for Panel 11, load step 7; prestress anchor at el 84 ft

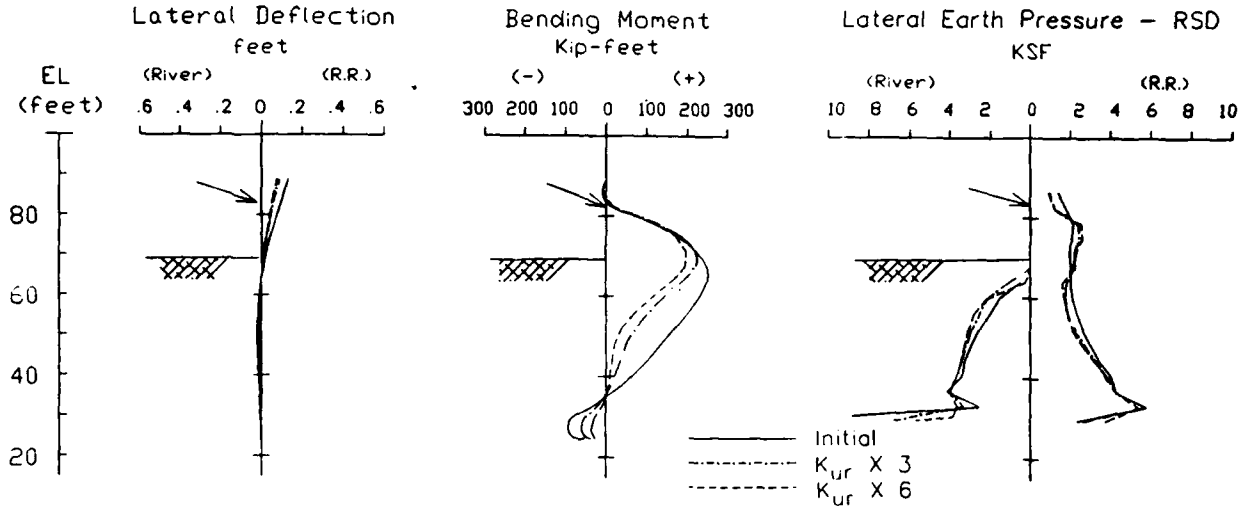

Figure 52. Deflection, moment, and earth pressure for Panel 11, load step 8; lock off anchor 1, excavate to el 69.3 ft

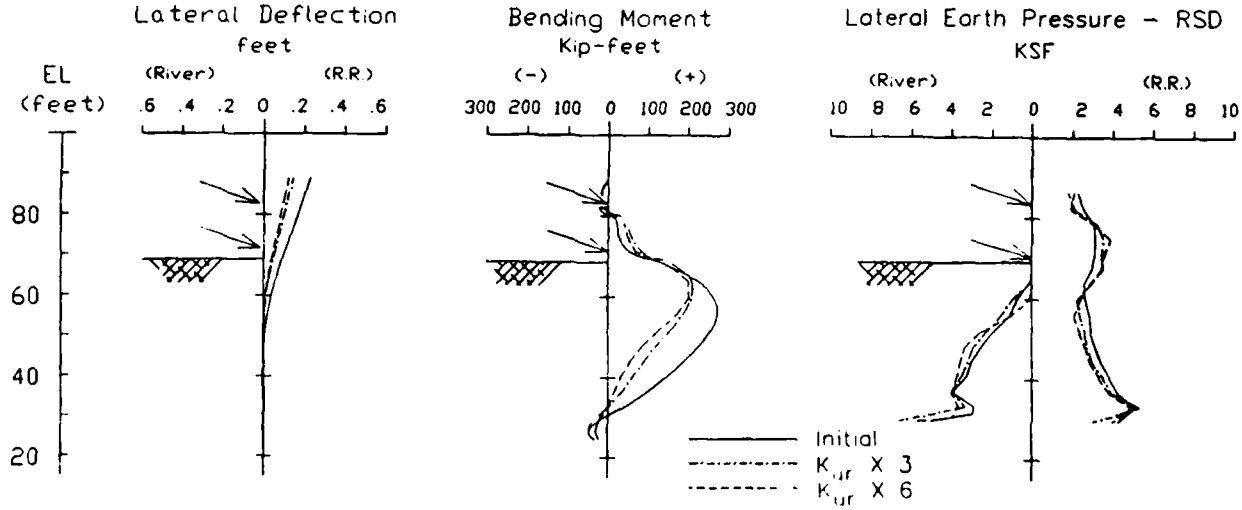

Figure 53. Deflection, moment, and earth pressure for Panel 11, load step 9; prestress anchor at 73 ft

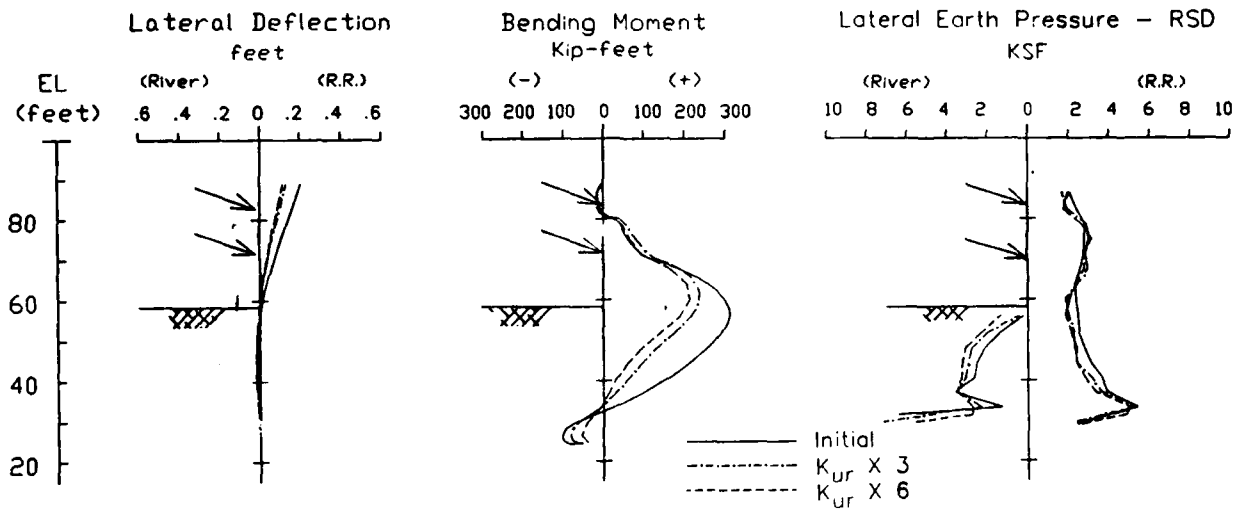

Figure 54. Deflection, moment, and earth pressure for Panel 11, load step 10; lock off anchor 2, excavate to el 57.9 ft

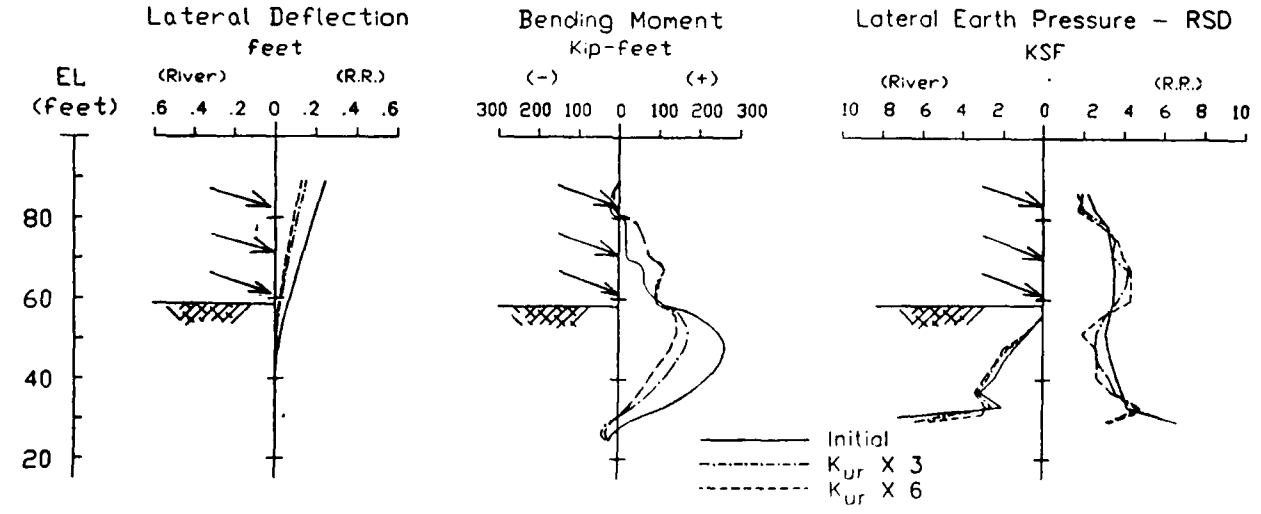

Figure 55. Deflection, moment, and earth pressure for Panel 11, load step 11; prestress anchor at el 62 ft

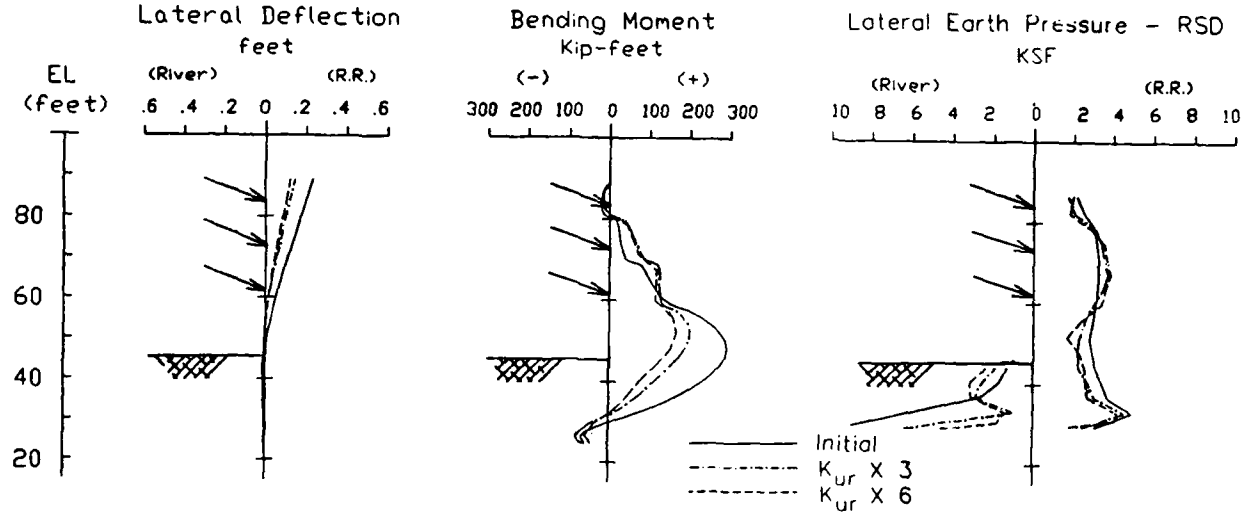

Figure 56. Deflection, moment, and earth pressure for Panel 11, load step 12; lock off anchor 3, excavate to el 46 ft

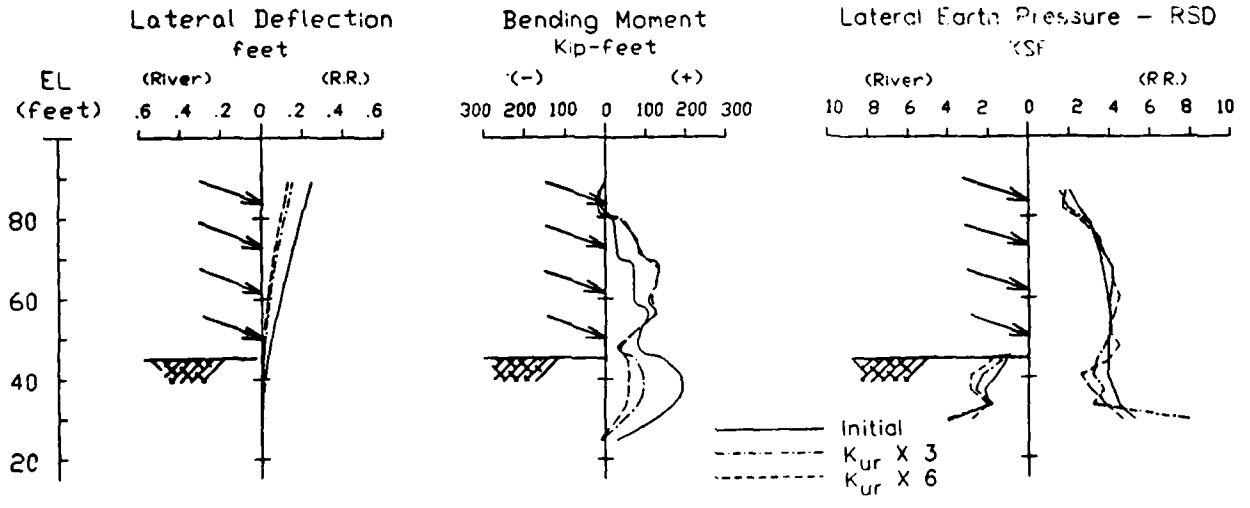

Figure 57. Deflection, moment, and earth pressure for Panel 11, load step 13; prestress anchor at el 49.67 ft

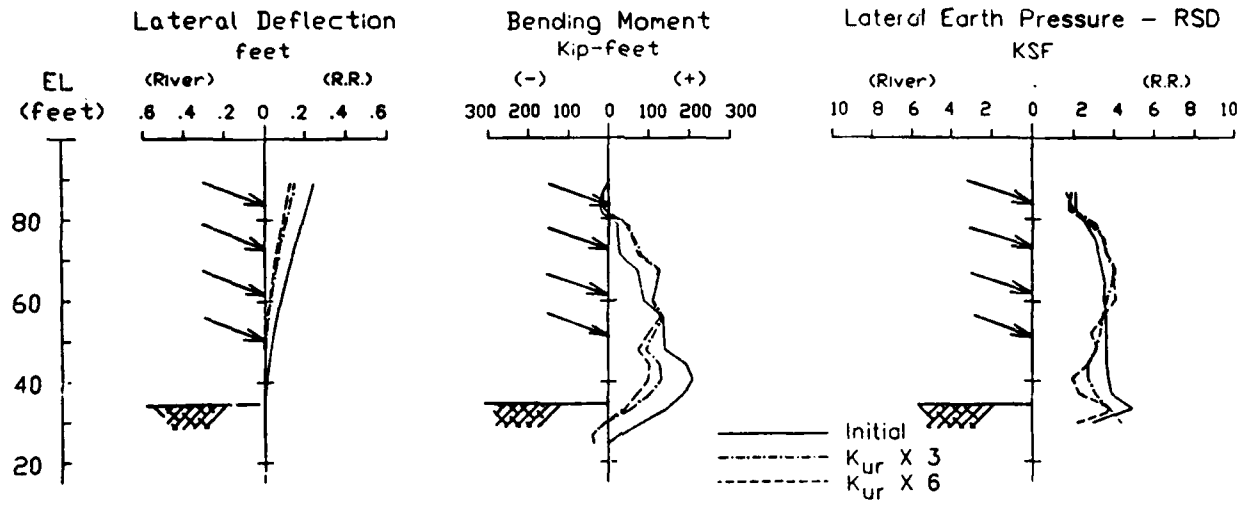

Figure 58. Deflection, moment, and earth pressure for Panel 11, load step 14; lock off anchor 4, excavate to el 35 ft

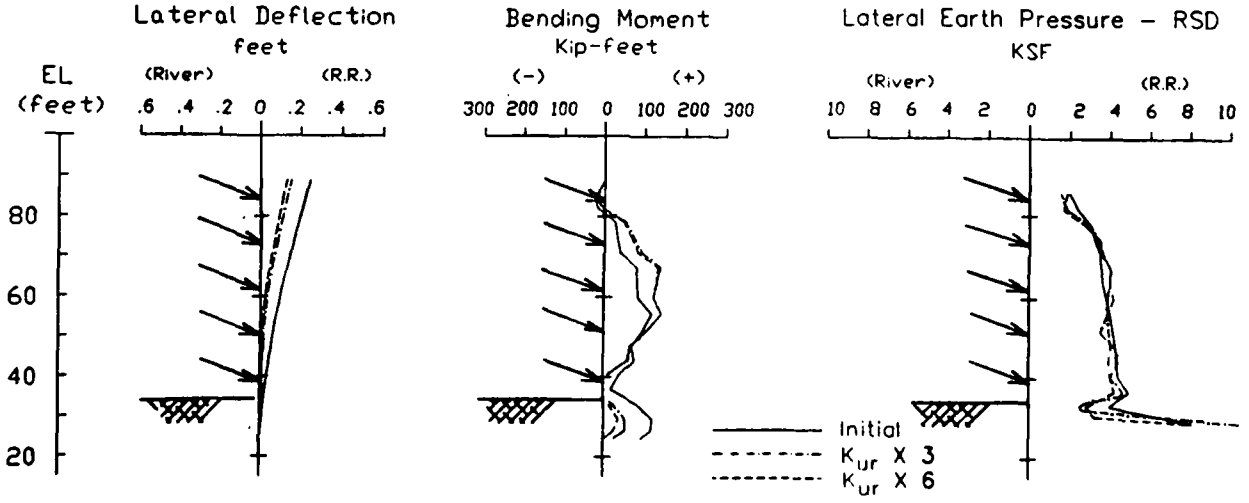

Figure 59. Deflection, moment, and earth pressure for Panel 11, load step 15; prestress anchor at el 38.67 ft

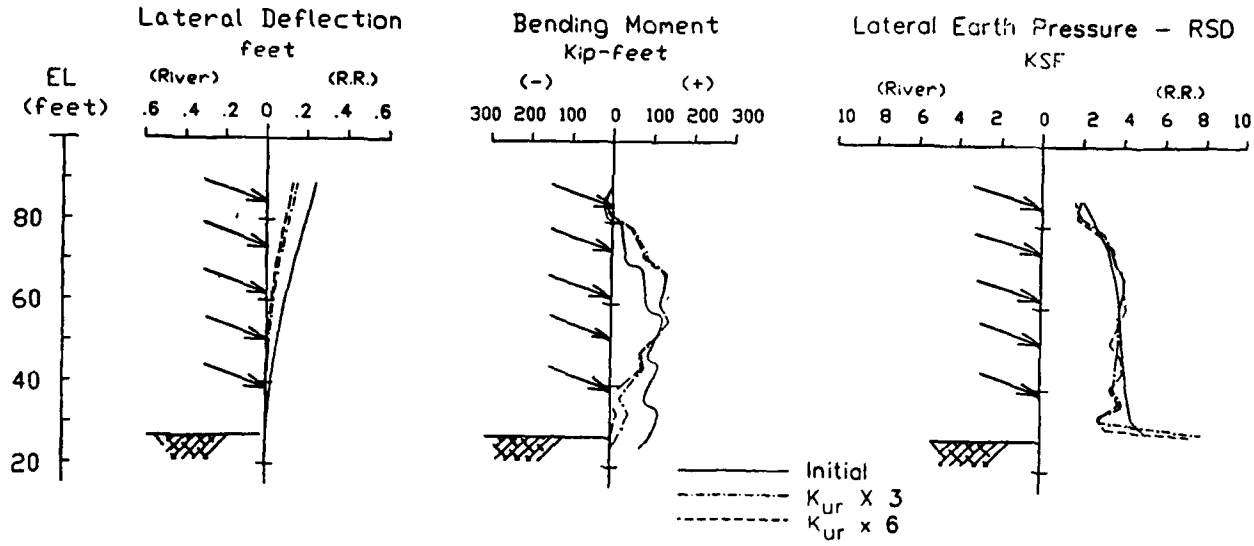

Figure 60. Deflection, moment, and earth pressure for Panel 11, load step 16; lock off anchor 5, excavate to el 27.67 ft

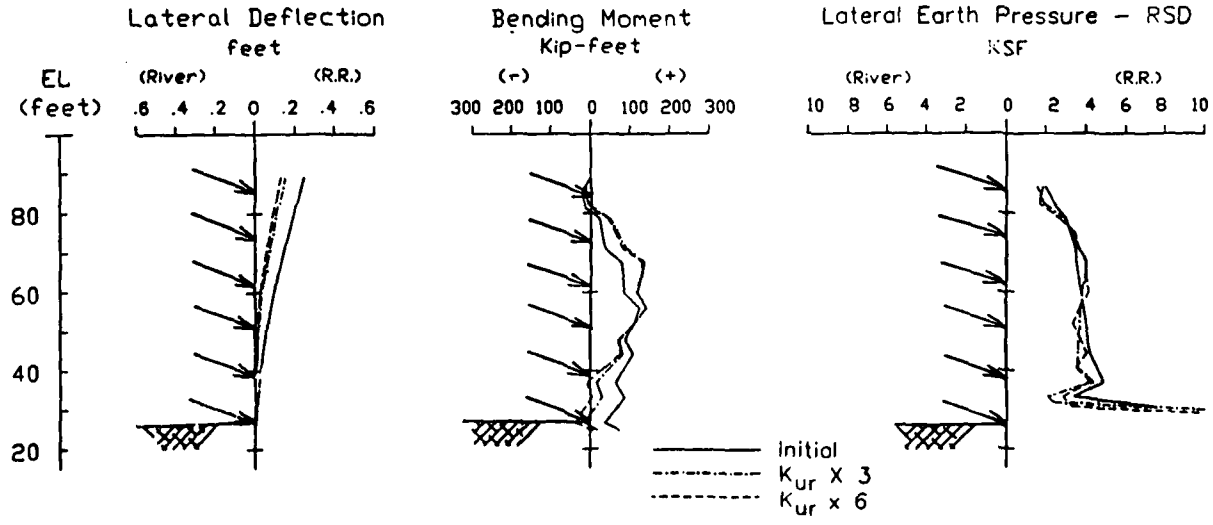

Figure 61. Deflection, moment, and earth pressure for Panel 11, load step 17; prestress anchor at el 27.67 ft

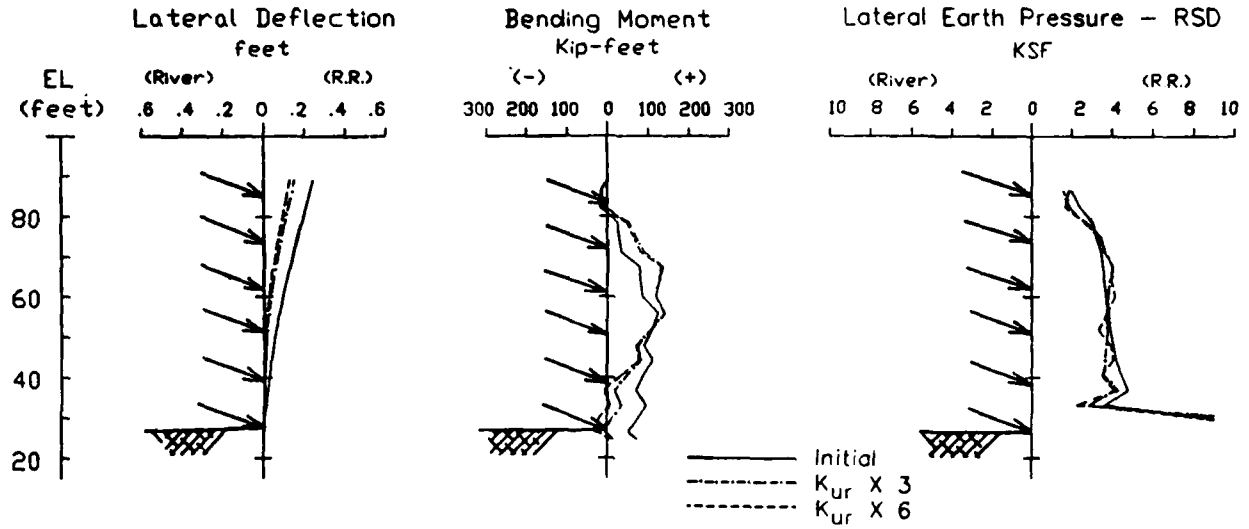

Figure 62. Deflection, moment, and earth pressure for Panel 11, load step 18; lock off anchor 6

reflected very little in the pressure it distributes on the wall. This is because the forces applied to the earth are the same in all three cases. As noted earlier in the report, these earth pressures are mainly a response to the magnitudes of the anchor loads.

138. Anchor prestressing is displayed by increases in the pressure diagram behind the wall at the anchor locations. With excavations and anchor lockoffs, the pressure diagram, as a whole, decreases but maintains the form it had from the previous load step. These pressure increases, due to anchor prestressing, are not as defined as the bulges seen in the Panel 6 results but are more uniformly distributed over the wall behind the anchor locations. This confirms the suggestion that the pressure bulges discussed in Part II could be influenced more by the Weigle material characteristics than by the anchor loads alone.

139. The bottom of the pressure diagram shows sharp changes in pressure values. These extreme changes reflect the interaction of the RSD with the diabase at the interface of these materials, el 27.67 ft. This behavior results from stress transfer and different magnitudes of movement between the strong, stiff, cohesive material (diabase) and the softer cohesionless

material (RSD). At Panel 6, the Tw material acted as an interface or median between the RSD and Ti, and this sharp contrast in earth pressures does not appear.

Anchor loads

140. Table 10 lists the FE resulting anchor loads during the construction procedure from the $K_{ur} \times 3$ analyses of Panel 11. The changes in an anchor's load are directly related to either excavation and anchor lockoff or prestressing of another anchor. At the end of construction, the loads in the lower four anchors show little change from their initial lockoff value. The top and second anchors have loads less than their lockoff loads by 9 and 4 percent, respectively.

Table 10

Panel 11 Anchor Loads During Construction Steps (K_{ur} X 3 Analysis)

Anchor Elevation	Lockoff Load (kips)	Step 8	Step 9	Step 10	Step 11	Step 12	Step 13	Step 14	Step 15	Step 16	Step 17	Step 18
84'	386	404	360	370	352	357	350	353	350	351	351	351
73'	386	---	---	399	374	382	370	375	370	372	371	371
62'	388	---	---	---	---	400	381	388	380	383	382	382
49.67'	388	---	---	---	---	---	---	399	385	390	388	389
38.67'	402	---	---	---	---	---	---	---	---	407	405	406
27.67'	378	---	---	---	---	---	---	---	---	---	---	379

Notes:
Refer to Table 9 for Panel 11 load step description.
Anchor loads in kips (tension).

Ground surface movement

141. Figure 63 shows the maximum deflection of the ground surface from the wall to the railroad tracks, for the three analyses of Panel 11. The maximum movement at the tracks decreased by over 50 percent as the K_{ur} value of the RSD is increased. Specifically, the ground movement is 0.68, 0.31, and 0.12 in. at the tracks for $K_{ur} \times 1$, $K_{ur} \times 3$, and $K_{ur} \times 6$, respectively. The actual movement for any of these soil cases is more likely to be less than these reported because the weight of the tracks themselves, the presence of

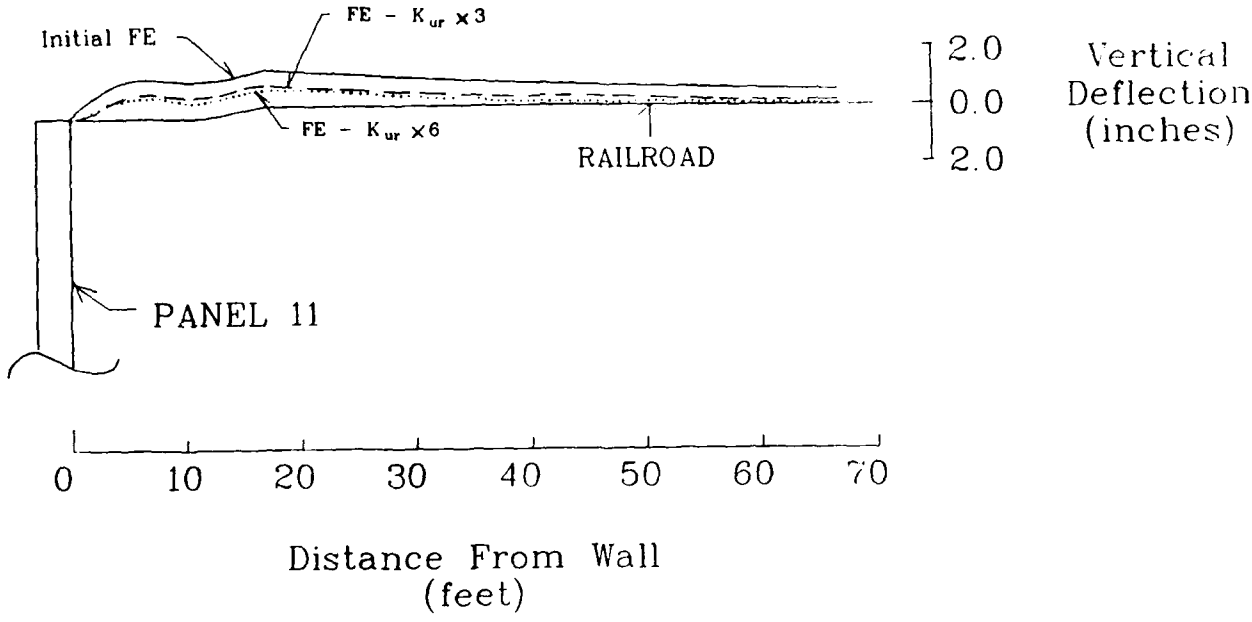

Figure 63. Maximum ground surface movement behind Panel 11 for three FE analyses

trains on the tracks, and other surface loads were not taken into account in these analyses.

Summary of Results

142. Table 11 lists the overall maximum, and the final maximum values of wall deflection, bending moment, and ground deflection for the three analyses performed on Panel 11.

Table 11
Summary of Results - Panel 11

Analysis	Wall Deflection (feet) overall maximum	final maximum	Bending Moment (kip-ft) overall maximum	final maximum	Ground Surface Deflection (inch) overall maximum	final maximum
Initial	0.246 (13)*	0.244	311 (10)	124	0.68 (15)	0.66
K_{ur} x 3	0.153 (13,15)	0.152	236 (10)	142	0.31 (15)	0.30
K_{ur} x 6	0.130 (13)	0.129	213 (10)	140	0.12 (15)	0.12

* Load step in which maximum occurred. See Table 9.

Analyses Comparison of Panels 6 and 11

143. The Panel 11 analyses mirrored those of Panel 6 in many respects. Similar trends in deflected wall form, bending moment, and earth pressures can be observed between the two panels in corresponding analyses. It is because of these similarities that the instrumentation results from Panel 6 can be expected to reflect the Panel 11 response as well, on a larger scale. The greater height and higher anchor forces of Panel 11 caused the maximum calculated wall deflection, moment, and the ground surface deflection to be greater than those of Panel 6. The decreases in these maximums with each increase of the RSD material stiffness is about the same, percentage-wise, for both panels.

144. As noted in Part I, the soil properties and parameters used in the initial analyses were chosen conservatively. Therefore, the resulting calculated deflections and moments were anticipated to be greater than the actual response. This is confirmed by the instrumentation results compared with the Panel 6 initial analytical results. Also, the effective elastic modulus, that lowered the FE computed bending moment by about 12 percent as shown in Part V, was not used in the Panel 11 analyses. Therefore, the moments shown for the initial Panel 11 model are conservative.

145. Ground surface movement would, most likely, be less than that predicted by the analyses. Based on instrumentation results and soil test data, the RSD is a very stiff material, exhibiting little deformation with loading. Also, the weights of trains, the railroad tracks, and any other surface loads were not included in any of the analyses. These loads would largely eliminate potential surface movement due to wall deflection into the soil. Therefore, the possibility of misalignment at the railroad tracks is believed to be negligible.

REFERENCES

BCA Geophysics, Inc. 1988 (Mar). "Bonneville Navigation Lock Excavation Weekly Instrumentation Report, No. 32," Tiburon, CA.

Broms, Bengt B. 1988 (Jun). "Design and Construction of Anchored and Strutted Sheet Pile Walls in Soft Clay," Proceedings: Second International Conference on Case Histories in Geotechnical Engineering, St. Louis, MO, Vol 2, pp 1515-1530.

Clough, G. Wayne. 1976. "Deep Excavations and Retaining Structures," Analysis and Design of Building Foundations, H. Y. Fang, ed., Envo Publishing Co., Inc., Lehigh Valley, PA, pp 417-465.

Clough, G. Wayne, Weber, P. R., and Lamont, J. 1972 (June). "Design and Observation of a Tied-Back Wall," Proceedings, Specialty Conference on Performance of Earth and Earth-Supported Structures, Purdue University, IN, Vol I, Part 2, pp 1367-1389.

Department of the Navy. 1982 (May). Naval Facilities Engineering Command, Foundations and Earth Structures, Design Manual 7.2, Alexandria, VA.

Doherty, W. P., Wilson, E. L., and Taylor, R. L. 1969. "Stress Analysis of Axisymmetric Solids Utilizing Higher-Order Quadrilateral Finite Elements," Report No. SESM 69-3, Structural Engineering Laboratory, University of California, Berkeley, CA.

Duncan, J. M., and Chang, C. Y. 1970 (Sep). "Nonlinear Analysis of Stress and Strain in Soils," Journal, Geotechnical Division, American Society of Civil Engineering, Vol 96, No. SM5, pp 1629-1653.

Duncan, J. M., Byrne, P., Wong, K. S., and Mabry, P. 1980. "Strength, Stress-Strain and Bulk Modulus Parameters for Finite Element Analyses of Stresses and Movements in Soil Masses," Report No. UCB/GT/80-01, University of California, Berkeley, CA.

Ferguson, Phil M. 1979. Reinforced Concrete Fundamentals, 4th ed., Wiley, New York.

Goodman, R. E., Taylor. R. L., and Brekke, T. L. 1968. "A Model for the Mechanics of Jointed Rock," Journal, Soil Mechanics and Foundations Division, Proceedings of the American Society of Civil Engineering, SM3, pp 637-659.

Headquarters, Department of the Army. 1987 (Nov). "Bonneville Navigation Lock, Geology, Excavation, and Foundation," Design Memorandum No. 3, Supplement 1, Washington, DC.

Johnson, Lawrence D. 1988. "Design and Construction of Mat Foundations," Miscellaneous Paper GL-88-6, US Army Engineer Waterways Experiment Station, Vicksburg, MS.

Leonhardt, Fritz. 1988. "Cracks and Crack Control in Concrete Structures," PCI Journal, Prestressed Concrete Institute, Chicago, IL, Vol 33, No. 4, pp 124-143.

Peters, J. F., Leavell, D. A., Holmes, T. L., and Edris, E. V. "Analysis of Sheetpile Floodwalls in Soft-Clay Foundations" (in preparation), US Army Engineer Waterways Experiment Station, Vicksburg, MS.

Potts, E. M., and Fourie, A. B. 1984. "The Behavior of a Propped Retaining Wall: Results of a Numerical Experiment," Geotechnique, The Institute of Civil Engineers, London, Vol 34, No. 3, pp 383-404.

Schultz, Michael S. 1981 (Jun). "An Empirical Investigation into the Behavior of Diaphragm Walls," M.S. thesis, Massachusetts Institute of Technology, Cambridge, MA.

Smith, Trevor. 1985 (Sep). "Pressuremeter Testing and Design Considerations for Upstream Temporary Diaphragm Wall, Buttress Diaphragm Wall, and Downstream Approach Walls, Bonneville Navigation Lock," Letter report prepared by the Department of Civil Engineering, Portland State University, Portland, OR, for US Army Engineer District, Portland, OR.

Tamano, T. 1985 (Mar). "A Case Study of a Sheet Pile Wall Multi-Tied with Anchors," Transactions of the Japan Society of Civil Engineers, Tokyo, 160 Japan, Vol 15, pp 357-358.

US Army Engineer District, Portland. 1986 (14 Nov). "Phase II, Tieback Test Program, Bonneville Navigation Lock, Columbia River, Oregon/Washington," Portland, OR; prepared by L. R. Squier Associates, Lake Oswego, OR.

BIBLIOGRAPHY

Bowles, Joseph E. 1982. Foundation Analysis and Design, 3rd ed., McGraw-Hill, New York.

Clough, G. Wayne. 1984. User's Manual for Program SOILSTRUCT, Virginia Polytechnic Institute, Blacksburg, VA.

Clough, G. Wayne, and Tsui, Y. 1974. "Performance of Tied-Back Walls in Clay," Journal, Geotechnical Division, American Society of Civil Engineering, Vol 100, No. GT12, pp 1259-1274.

APPENDIX A: USE OF BAR ELEMENTS IN SOILSTRUCT TO DETERMINE BENDING MOMENT

Introduction

1. The finite element (FE) procedure used in the program SOILSTRUCT is a proven method for determining stresses and displacements in the materials; however, it provides no direct calculation of the bending moment in structural elements. In this study, it was important to assess the bending moment in the temporary wall section to more fully analyze the wall behavior and to compare analytical results with instrument results.

2. A method for determining moment in structural elements was developed by Peters, et al. (1989)* and used in the SOILSTRUCT analyses of this study. This method is described in the following paragraphs.

Bending Moment in Structural Elements

3. One-dimensional bar elements, described in Part I, were added to each exterior side of the wall elements in the FE grid. This is shown in Figure A1.

4. As the wall elements move due to the various loadings, the bar elements move with them. Since the bar elements are one-dimensional members, movement is either axial elongation or axial shortening. This movement is recorded for each load case in the analysis.

5. The bar elements on the wall can be considered as the extreme fibers of a beam-column. The strain, ϵ ,** of these extreme fibers is found by dividing the axial movement of the bar element by its original length.

6. The stress, σ , in the extreme wall fibers is then obtained by multiplying the strain with the wall's elastic modulus, E . Figure A2 shows this behavior.

7. Using the flexure formula, $\sigma = \pm (P/A) \pm (M_c/I)$, the bending

---

* References cited in this appendix are listed following the main text of this report.

** For convenience, symbols and abbreviations used in this appendix are listed in the Notation (Appendix E).

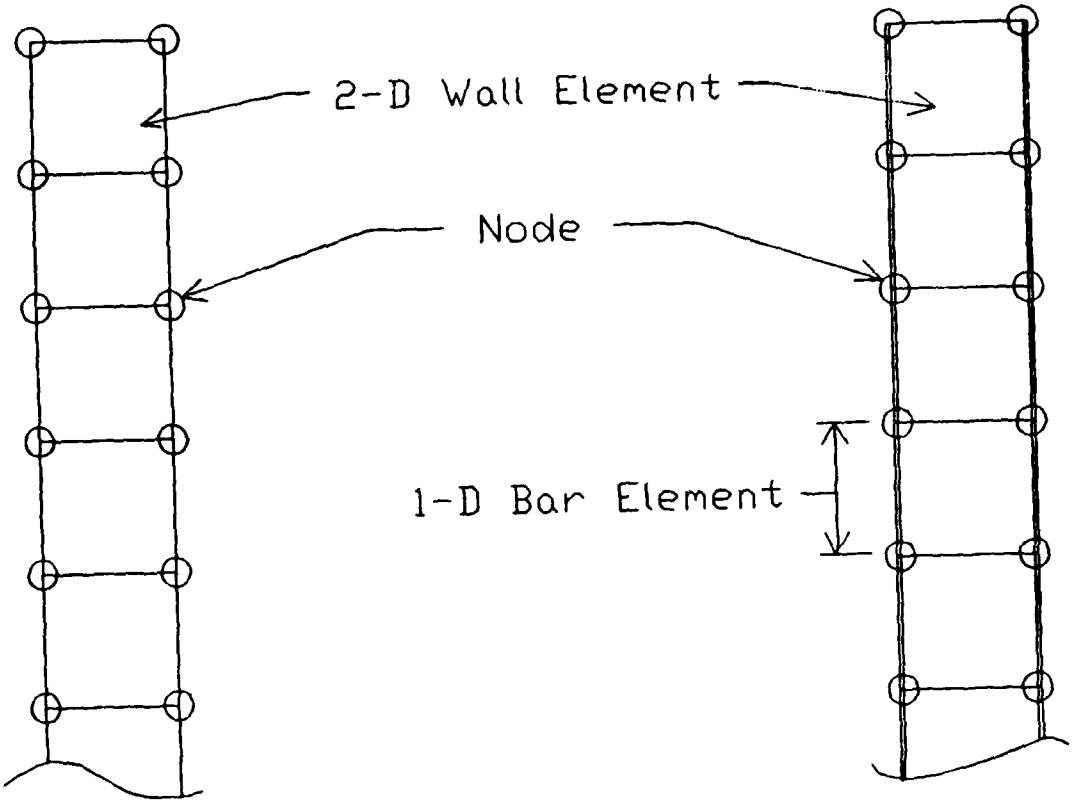

a. Wall initially built

b. Bar element added to outside of each wall element

Figure A1. FE grid components of wall

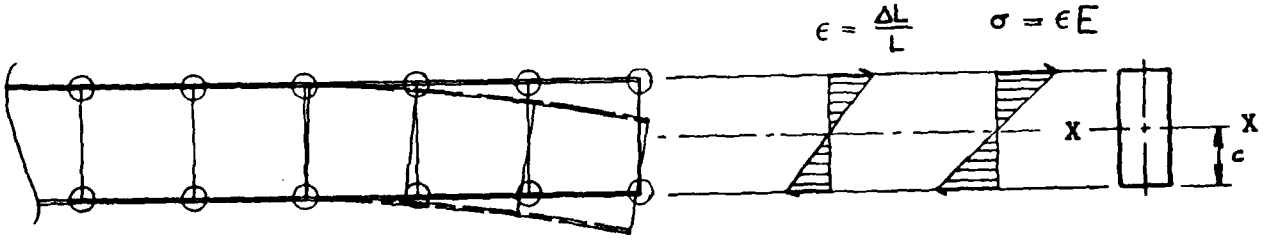

Figure A2. Wall deflection, strain diagram, and stress diagram (L = length; ΔL = change in length; c = distance to centroid of section)

moment is calculated as shown in the following equations and Figure A3. The sign convention is: compression is negative, tension is positive.

$$\frac{P}{A} = \frac{\sigma_t + \sigma_b}{2} \quad \text{and} \quad M = \frac{I}{c}\left(\sigma_b - \frac{P}{A}\right)$$

where

P = axial load

A = axial cross-sectional area

σ_t = stress in top beam fibers

σ_b = stress in bottom beam fibers

M = internal bending moment

I = section moment of inertia about the X-X axis

c = distance to centroid of section

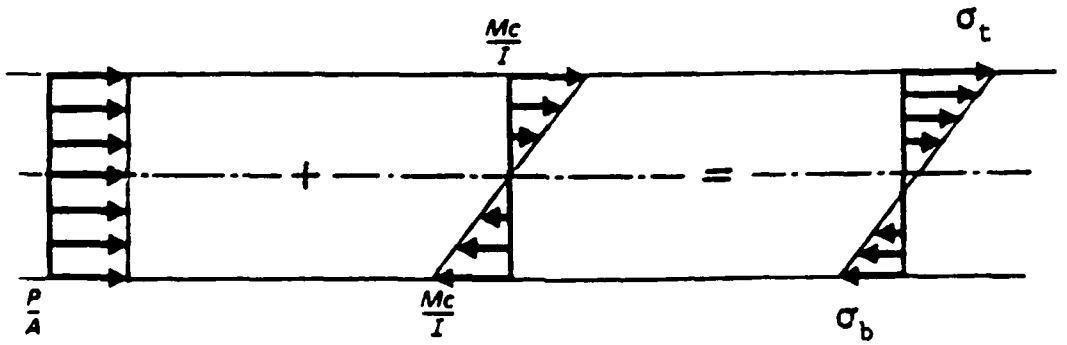

Figure A3. Components of stress in a beam-column

APPENDIX B: FINITE ELEMENT GRID MODEL STUDY FOR TEMPORARY WALL AND ANCHORS

1. To analyze the temporary tieback wall and soil behavior, an appropriate finite element (FE)* grid had to be developed. The system being modeled is made up of two basic components: soil strata and structural members. The structural members are the wall and the anchors. Various designs were studied in the development of these models. These are described in the following paragraphs.

Wall Model Study

2. Behavior of the wall and surrounding soil was of most importance in this project. The FE grid in this region had to be fine enough to accurately model behavior but not so fine that it was unworkable. Therefore, it was necessary to determine how dense the FE grid should be in the wall vicinity. This was done by comparing analysis results from five simple grids of different densities with results from elastic beam theory.

3. The objective of this study was to determine the size and aspect ratio (length/width) of wall elements that, used in SOILSTRUCT, produce results in closest agreement with elastic beam calculations.

Method

4. A fixed-end cantilever beam, with a point load at the free end, was used as the model. This model beam is 50 ft long and 3 ft thick, as is Panel 6. This is shown in Figure B1. From beam theory, the fixed-end moment is $M = PL$, and the deflection, Δ, is

$$\Delta = \frac{PL^3}{3EI}$$

5. The five wall grids analyzed are shown in Figure B2. Grid 5 is 1 ft longer than the other four, to produce an even 3- by 3-ft model. A separate beam theory calculation is made for this model. Bar elements were placed on the outsides of the wall elements to be used as strain gages. The strain due to wall bending was used to calculate wall moment as described in Appendix A.

---

* For convenience, symbols and abbreviations used in this appendix are listed in the Notation (Appendix E).

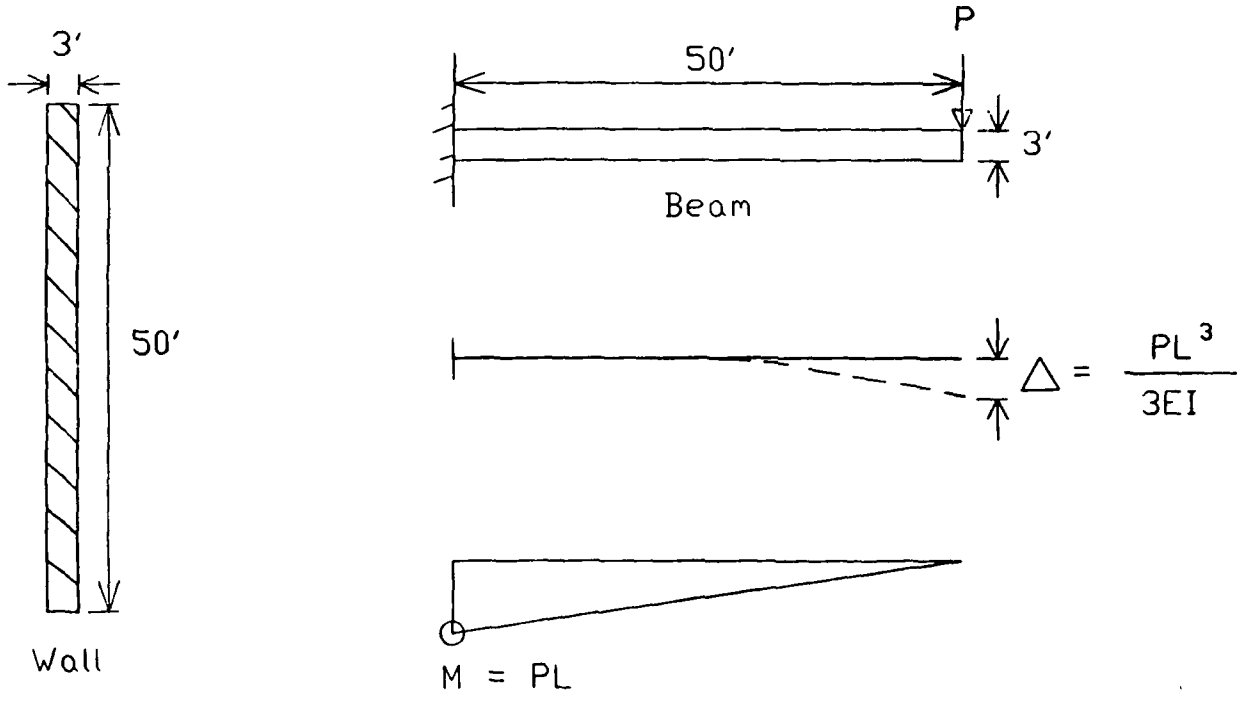

Figure B1. Beam modeled by FE grid and elastic theory

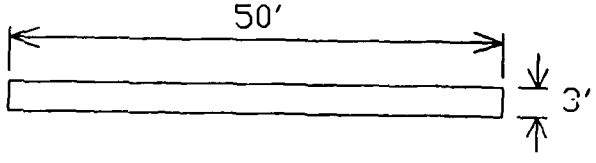

MODEL	SIZE	ASPECT RATIO
1	3' X 5'	1.67
2	1.5' X 5'	3.33
3	0.75' X 5'	6.67
4	0.75' X 1.25'	1.67
5	3' X 3'	1.0

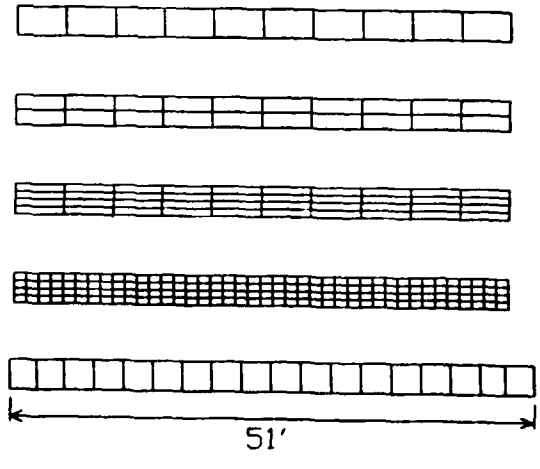

Figure B2. Five FE grid models of beam

Results

6. Results from beam theory and the five FE analyses are presented in Table B1. Comparison of results shows the best FE model of the wall is the one-element-thick, 3- by 5-ft model. Not only does this model's results agree with the elastic theory results better than the others in both moment and end deflection, it also is much easier to use in the complete grid because of its proportions and size.

Table B1
Summary of Wall Study Results

Model #	Description	Element Aspect ratio (length/width)	Deflection at end of Beam (Ft.)	Percent Error, Deflection	Bending Moment at 2.5' from fixed end (Ft.- Lbs.)	Percent Error, Moment
	Static Beam Equilibrium	---	0.002058	---	2375	---
1	1-element width (3' X 5' elements)	1.67	0.001929	6.27	2227	6.23
2	2-element width (1.5' X 5')	3.33	0.001915	6.95	2154	9.30
3	4-element width (0.75' X 5')	6.67	0.001913	7.05	2146	9.64
4	4-element width (0.75' X 1.25')	1.67	0.001929	6.27	2218	6.61
5	1-element width, 51-foot beam (3' X 3')	1.0	Beam: 0.002184 FE: 0.002050	6.14	Beam: 2475 FE: 2320	6.26

Conclusions

7. This study showed the SOILSTRUCT elements and methods to be more sensitive to the aspect ratio of the QM5 element than to the fineness of the grid. Often in FE analyses, it is expected that the finer grid gives the best results. Deflections match for models 1 and 4 (Table B1), but the fixed-end moment of model 4 is not as close to the elastic beam moment as that of model 1. The grid of model 4 is much finer than that of model 1, but the element aspect ratios are the same. Model 5, with aspect ratio of 1.0, more

nearly matched beam theory deflection than did any of the others, but surprisingly did no better than model 1 in modeling bending.

Anchor Model Study

8. Much time and effort were spent developing an FE grid model for the anchors of the tieback wall. A variety of combinations of two-dimensional elements, bar elements, and interface elements were tested in a small grid of soil elements. Some of these anchor schemes are shown in Figure B3. The system initially chosen for use in the full grid is shown in Figure B4.

9. After some initial analyses of the full model, a new anchor model system was tried. This consisted simply of a bar element for each anchor connected to the appropriate wall location at one end and connected to a fixed boundary node at the other. This configuration is shown in Figure B5.

10. Results from analyses using this new anchor model showed only a slight and essentially negligible increase in wall deflection due to the one fixed end of the bar and no major changes in soil stresses in the vicinity of the wall. Since this system was much simpler to use and provided reliable, slightly conservative results, it was used in all FE analyses.

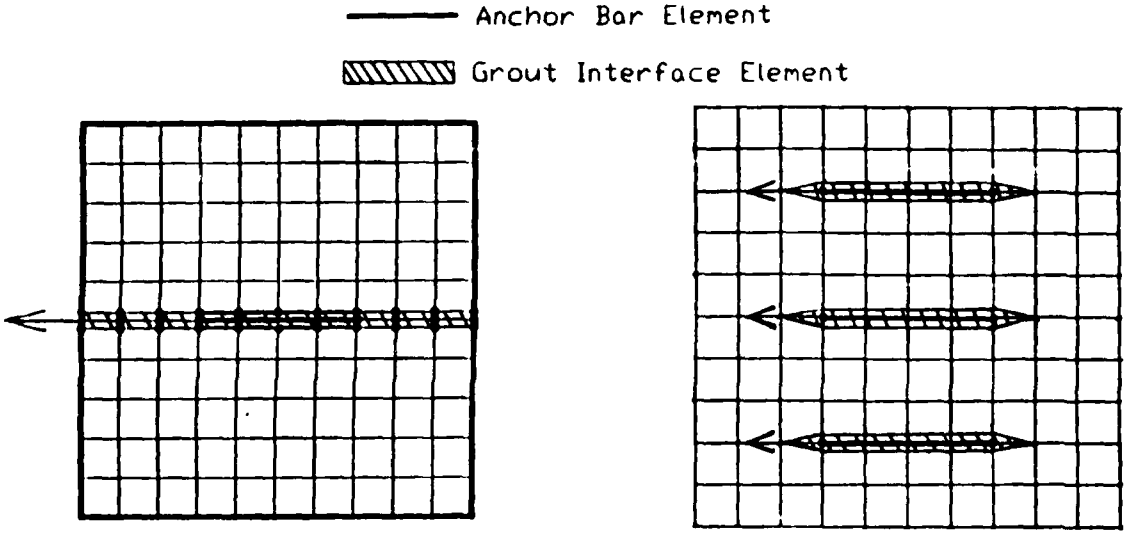

Figure B3. FE anchor models tested for use in the grid of the Panel 6 section

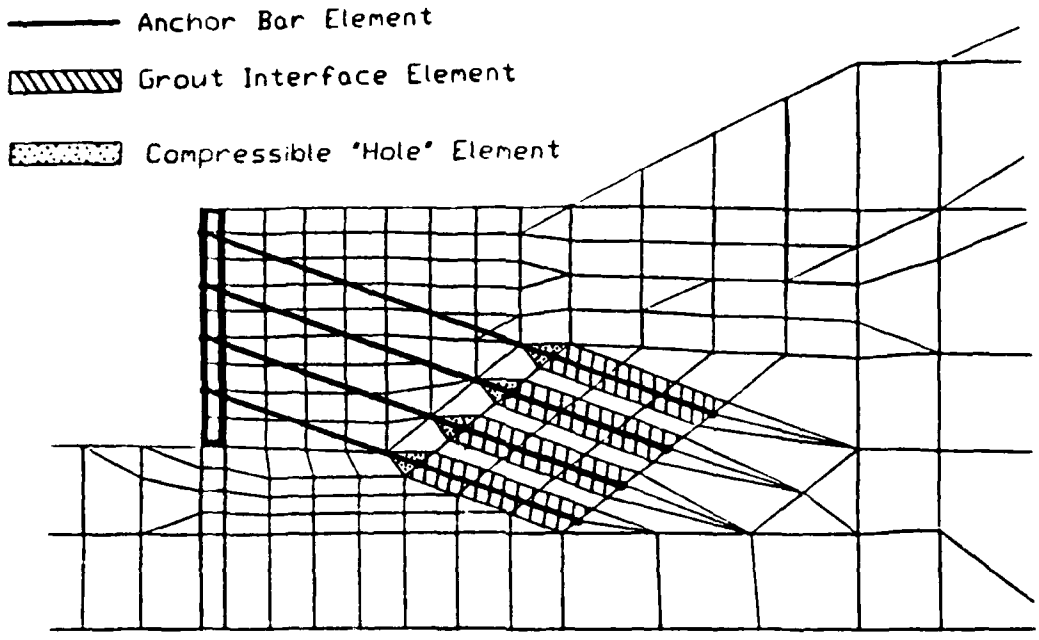

Figure B4. Anchor model system initially chosen for use in the FE grid of Panel 6

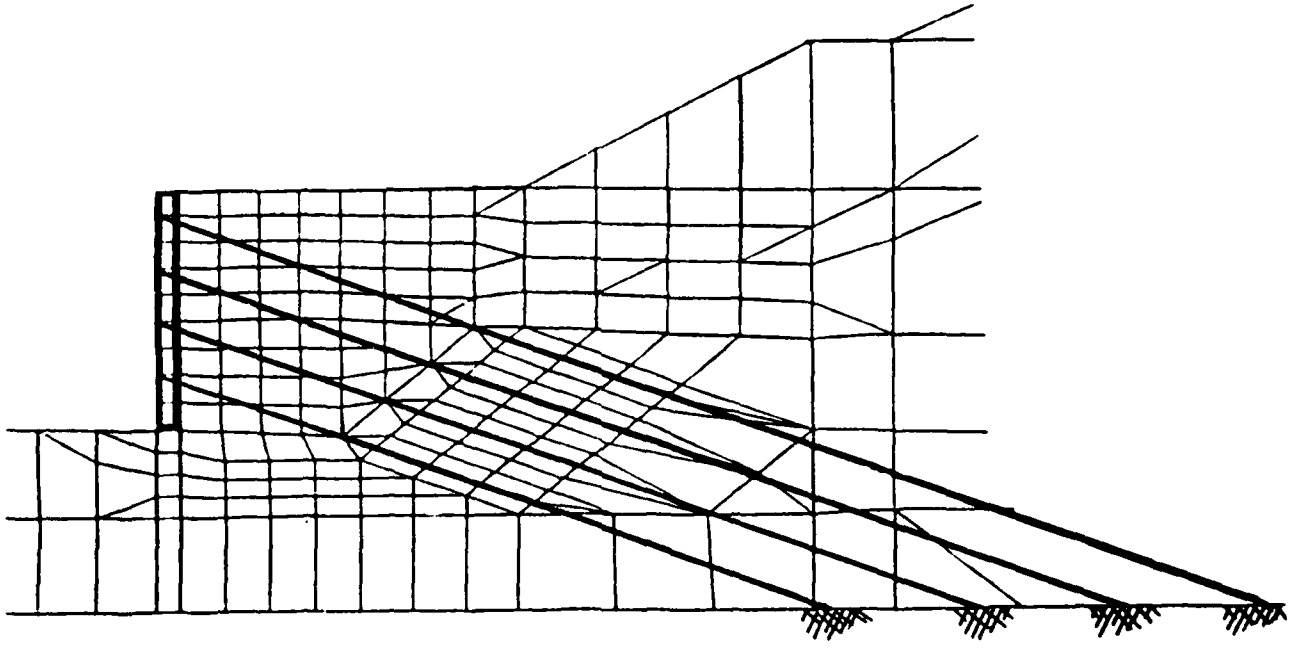

Figure B5. Simplified anchor model used in all FE analyses

APPENDIX C: INSTRUMENTATION DATA FOR PANEL 6

1. The monitoring of behavior at the navigation lock construction site was performed by an extensive program of instrumentation (BCA Geophysics, Inc. 1988).* Some of this includes piezometers, slope inclinometers, extensometers, load cells, and strain gages. Panel 6 was instrumented with a slope inclinometer (SI),** installed in a 6-in. steel pipe in the panel, and with 10 pairs of strain gages, one of each pair on the inside (railroad) and one on the outside (river) of the reinforcing steel cage in the panel.

2. Figures C1 through C9 (BCA Geophysics, Inc. 1988) show the SI data from Jan 6, 1988, the start of excavation in front of the wall, to Mar 14, 1988, the end of construction. Figure C10 (BCA Geophysics, Inc. 1988) is the SI data for Oct 4, 1988, about 7 months after the end of construction. Note that the SI data of Figures C1 through C10 are shown in the opposite direction (looking downstream) from the deflection plots shown in the report (looking upstream). The vertical axis shows depth below the top of the wall in feet. Those SI plots used for comparison with finite element (FE) results are indicated in each figure caption.

3. Figures C11 and C12 show the strains for the inner and outer strain gages, from Dec 29, 1987, through Oct 10, 1988. A computer program was used to calculate bending moments from the strains. The program was written to follow the procedure outlined in Appendix A. The strains are input to the program with the opposite sign of their reading, due to the sign convention used in the FE analyses: compression is negative, tension is positive.

---

* References cited in this appendix are listed following the main text of this report.

** For convenience, symbols and abbreviations used in this appendix are listed in the Notation (Appendix E).

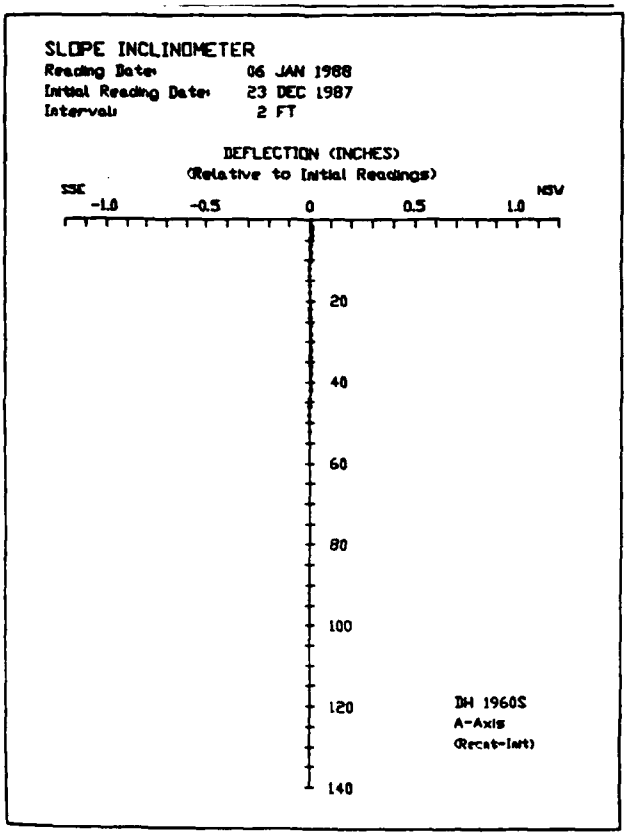

Figure C1. Panel 6 deflection at start of excavation

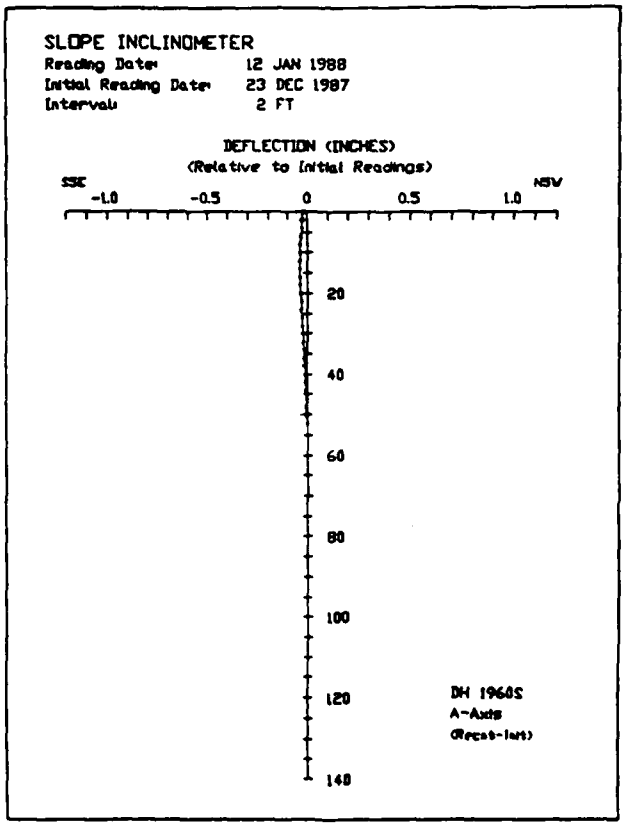

Figure C2. Panel 6 deflection after first excavation (about 10 ft), used with FE load step 7, first excavation

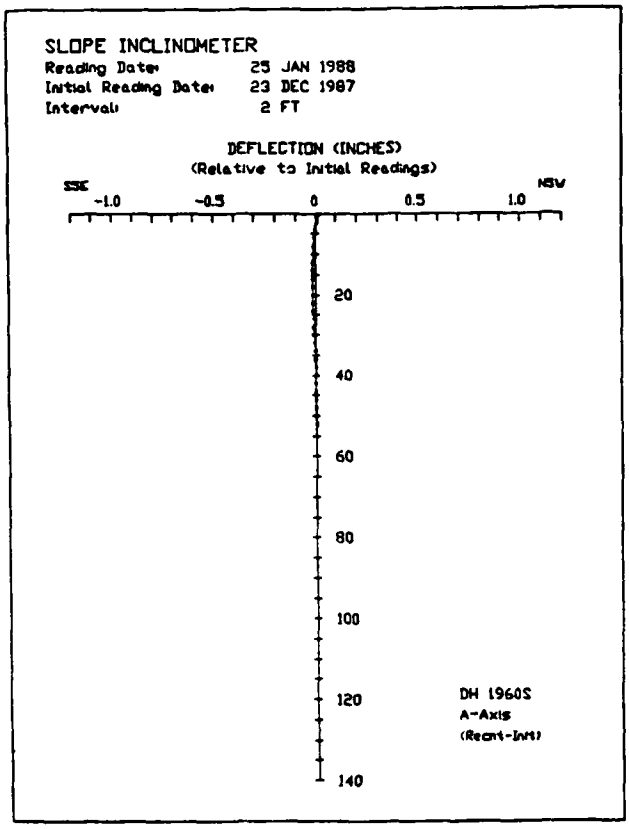

Figure C3. Panel 6 deflection after first excavation, with drilling for anchor holes begun (at el 84 ft)

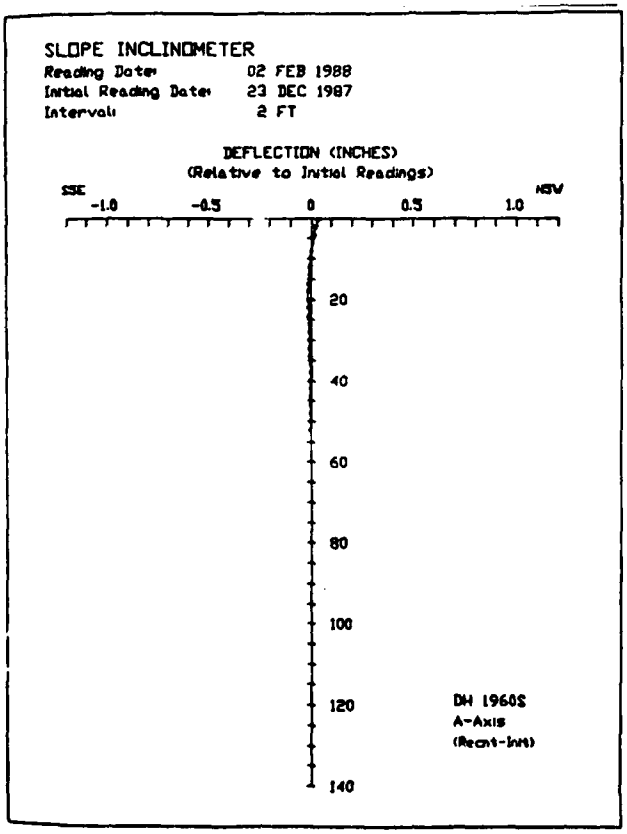

Figure C4. Panel 6 deflection at beginning of el 84-ft anchor installation

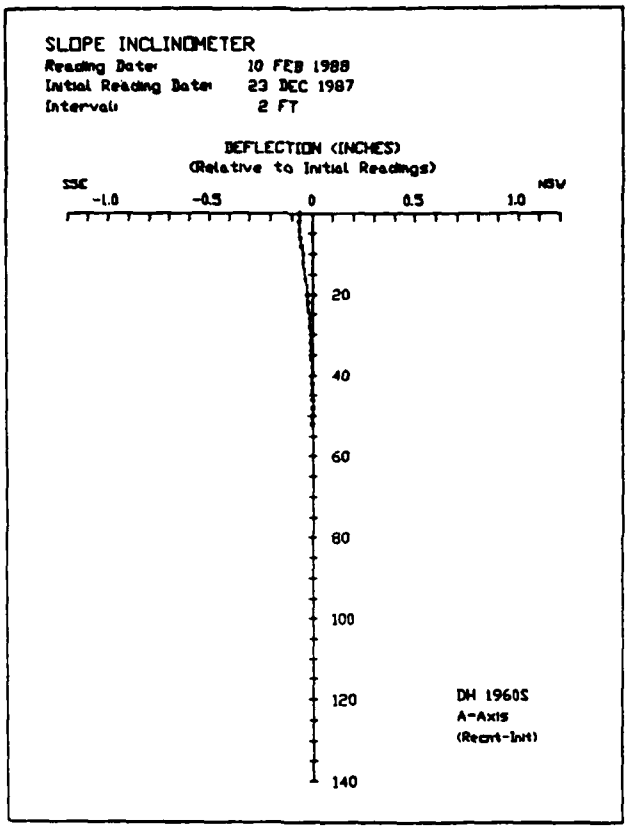

Figure C5. Panel 6 deflection after el 84-ft anchor is prestressed and locked off, used with FE load step 9, lock off first anchor, second excavation

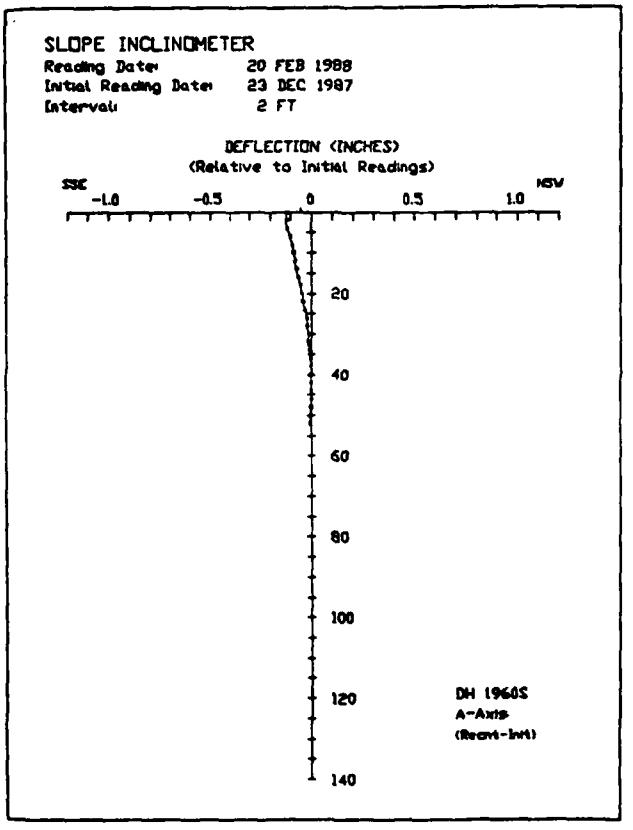

Figure C6. Panel 6 deflection after one el 73-ft anchor is installed

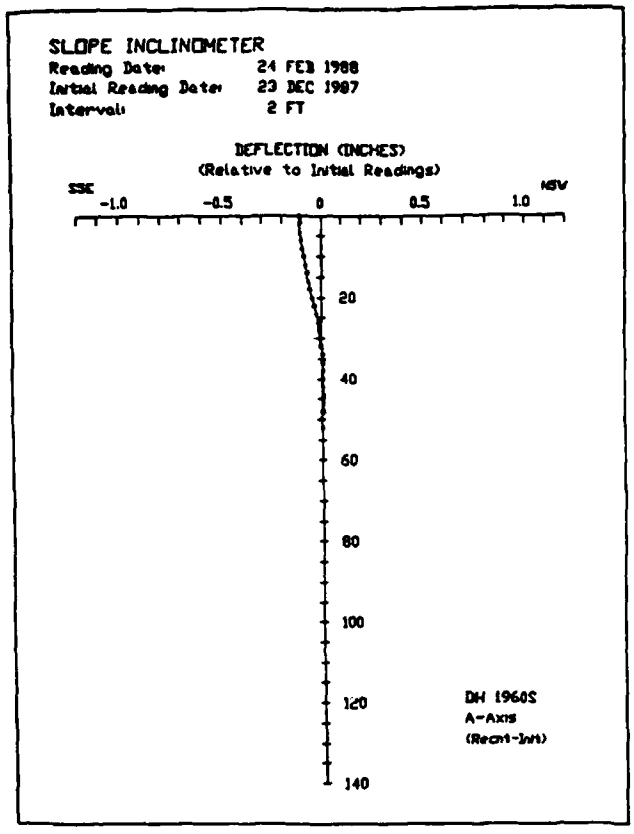

Figure C7. Panel 6 deflection after both el 73-ft anchors are prestressed and locked off, used with FE load step 11, lock off second anchor, third excavation

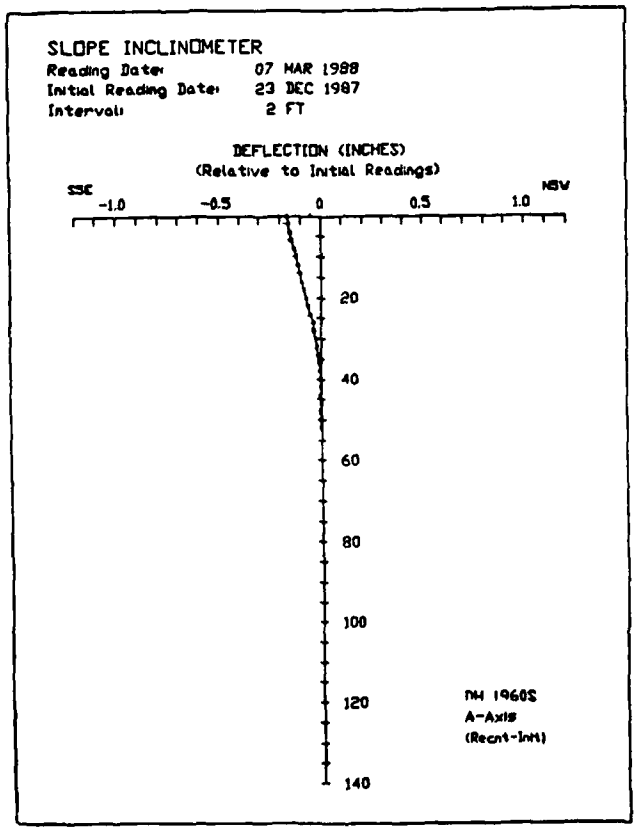

Figure C8. Panel 6 deflection after both el 62-ft anchors are prestressed and locked off, used with FE load step 13, lock off third anchor, fourth excavation

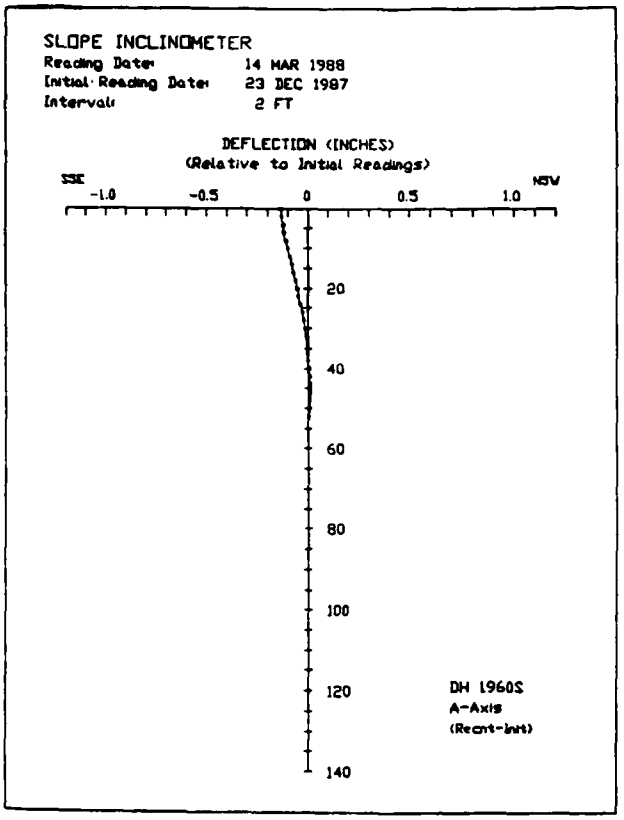

Figure C9. Panel 6 deflection after both el 51-ft anchors are prestressed and locked off, used with FE load step 15, end of construction

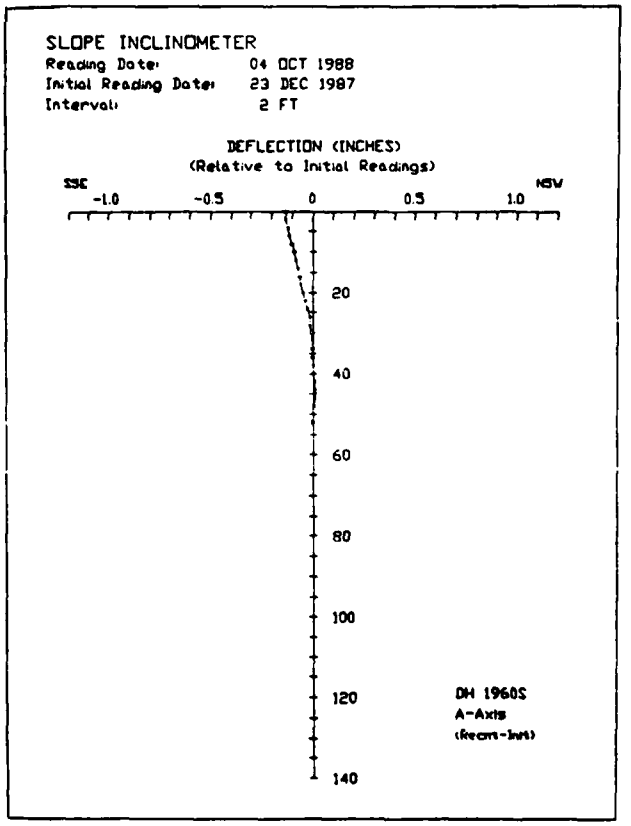

Figure C10. Panel 6 deflection at 7 months following end of construction

Date	Gauge No. 1 Depth: 5 Ft		Gauge No. 2 Depth: 10 Ft		Gauge No. 3 Depth: 15 Ft		Gauge No. 4 Depth: 20 Ft		Gauge No. 5 Depth: 24 Ft		Gauge No. 6 Depth: 28 Ft		Gauge No. 7 Depth: 32 Ft		Gauge No. 8 Depth: 36 Ft		Gauge No. 9 Depth: 40 Ft		Gauge No. 10 Depth: 44 Ft	
	Field Read	Cumul. ue	Field Read	Cumul. ue	Field Read	Cumul. ue	Field Read	Cumul. ue	Field Read	Cumul. ue	Field Read	Cumul. ue	Field Read	Cumul. ue	Field Read	Cumul. ue	Field Read	Cumul. ue	Field Read	Cumul. ue
871229*	573		-84		19		-189		-187		-211		-385		-36		63		138	
880107	579	6	-81	3	24	5	-184	5	-184	3	-207	4	-382	3	-32	4	65	2	138	0
880111	576	3	-81	3	23	4	-183	6	-183	4	-205	6	-380	5	-29	7	66	3	139	1
880119	593	20	-75	9	31	12	-182	7	-183	4	-204	7	-378	7	-26	10	66	3	139	1
880125	600	27	-69	15	36	17	-180	9	-182	5	-202	9	-377	8	-23	13	67	4	141	3
880204	601	28	-65	19	41	22	-177	12	-180	7	-199	12	-375	10	-21	15	68	5	141	3
880209	608	35	-67	17	33	14	-189	0	-189	-2	-205	6	-380	5	-24	12	65	2	139	1
880217	611	38	-82	2	6	-13	-218	-29	-213	-26	-219	-8	-389	-4	-25	11	66	3	140	2
880225	613	40	-76	8	27	8	-223	-34	-231	-44	-241	-30	-414	-29	-45	-9	55	-8	135	-3
880304	617	44	-73	11	32	13	-216	-27	-221	-34	-226	-15	-416	-31	-49	-13	52	-11	134	-4
880311	616	43	-74	10	31	12	-216	-27	-221	-34	-228	-17	-425	-40	-65	-29	43	-20	132	-6
880314	621	48	-69	15	40	21	-209	-20	-214	-27	-220	-9	-416	-31	-56	-20	48	-15	134	-4
880324	627	54	-64	20	48	29	-198	-9	-195	-8	-216	-5	-410	-25	-50	-14	61	-2	141	3
880401	631	58	-59	25	58	39	-191	-2	-190	-3	-209	2	-405	-20	-46	-10	65	2	143	5
880407	633	60	-59	25	57	38	-191	-2	-189	-2	-208	3	-404	-19	-45	-9	68	5	145	7
880415	641	68	-52	32	68	49	-180	9	-190	-3	-201	10	-398	-13	-38	-2	74	11	147	9
880419	643	70	-51	33	70	51	-179	10	-189	-2	-200	11	-398	-13	-37	-1	74	11	147	9
880427	648	75	-46	38	79	60	-173	16	-172	15	-193	18	-393	-8	-32	4	78	15	149	11
880503	641	68	-55	29	63	44	-185	4	-182	5	-202	9	-399	-14	-38	-2	75	12	148	10
880510	651	78	-44	40	80	61	-171	18	-169	18	-191	20	-391	-6	-29	7	81	18	151	13
880516	653	80	-43	41	80	61	-169	20	-179	8	-190	21	-391	-6	-28	8	83	20	151	13
880523	656	83	-42	42	78	59	-170	19	-178	9	-191	20	-391	-6	-29	7	83	20	151	13
880531	653	80	-48	36	71	52	-177	12	-183	4	-194	17	-393	-8	-31	5	82	19	152	14
880608	657	84	-41	43	82	63	-168	21	-176	11	-186	25	-388	-3	-25	11	87	24	155	17
880614	665	92	-34	50	93	74	-160	29	-168	19	-180	31	-383	2	-21	15	90	27	155	17
880622	672	99	-31	53	94	75	-156	33	-163	24	-178	33	-381	4	-19	17	93	30	156	18
880627	668	95	-37	47	82	63	-165	24	-159	28	-186	25	-387	-2	-26	10	89	26	155	17
880705	665	92	-41	43	77	58	-170	19	-175	12	-188	23	-388	-3	-27	9	88	25	155	17
880711	671	98	-34	50	86	67	-162	27	-167	20	-183	28	-384	1	-23	13	91	28	156	18
880719	677	104	-30	54	93	74	-157	32	-163	24	-178	33	-381	4	-20	16	94	31	157	19
880727	682	109	-27	57	95	76	-153	36	-158	29	-177	34	-379	6	-20	16	95	32	158	20
880801	675	102	-36	48	79	60	-165	24	-168	19	-186	25	-385	0	-27	9	90	27	157	19
880811	678	105	-33	51	82	63	-163	26	-166	21	-182	29	-382	3	-24	12	92	29	159	21
880818	672	99	-38	46	76	57	-168	21	-171	16	-185	26	-384	1	-26	10	90	27	159	21
880822	674	101	-35	49	80	61	-165	24	-168	19	-183	28	-382	3	-25	11	91	28	160	22
880901	680	107	-32	52	84	65	-161	28	-164	23	-181	30	-381	4	-23	13	94	31	161	23
880907	680	107	-33	51	82	63	-162	27	-152	35	-181	30	-381	4	-23	13	96	33	162	24
880914	678	105	-33	51	81	62	-163	26	-165	22	-181	30	-380	5	-23	13	94	31	162	24
880919	670	97	-41	43	70	51	-172	17	-172	15	-186	25	-383	2	-25	11	93	30	163	25
880926	671	98	-37	47	80	61	-165	24	-167	20	-179	32	-379	6	-20	16	97	34	165	27
881004	670	97	-36	48	81	62	-164	25	-167	20	-179	32	-379	6	-20	16	97	34	166	28

* Initial Reading

Figure C11. Strain gage data from inside (railroad face) bars of Panel 6

	Gauge No. 1 Depth: 5 Ft		Gauge No. 2 Depth: 10 Ft		Gauge No. 3 Depth: 15 Ft		Gauge No. 4 Depth: 20 Ft		Gauge No. 5 Depth: 24 Ft		Gauge No. 6 Depth: 28 Ft		Gauge No. 7 Depth: 32 Ft		Gauge No. 8 Depth: 36 Ft		Gauge No. 9 Depth: 40 Ft		Gauge No. 10 Depth: 44 Ft	
Date	Field Read	Cumul. ue	Field Read	Cumul. ue	Field Read	Cumul. ue	Field Read	Cumul. ue	Field Read	Cumul. ue	Field Read	Cumul. ue	Field Read	Cumul. ue	Field Read	Cumul. ue	Field Read	Cumul. ue	Field Read	Cumul. ue
871229*	322		-31		-209		-159		249		-126		-274		150		259		-25	
880107	321	-1	-33	-2	-213	-4	-161	-2	248	-1	-122	4	-274	0	143	-7	264	5	-24	1
880111	340	18	-31	0	-212	-3	-161	-2	249	0	-120	6	-273	1	160	10	267	8	-23	2
880119	353	31	-27	4	-212	-3	-162	-3	248	-1	-118	8	-271	3	164	14	268	9	-18	7
880125	358	36	-23	8	-209	0	-161	-2	249	0	-116	10	-270	4	166	16	270	11	-16	9
880204	369	47	-17	14	-205	4	-160	-1	249	0	-115	11	-271	3	154	4	271	12	-14	11
880209	374	52	-8	23	-194	15	-153	6	256	7	-110	16	-269	5	156	6	272	13	-13	12
880217	373	51	7	38	-153	56	-135	24	272	23	-104	22	-265	9	160	10	273	14	-11	14
880225	371	49	12	43	-163	46	-133	26	281	32	-92	34	-258	16	163	13	268	9	-14	11
880304	379	57	16	47	-156	53	-128	31	282	33	-54	72	-259	15	167	17	270	11	-14	11
880311	381	59	18	49	-150	59	-122	37	291	42	-45	81	-238	36	192	42	282	23	-7	18
880314	377	55	16	47	-160	49	-125	34	288	39	-47	79	-242	32	185	35	280	21	-9	16
880324	379	57	17	48	-157	52	-124	35	287	38	-49	77	-239	35	162	12	253	-6	-20	5
880401	382	60	15	46	-158	51	-123	36	288	39	-48	78	-237	37	163	13	254	-5	-20	5
880407	383	61	19	50	-155	54	-122	37	289	40	-46	80	-237	37	165	15	254	-5	-20	5
880415	377	55	15	46	-170	39	-130	29	279	30	-54	72	-246	28	150	0	243	-16	-26	-1
880419	384	62	22	53	-164	45	-125	34	284	35	-50	76	-241	33	153	3	243	-16	-26	-1
880427	385	63	25	56	-167	42	-124	35	287	38	-46	80	-240	34	147	-3	238	-21	-26	-1
880503	386	64	25	56	-149	60	-117	42	295	46	39	165	-232	42	166	16	253	-6	-18	7
880510	381	59	19	50	-170	39	-129	30	281	32	-48	78	-241	33	152	2	240	-19	-24	1
880516	381	59	21	52	-166	43	-126	33	284	35	-47	79	-240	34	154	4	242	-17	-23	2
880523	377	55	15	46	-169	40	-130	29	279	30	-52	74	-245	29	152	2	238	-21	-22	3
880531	390	68	30	61	-148	61	-115	44	298	49	-34	92	-230	44	165	15	249	-10	-17	8
880608	393	71	33	64	-152	57	-116	43	295	46	-37	89	-230	44	160	10	243	-16	-20	5
880614	392	70	29	60	-162	47	-121	38	286	37	-46	80	-236	38	152	2	233	-26	-25	0
880622	385	63	24	55	-171	38	-127	32	280	31	-54	72	-244	30	140	-10	225	-34	-27	-2
880627	388	66	27	58	-157	52	-120	39	289	40	-47	79	-237	37	150	0	230	-29	-23	2
880705	385	63	27	58	-154	55	-118	41	294	45	-40	86	-234	40	156	6	235	-24	-18	7
880711	387	65	27	58	-159	50	-120	39	290	41	-46	80	-236	38	150	0	228	-31	-23	2
880719	383	61	25	56	-166	43	-125	34	285	36	-50	76	-244	30	142	-8	222	-37	-23	2
880727	387	65	26	57	-164	45	-122	37	286	37	-54	72	-242	32	143	-7	220	-39	-24	1
880801	386	64	29	60	-148	61	-114	45	286	37	-44	82	-235	39	153	3	227	-32	-17	8
880811	385	63	31	62	-146	63	-111	48	299	50	-38	88	-232	42	155	5	233	-26	-15	10
880818	385	63	33	64	-140	69	-109	50	303	54	-34	92	-228	46	161	11	238	-21	-11	14
880822	383	61	31	62	-146	63	-112	47	298	49	-37	89	-231	43	159	9	236	-23	-11	14
880901	385	63	33	64	-146	63	-111	48	299	50	-38	88	-232	42	156	6	231	-28	-12	13
880907	382	60	30	61	-146	63	-109	50	298	49	-39	87	-235	39	154	4	228	-31	-12	13
880914	379	57	30	61	-143	66	-109	50	298	49	-39	87	-235	39	156	6	231	-28	-6	19
880919	380	58	33	64	-130	79	-102	57	307	58	-28	98	-225	49	165	15	241	-18	0	25
880926	382	60	33	64	-139	70	-106	53	303	54	-30	96	-228	46	162	12	242	-17	-4	21
881004	381	59	32	63	-140	69	-106	53	303	54	-30	96	-228	46	178	28	244	-15	-3	22

* Initial Reading

Figure C12. Strain gage data from outside (river face) bars of Panel 6

APPENDIX D: COMPUTATION OF EFFECTIVE ELASTIC MODULUS AND MOMENT OF INERTIA FOR PANEL 6 SECTION

Effective Moment of Inertia of Wall Section

Section

A_s' = 1.03 in.^{2}/ft*

A_s = 2.11 in.^{2}/ft

width , b = 1.0 ft

height , h = 3.0 ft

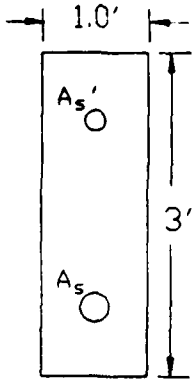

Modular ratio

$$n = E_s/E_c = \frac{29 \times 10^6 \text{ psi}}{4.03 \times 10^6 \text{ psi}}$$

$$n = 7.2$$

where

n = modular ratio
E_s = elastic modulus of steel
E_c = elastic modulus of 5,000 psi concrete

Transformed Section

nA_s' = 7.2(1.03 in.^{2}/ft)
= 7.416 in.^{2}

nA_s = 7.2(2.11 in.^{2}/ft)
= 15.192 in.^{2}

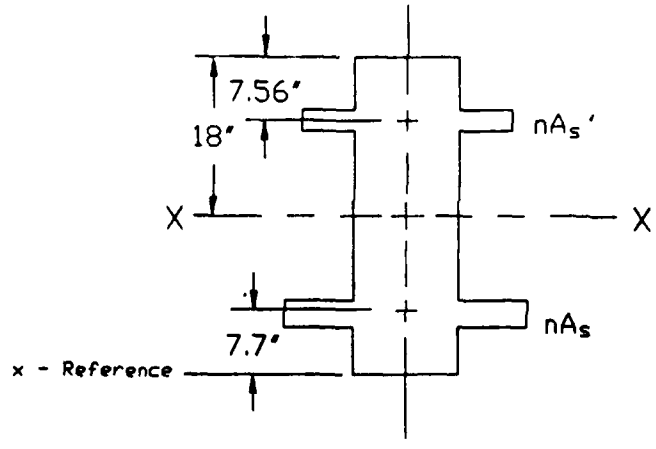

---

* For convenience, symbols and abbreviations used in this appendix are listed in the Notation (Appendix E).

To find centroid

$\bar{x}$ = centroid of composite section

$$\bar{x} = \frac{\Sigma Ax}{\Sigma A}$$

$$= \frac{(nA'_s)(36 \text{ in.} - 7.56 \text{ in.}) + (nA_s)(7.7 \text{ in.}) + [(12 \text{ in.} \times 36 \text{ in.}) - (1.03 \text{ in.}^2 + 2.11 \text{ in.}^2)] (18 \text{ in.})}{nA'_s + nA_s + [(12 \text{ in.} \times 36 \text{ in.}) - (1.03 \text{ in.}^2 + 2.11 \text{ in.}^2)]}$$

$$= \frac{210.91 + 116.98 + 7,719.48}{7.416 + 15.192 + 428.86}$$

where

A = geometric area
x = distance from centroid of area A to x reference line

Centroid: $\bar{x}$ = 17.82 in. (from the x reference line shown)

To compute effective moment of inertia

I_{xx} = moment of inertia of the section, about the x-x axis

$I_{xx} = \Sigma(I + Ad^2)$

$= 1/12 (12 \text{ in.})(36 \text{ in.})^3 + [(12 \text{ in.} \times 36 \text{ in.}) - (1.03 \text{ in.}^2 + 2.11 \text{ in.}^2)] (18 \text{ in.} - 17.82 \text{ in.})^2$ (concrete)

$+ [\sim 0 + (7.416 \text{ in.}^2)(18.18 \text{ in.} - 7.56 \text{ in.})^2]$ (top steel)

$+ [\sim 0 + (15.192 \text{ in.}^2)(17.82 \text{ in.} - 7.7 \text{ in.})^2]$ (bottom steel)

$= (46,670 + 836.4 + 1,555.9) \text{in.}^4$

$= 49,062 \text{ in.}^4 = 2.36 \text{ ft}^4$

Effective Modulus of Elasticity for Wall Section

$$E_{eff} = \frac{E_s I_s + E_c (I_c - I_s)}{I_c}$$

where

E_{eff} = effective elastic modulus for an uncracked composite section of steel and concrete (Johnson 1988)*

E_s and E_c, as defined on page D1.

I_c = moment of inertia of the concrete in the section

$$I_c = \frac{bh^3}{12} = \frac{12 \text{ in.}(36 \text{ in.})^3}{12} = 46{,}656 \text{ in.}^4$$

I_s = moment of inertia of the four steel bars in the section

= 332.3 in.^{4} (shown in following drawing)

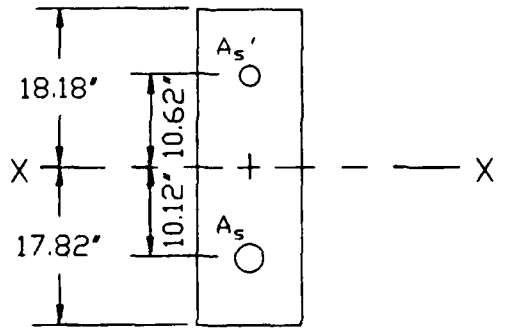

A_s' = 1.03 in.^{2}/ft × 1-ft section

A_s = 2.11 in.^{2}/ft × 1-ft section

$$I_s = \Sigma Ad^2$$

$$= (1.03 \text{ in.}^2)(10.62 \text{ in.})^2 + (2.11 \text{ in.}^2)(10.12 \text{ in.})^2$$

$$= 332.3 \text{ in.}^4$$

$$E_{eff} = \frac{29 \times 10^6 \text{ psi}(332.3 \text{ in.}^4) + 4.03 \times 10^6 \text{ psi}(46{,}656 - 332.3)\text{in.}^4}{46{,}656 \text{ in.}^4}$$

$$= 4.21 \times 10^6 \text{ psi}$$

---

* References cited in this appendix are listed following the main text of this report.

APPENDIX E: NOTATION

A	Geometric area
A_s	Cross-sectional area of bottom steel in beam section
A_s'	Cross-sectional area of top steel in beam section
b	Width of beam section
c	Distance to centroid of beam section, from extreme fiber
d	Distance from $\bar{x}$ (centroid of composite section) to the centroid of a component of the section
D	Depth of excavation
DL	Design load
E	Elastic modulus
E_c	Elastic modulus of concrete
E_{eff}	Effective elastic modulus for uncracked composite section of steel and concrete
E_I	Initial stress-strain soil modulus in hyperbolic model
E_s	Elastic modulus of steel
E_{ur}	Soil unload-reload modulus of nonlinear hyperbolic model
EI	Structural section stiffness
E_T	Tangent stress-strain soil modulus in hyperbolic model
f_c'	Concrete compressive strength
f_t'	Concrete tensile strength
FE	Finite element
h	Height of beam section
I	Moment of inertia
I_c	Moment of inertia of concrete
I_{eff}	Effecive moment of inertia including concrete and steel
I_s	Moment of inertia of steel in a beam section
I_{xx}	Moment of inertia of a section about the x-x axis
K_a	Rankine active earth pressure coefficient
K_m	Hyperbolic modulus constant for initial modulus
K_o	Initial horizontal, at-rest earth pressure coefficient
K_{ur}	Hyperbolic modulus constant for unload-reload modulus
L	Length
M	Internal bending moment about major axis of beam section
N	Hyperbolic model modulus exponent
n	Modular ratio of composite section

P	Force
QM5	Two-dimensional, plane strain, subparametric, quadilateral finite element used in the SOILSTRUCT program
R	Hyperbolic model material strength ratio of failure to ultimate strengths
RSD	Reworked slide debris
S	Section modulus
SB	Slide blocks
SD	Slide debris
SI	Slope inclinometer
Ti	Bonney rock intrusion
Tw	Weigle formation
UPRR	Union Pacific Railroad
x	Distance to centroid of area from a reference
$\bar{x}$	Centroid of composite section from a reference
$\mu\epsilon$	microstrain = 1×10^{-6} ϵ
Δ	Deflection
ΔL	Change in length
ϵ	Strain
σ	Stress
σ_H	Horizontal stress
σ_V	Vertical stress
σ_t	Stress in top beam fibers
σ_b	Stress in bottom beam fibers
σ_1	Major principal stress
σ_3	Minor principal or confining stress
$(\sigma_1 - \sigma_3)$	Deviator stress level
$(\sigma_1 - \sigma_3)_{ult}$	Ultimate stress level
ϕ	Internal friction angle of soil